INTERNATIONAL ATOMIC ENERGY AGENCY
UNITED NATIONS EDUCATIONAL, SCIENTIFIC AND CULTURAL ORGANIZATION
INTERNATIONAL CENTRE FOR THEORETICAL PHYSICS
I.C.T.P., P.O. BOX 586, 34100 TRIESTE, ITALY, CABLE: CENTRATOM TRIESTE

SMR. 758 - 26

SPRING COLLEGE IN CONDENSED MATTER ON QUANTUM PHASES

(3 May - 10 June 1994)

==========

Background information on the lecture

THE DENSITY MATRIX RENORMALIZATION GROUP

Steven R. WHITE
Department of Physics
University of California
Irvine, CA-92717, U.S.A.

==========

These are preliminary lecture notes, intended only for distribution to participants.

==========

```
#include "utilities.h"
#include "matrix.h"

Matrix reverserows(const Matrix& mat)
{
Matrix res = mat;
Vector temp;
int nr = res.Nrows();
for(int i=1; i <= nr/2; i++)
    {
    temp = res.Row(i);
    res.AccessRow(i) = res.Row(nr+1-i);
    res.AccessRow(nr+1-i) = temp;
    }
return res;
}

Matrix reversecols(const Matrix& mat)
{
Matrix res = mat;
Vector temp;
int nc = res.Ncols();
for(int i=1; i <= nc/2; i++)
    {
    temp = res.Column(i);
    res.AccessColumn(i) = res.Column(nc+1-i);
    res.AccessColumn(nc+1-i) = temp;
    }
return res;
}

Matrix reverse(const Matrix& mat)
{
return reversecols(reverserows(mat));
}

Matrix colmat(const Vector& vec)
{
Matrix res(vec.Length(),1);
res.AccessColumn(1) = vec;
return res;
}


void main()
{
int i,j,newcurm=1,L,m,curm=1,blocksize,numiter;
cout << "Input length, number of states to keep m" << endl;
cin >> L >> m >> nextline;
cout << "numiter, do psikeep?, do local?" << endl;
cin >> numiter >> nextline;
int toadd,extra;
cout << "sites to add, extra sites?" << endl;
cin >> toadd >> extra >> nextline;
int centersize = toadd+extra;

Matrix *Hstore;
Vector *tstore;
Hstore = new Matrix[L+1];
tstore = new Vector[L+1];
```

```
Matrix H(1,1);
H = 2.0;
Hstore[1] = H;
Vector t(1);
t(1)=-1;
tstore[1] = t;
Matrix bigcenter(centersize,centersize);
bigcenter = 2.0;
for(j=1; j <= centersize-1; j++)
    bigcenter(j,j+1)=bigcenter(j+1,j)=-1.0;
Matrix Hbig,psikeep(1,1),evecs,V,Htilde,psitilde,colt,Hright;
Matrix coltright;
Vector evals;
psikeep=1.0;
for(int iter=1; iter <= numiter; iter++)
  {
  H = Hstore[1];
  t = tstore[1];
  newcurm=1;
  blocksize = 1;
  while(1)
    {
    if(blocksize+centersize
    if(iter == numiter && 2*blocksize > L) break;
    curm = newcurm;
    newcurm = min(m,curm+1);
    int bigdim;
    Htilde.ReDimension(curm+1,curm+1);
    Htilde.AccessSubMatrix(1,curm,1,curm) = H;
    colt = colmat(t);
    Htilde.AccessSubMatrix(1,curm,curm+1,curm+1) = colt;
    Htilde.AccessSubMatrix(curm+1,curm+1,1,curm) = Transpose(colt);
    Htilde(curm+1,curm+1) = center(1,1);

    if(iter == 1 && 2*blocksize <= L)
        {
        Hright = Htilde;
        bigdim = 2*curm+2;
        }
    else
        {
        int cr = Hstore[L-blocksize-1].Nrows();
        Hright.ReDimension(cr+1,cr+1);
        Hright.AccessSubMatrix(1,cr,1,cr) = Hstore[L-blocksize-1];
        coltright = tstore[L-blocksize-1];
        Hright.AccessSubMatrix(1,cr,cr+1,cr+1) = coltright;
        Hright.AccessSubMatrix(cr+1,cr+1,1,cr) = Transpose(coltright);
        Hright(cr+1,cr+1) = center(1,1);
        bigdim = curm+2+cr;
        }
    Hbig.ReDimension(bigdim,bigdim);
    Hbig = 0.0;
    Hbig.AccessSubMatrix(1,curm+1,1,curm+1) = Htilde;
    Hbig.AccessSubMatrix(curm+1,curm+2,curm+1,curm+2) = center;
    Hbig.AccessSubMatrix(curm+2,bigdim,curm+2,bigdim) = reverse(Hright);

    EigenValues(Hbig,evals,evecs);
    cout << iter SP blocksize;
    for(j=1; j <= curm; j++)
        cout << evals(j);
```

```
    cout << endl;

    V = evecs.SubMatrix(1,curm+1,1,newcurm);
    Orthog(V);
    V = Transpose(V);
    H = V * Htilde * Transpose(V);
    t = -V.Column(curm+1);
    Hstore[blocksize] = H;
    tstore[blocksize] = t;
    }
  }
blocksize--;
cout << "size = " <<  2*blocksize << endl;
cout << "energies are " << endl;
for(j=1; j <= curm; j++)
    cout << j SPACC evals(j) SPACC 2*(1.0-cos(j*Pi/(2*blocksize+1))) << endl;
}
```

PRL 68, 3487 (1992)
January, 1992

Real-space Quantum Renormalization Groups

S.R. White and R.M. Noack
Department of Physics
University of California
Irvine, CA 92717

Although originally thought to show great promise in solving quantum many-body problems on a lattice, numerical real-space renormalization group techniques have had little success for such problems. We explore the nature of the difficulties involved by studying the application of the method to the simple tight-binding model in one dimension. The standard approach fails dramatically for this model. We show that the key to successfully applying the renormalization group technique lies in applying a variety of boundary conditions to a block in order to simulate the effect of neighboring blocks.

PACS Numbers: 05.30.Fk, 05.70.Fh, 71.10.+x

Shortly after Wilson's dramatic success in solving the Kondo problem with a numerical renormalization group (RG) method[1], there was considerable excitement about the possibility of applying the same type of approach in a real-space form to a variety of difficult quantum lattice problems. These real-space RG techniques quickly developed a bad reputation, however, after several different applications of the methods gave poor results. For example, Lee [2] applied a real-space RG technique to the problem of Anderson localization on a two-dimensional square lattice. The major conclusion of this study, that there was a critical parameter that separated scaling towards extended or localized states, later was shown by Lee and Fisher [3] to be incorrect. RG studies of other systems, such as the one-dimensional (1D) Hubbard model [4], also gave poor results, and today the technique is little used. It has not been very well understood why the method fails.

In this letter [5] we examine real-space RG methods for an extremely simple model, a 1D tight-binding lattice. The importance of understanding real-space RG in the context of this model was pointed out by Wilson several years ago in an informal, unpublished talk. The standard RG approach fails spectacularly in this model, and it is quite easy to see why. Here, in addition to showing why if fails, we provide several closely related variations of the standard approach which perform extremely well. Although the calculations reported here are for this very simple model, we believe the problem is generic and the general type of solution we give can be applied to virtually any quantum lattice model.

We consider a 1-D chain of sites i with the single-particle Hamiltonian matrix

$$H_{ij} = \begin{cases} 2 & i = j \\ -1 & |i - j| = 1 \\ 0 & \text{otherwise.} \end{cases} \tag{1}$$

This problem is equivalent in the continuum limit to a 1-D particle in a box.

The standard real-space RG approach consists of considering a group of sites to be a "block", and diagonalizing that block to find a set of eigenstates. One then truncates the set of eigenstates, keeping only the lowest m states (ordered by energy), and uses those states to construct an approximate Hamiltonian for a new, larger block composed of two of the old blocks. At each iteration s we can write the Hamiltonian of the infinite chain as a block tridiagonal matrix in terms of diagonal blocks H^s and off-diagonal blocks T^s

$$H = \begin{pmatrix} H^s & T^s & 0 & 0 & \dots \\ T^{s\dagger} & H^s & T^s & 0 & \dots \\ 0 & T^{s\dagger} & H^s & T^s & \dots \\ \vdots & \vdots & \vdots & \vdots & \end{pmatrix} \tag{2}$$

Initially, the block size is 1 and H^1 and T^1 are 1×1 matrices equal to 2 and -1, respectively. We start iteration s by forming the Hamiltonian matrix for a block composed of two blocks from the previous iteration

$$\bar{H}^s = \begin{pmatrix} H^{s-1} & T^{s-1} \\ (T^{s-1})^\dagger & H^{s-1} \end{pmatrix} \tag{3}$$

and

$$\bar{T}^s = \begin{pmatrix} 0 & 0 \\ T^{s-1} & 0 \end{pmatrix} \tag{4}$$

We diagonalize $\bar{H}^s$ and take the lowest m eigenvalues E^s_ℓ and eigenstates, V^s_ℓ, $\ell = 1, \dots m$, discarding the rest. We then perform a change of basis to the eigenstates via

$$H^s_{\ell\ell'} = \sum_{i,j} V^s_{\ell i} \bar{H}^s_{ij} V^s_{\ell' j}. \tag{5}$$

and

$$T^s_{\ell\ell'} = \sum_{i,j} V^s_{\ell i} \bar{T}^s_{ij} V^s_{\ell' j}. \tag{6}$$

Note that Eq. (5) puts H^s into diagonal form. We then proceed on to the next iteration, starting with Eq. (3) and (4). The idea is that the higher energy states which are discarded at the current iteration are unimportant in making up the low energy states at a later iteration. The accuracy can be increased by keeping more states, i.e., increasing m.

It is easy to see in this simple example, however, that this procedure is quite *poor* in describing large scale, low energy behavior. The Hamiltonian in this example is just a finite-difference discretization of the kinetic energy of a 1-D particle, and in the limit of large block size, the eigenstates are just particle-in-a-box eigenstates. The boundary condition of ignoring the connections T to neighboring blocks corresponds to setting the wavefunction to 0 at the sites just outside the block. Fig. 1 illustrates the difficulty. Any state made only of low-lying states from the previous iteration must have a "kink" in the middle. In order to accurately represent states in the larger block, one must make use of nearly all the states in the smaller block: any truncation leads to large errors.

Wilson suggested one possible way to cure this problem. He suggested integrating out the higher energy states via a unitary transformation, taking into account the interactions with other blocks perturbatively rather than ignoring them. (This approach is closely related to degenerate perturbation theory.) Ingersent and White [6] recently tried a variety of ways of implementing this, but were unable to find a satisfactory approach. We now believe that the set of low-lying states kept in the standard approach is too incomplete for the perturbative unitary transformation to help.

The key to fixing this simple example lies in the treatment of boundary conditions (BCs). However, simply choosing an alternative set of BSs is not adequate. The standard approach uses BCs in which the eigenstates vanish (in the large block limit)

at the edges of a block. We call this type of BCs "fixed". Because fixed BCs must be used on the inside edges whenever two blocks are to be joined, fixed BCs are the most natural kind to use. However, the RG procedure can be modified to use other kinds of BCs. The alternative BCs would be used in forming the matrix that is diagonalized in order to determine the eigenfunctions V to be kept, but fixed BCs must still be used on the inner edges in forming larger blocks. Although H^s in Eq. (5) is no longer diagonal, the procedure is still well-defined in the sense that it is exact when all states are kept at each iteration.

One finds, however, that applying the RG procedure with BCs other than fixed does not eliminate the difficulties. For example, using periodic BCs results in the low-lying eigenstates being identical at the two edges, which prevents the accurate representation of anything but the ground state (which for periodic BCs is a constant function) on larger blocks. "Free" boundary conditions (obtained by changing H_{ii} from 2 to 1 on the edges) result in the slope of the eigenstate vanishing at the edges, and again excited states on larger blocks cannot be represented.

In order to obtain a working approach, we must *combine* eigenstates obtained from different boundary conditions. The block must be diagonalized several times, with different boundary conditions each time. We then extract a few low-lying eigenstates from each diagonalization, orthogonalize them, and keep this set of states for the next iteration. To be more specific, the following "fixed-free" procedure solves the simple problem *exactly* for fixed boundary conditions, in the sense that a finite number of the lowest energies of large blocks are obtained exactly even after many iterations, keeping only a few states at each iteration. This method uses the four possible combinations of free and fixed BCs at the two edges of each block. We keep track of four H matrices at each iteration, $\bar{H}^s_{bb'}$, where b represents the left edge and takes on the values "free" or "fixed", and b' similarly represents the right edge. For example, for an initial

two-site block one would have

$$H^1_{\text{free,fixed}} = \begin{pmatrix} 1 & -1 \\ -1 & 2 \end{pmatrix}. \tag{7}$$

We diagonalize $\bar{H}^s_{\text{free,fixed}}$ and extract the lowest $m/4$ eigenstates. Similarly, we extract the lowest $m/4$ eigenstates for $\bar{H}^s_{\text{free,free}}$, $\bar{H}^s_{\text{fixed,free}}$, and $\bar{H}^s_{\text{fixed,fixed}}$. This set of m states is not orthogonal, so we next orthonormalize them. This set of states forms the new basis, taking the place of the $V^s_\ell, \ell = 1, \cdots m$. (The orthogonal complement to these states are the states that are discarded.) We next perform a change of basis on the matrices $\bar{T}^s$ and $\bar{H}^s_{b,b'}$, as in Eq. (6). Finally, for the next iteration, we replace Eq. (3) by

$$H^s_{bb'} = \begin{pmatrix} H^{s-1}_{b,\text{fixed}} & T^{s-1} \\ (T^{s-1})^\dagger & H^{s-1}_{\text{fixed},b'} \end{pmatrix}. \tag{8}$$

Note the use of fixed BCs for the inner edges when joining two blocks together.

Table I compares the results of this procedure with the standard one. The eigenvalues of $\bar{H}^s_{\text{fixed,fixed}}$ are shown for the new procedure. A total of 8 states ($m = 8$) were kept for both procedures. Whereas the results from the standard procedure bear little relationship to the exact results, we find that the new procedure yields exact energies for the first four states even after 10 (or more) iterations to at least 15 digits with 64 bit precision. We have only numerical evidence that this procedure gives exact results; nevertheless, the results are quite convincing.

The lesson to be learned from this example is that the influence of the surrounding blocks not taken into account in the current iteration is to effectively apply a variety of boundary conditions to the current block. Hence, any approach using one set of boundary conditions on a block generates a set of states which is in some sense "incomplete", and it is very difficult to correct this incompleteness by keeping many states or by applying perturbative corrections.

The fact that the fixed-free method performs so well is not an accident specific to this problem or this choice of BCs. Very accurate, but *not exact* results are obtained using the combination of periodic and anti-periodic BCs. For periodic or anti-periodic BCs, the matrix elements at the corners of the blocked Hamiltonian matrix are affected by the boundary conditions. In order to perform the real-space blocking transformation, one has to keep track of two additional off-diagonal matrices, T^s_P, T^s_{AP}, for periodic and antiperiodic BCs, in addition to T^s. One diagonalizes the blocked Hamiltonian

$$\bar{H}^s_b = \begin{pmatrix} H^{s-1} & T^{s-1}_b \\ (T^{s-1}_b)^\dagger & H^{s-1} \end{pmatrix} \tag{9}$$

for both periodic ($b = P$) and anti-periodic ($b = AP$) boundary conditions, keeps $m/2$ states from each BC and orthonormalizes the resulting states. This set of states is then used to transform $\bar{H}^s$ and $\bar{T}^s$, formed using Eqs. (3) and (4), to the new basis. The new off-diagonal matrices can be formed from the T^{s-1} using

$$\bar{T}^s_b = \begin{pmatrix} 0 & \pm(T^{s-1})^\dagger \\ T^{s-1} & 0 \end{pmatrix} \tag{10}$$

and then transformed to the new basis as in Eq. (6). Here the positive sign is for periodic BCs and the negative sign for anti-periodic BCs. Table III compares the energies of the lowest four eigenstates using this method for periodic BCs with the exact results and with renormalization group results for which only periodic boundary conditions are kept. The results are calculated after 10 iterations of the renormalization group, keeping 8 states at each iteration.

A third approach to varying the BCs involves putting extra blocks around the block of interest. One diagonalizes a larger system containing p blocks (a "superblock"), where $p > 2$, but with only *one* type of BC (typically periodic). Two of these blocks

will form a larger block for the next iteration. The idea is that the surrounding blocks apply a variety of BCs to the block of interest. We extract m states from the diagonalization of the superblock, then project out the portion of each wavefunction corresponding to the two spatial blocks of interest. The system size doubles at each iteration. For $p = 2$, this procedure is equivalent to the conventional procedure for periodic BCs (results for which are given in Table II, Column 2). As in the other methods, these projected states must be orthogonalized before they can be used to transform the Hamiltonian matrices.

The results for the superblock procedure are summarized in Table III for various values of p, after 10 iterations, keeping 8 states at each iteration. The results are reasonably accurate even for $p = 3$, and become more accurate for larger p. The $p = 20$ results are accurate to 10 decimal places, suggesting that this procedure becomes exact in the large p limit.

In devising a procedure such as the three we have described here, it is important to make sure that the variation of the boundary conditions be sufficiently broad. For example, if one uses the superblock method with antiperiodic BCs, one finds that the ground state is not accurately obtained, but that excited states are. This is because the states kept are missing any very low momentum component. However, if one adds one extra state, the zero momentum state $V_i = \text{const}$, to the list of states kept at each iteration, the method becomes even more accurate than the periodic BC superblock method.

The next challenge is to discover how to apply the general ideas discussed here to more difficult models, such as the localization model studied by Lee [2], or interacting models, such as the 1D Hubbard model. We believe the most promising method of the three we have described here is the superblock method, since one does not have to choose what BCs to apply—in a sense, the system does it for us. One can also

envision hybrids of the superblock method with other variations of the BCs, in order to keep the number of extra blocks to a minimum.

We would like to thank K. Ingersent for an number of helpful discussions and collaboration. We would also like to thank S. Coppersmith and D.R. Hamann for helpful comments and suggestions. This work was supported by the Office of Naval Research under Grant No. N00014-91-J-1143 and in part by the University of California through an allocation of computer time on the UC Irvine Convex.

[1]K.G. Wilson, *Rev. Mod. Phys.* 47, 773 (1975).

[2]P.A. Lee, *Phys. Rev. Lett.* **42** , 1492 (1979).

[3]P.A. Lee and D.S. Fisher, *Phys. Rev. Lett.* **47** , 882 (1981).

[4]J.W. Bray and S.T. Chui, *Phys. Rev.* **B**19, 4876 (1979); S.T. Chui and J.W. Bray, *Phys. Rev.* **B**18, 2426 (1978); J.E. Hirsch,*Phys. Rev.* **B**22, 5259 (1980); C. Dasgupta and P. Pfeuty, *J. Phys.* C14, 717 (1981).

[5]Parts of this work have appeared in S.R. White, in *Proceedings of the International Meeting on Computational Physics for Condensed Matter Phenomena*, Osaka, October 1991 (to be published).

[6]K. Ingersent and S.R. White, unpublished.

FIGURE CAPTIONS

FIG. 1. Lowest eigenstates of two 8-site blocks (solid circles) and a 16-site block (open circles) for the one-dimensional tight-binding model with fixed boundary conditions.

TABLE I. Lowest energies after 10 blocking transformations for the noninteracting single particle on a 1-D chain with fixed boundary conditions.

	Exact	Standard	Fixed-Free
E_0	2.3508×10^{-6}	1.9207×10^{-2}	2.3508×10^{-6}
E_1	9.4032×10^{-6}	1.9209×10^{-2}	9.4032×10^{-6}
E_2	2.1157×10^{-5}	1.9214×10^{-2}	2.1157×10^{-5}
E_3	3.7613×10^{-5}	1.9217×10^{-2}	3.7613×10^{-5}

TABLE II. Lowest energies after 10 blocking transformations for the noninteracting single particle on a 1-D chain with periodic boundary conditions.

	Exact	Periodic only	Periodic–Antiperiodic
E_0	0.0	0.0	0.0
E_1	9.4124×10^{-6}	2.1281×10^{-3}	9.4161×10^{-6}
E_2	3.7649×10^{-5}	5.3888×10^{-3}	3.7659×10^{-5}
E_3	8.4711×10^{-5}	9.1936×10^{-3}	8.4732×10^{-5}

TABLE III. Average relative errors in the lowest three excited state energies after 10 blocking transformations for periodic boundary conditions using the superblock method with p blocks.

p	Ave. error (%)
3	5
4	0.08
5	0.002
6	0.0005
20	10^{-8}

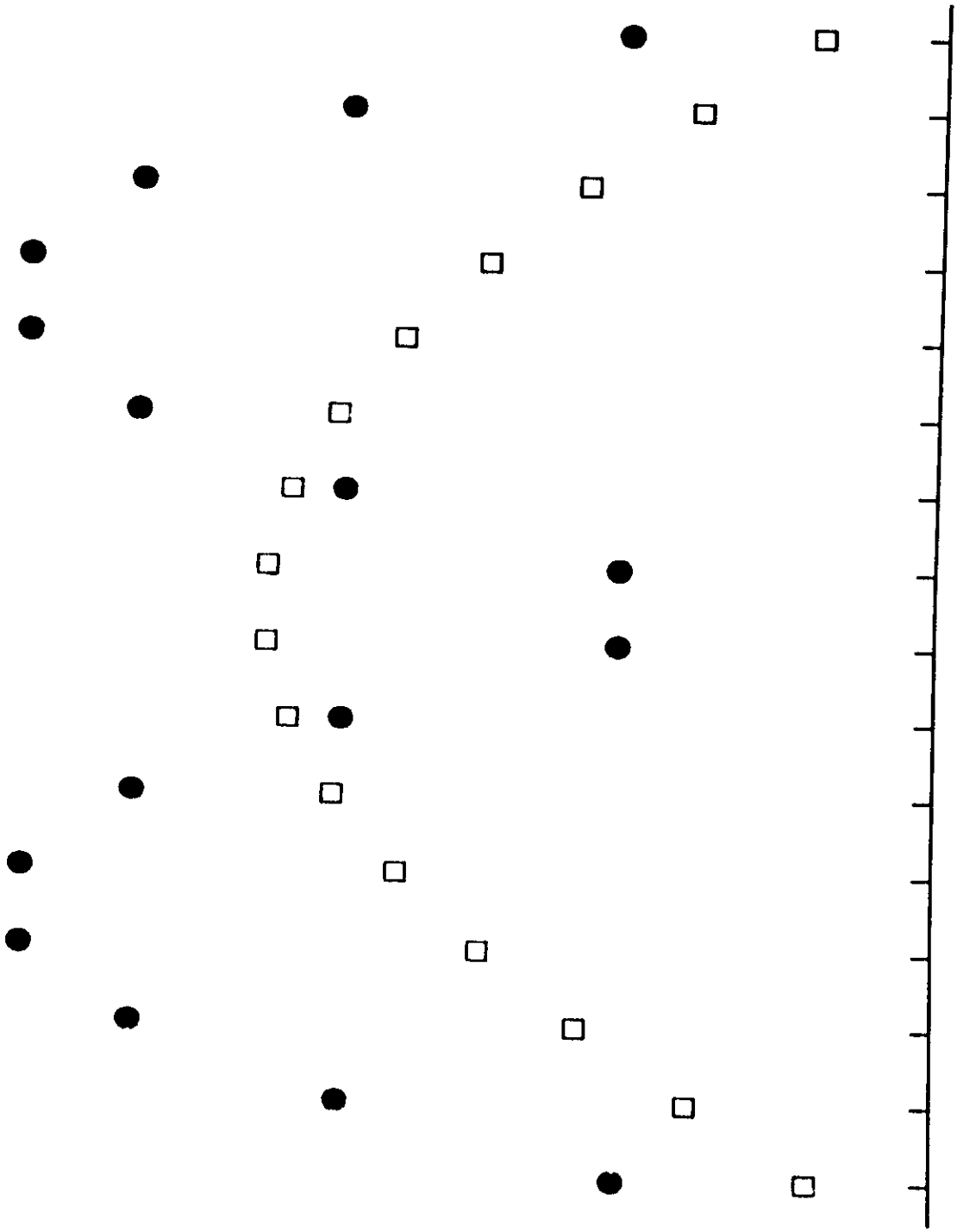

Fig. 1

Density Matrix Formulation for Quantum Renormalization Groups

Steven R. White

Department of Physics, University of California, Irvine, California 92717

(Received 22 May 1992)

A generalization of the numerical renormalization-group procedure used first by Wilson for the Kondo problem is presented. It is shown that this formulation is optimal in a certain sense. As a demonstration of the effectiveness of this approach, results from numerical real-space renormalization-group calculations for Heisenberg chains are presented.

PACS numbers: 75.10.Jm, 02.70.+d, 05.30.−d

While Wilson's solution of the Kondo problem [1] using a numerical renormalization-group (RG) technique was a dramatic breakthrough, the numerical approach he used has since had little success for anything but impurity problems. When applied to quantum lattice problems in a real-space blocking form, the approach is flawed in its treatment of the boundaries of a block [2]. The boundary errors make quantitatively accurate results impossible for most problems.

Here we show how to eliminate these flaws for an arbitrary interacting quantum lattice system. We reformulate the old approach in terms of density matrices, and show that the new approach is optimal in a certain sense. The density matrix framework provides an important conceptual basis for numerical RGs; for example, the zero-temperature, one-dimensional (1D), real-space algorithm we present here can easily be generalized to finite temperature, 2D or 3D, or momentum space (although the calculations may not always be practical). The approach does not require small couplings, can treat disordered systems, and of course, does not have the minus sign problem that plagues the quantum Monte Carlo approach.

We demonstrate the approach on $S=\frac{1}{2}$ and $S=1$ Heisenberg antiferromagnetic spin chains. Results are substantially better than the best available from Monte Carlo calculations, similar in accuracy and the variety of properties measured to what one expects from exact diagonalization, but one can treat lattices hundreds of sites long. We present results for the spatial spin density distribution of the fractional $S=\frac{1}{2}$ spins at the ends of open $S=1$ chains, and provide improved results for the ground-state energy and Haldane gap of $S=1$ chains. The computational resources required for these calculations are relatively small; if extreme accuracy is not required, a modest workstation is adequate.

We first describe the standard numerical RG procedure, as applied in a 1D real-space blocking context. One first breaks the infinite chain into a set of identical blocks A. One diagonalizes the Hamiltonian matrix H_{AA} for two neighboring blocks considered together, and uses m of its lowest-lying eigenstates to form a new, simpler Hamiltonian $H_{A'}$ representing a block twice as large [see Fig. 1(a)]. One repeats this procedure using the new larger blocks and the new effective Hamiltonian. One assumes in using this procedure that only the lowest-lying block eigenstates play a dominant role in forming states of larger blocks at later iterations.

For the formation of the effective Hamiltonian out of the low-lying eigenstates, we will only consider the approach used by Wilson for the Kondo problem, involving a change of basis to the new set of block eigenstates. We can write this procedure formally as

$$H_{A'}=OH_{AA}O^{\dagger}, \tag{1}$$

where O is an $m\times l$ matrix, and l is the dimension of H_{AA}. The rows of O are the m lowest eigenstates of H_{AA} [3].

Although the eigenstates of H_{AA} are natural states to use in forming O (the states kept), they are not optimal. In particular, because H_{AA} does not include any connections to surrounding blocks, its eigenstates have inappropriate features at the edges of a block. They are optimal only in the limit that the connections to other blocks vanish. Recently White and Noack [2] considered these problems with real-space RGs in the context of a very simple single-particle model. Several solutions, involving different treatments of boundary conditions, were proposed and shown to work very well for the single-particle model. These solutions all involved different

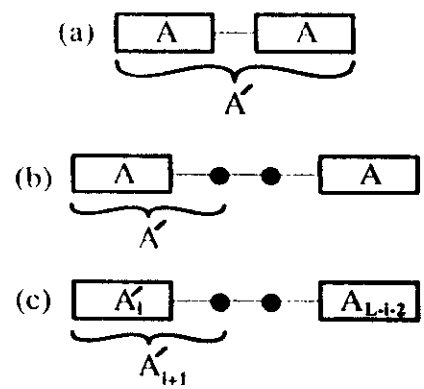

FIG. 1. Various blocking schemes for real-space renormalization groups on a 1D system. The standard approach is shown in (a). In the infinite-system method (b) and the finite-system method (c), one diagonalizes the entire system and forms the reduced density matrix for the part labeled A'. The solid circles represent single sites.

choices for the states kept. Here we show how to choose the *optimal* set of states to keep in a way appropriate for *interacting systems* as well as noninteracting.

The density matrix approach we present here is most closely related to the superblock method discussed by White and Noack, where one diagonalizes a larger system of three or more blocks (the superblock), of which AA is a part. The states one keeps are the projections of the low-lying states of the superblock onto AA. In the single-particle case, the projection operation is trivial. However, for a many-particle wave function, the projection of a wave function onto AA is not uniquely defined, nor does it produce only one state. In general, one expects it to project onto a complete set of block states. However, some of these states are more important than others; the density matrix tells us which states are the most important.

Let us assume that we know the state of the entire lattice (or a superblock in a practical calculation). We wish to generate a set of states for AA which are especially appropriate to represent the properties of AA when the lattice has this given state. It is straightforward to show that the eigenvectors with the largest eigenvalues of the density matrix of AA are the optimal states to keep, in the sense that they most accurately reproduce the state of the lattice. Suppose that the lattice is in a pure state $|\psi\rangle$. (One obtains the same conclusion if one considers the lattice to be in a mixed state, or at a finite tempreature.) Let $|i\rangle$, $i=1,\ldots,I$, be a complete set of states of AA and $|j\rangle$, $j=1,\ldots,J$, be the states of the rest of the lattice. We can write $|\psi\rangle=\sum_{i,j}\psi_{ij}|i\rangle|j\rangle$. We will assume for simplicity that ψ_{ij} is real. The reduced density matrix is [4]

$$\rho_{ii'}\equiv\sum_j \psi_{ij}\psi_{i'j}\,. \tag{2}$$

Let $|u^\alpha\rangle$, $\alpha=1,\ldots,m$, with $m<I$, be the optimal set of states we seek. The most general expansion for ψ in terms of the $|u^\alpha\rangle$ is

$$|\psi\rangle\approx\sum_{\alpha,j} a_{\alpha,j}|u^\alpha\rangle|j\rangle\,. \tag{3}$$

If we minimize the error in the representation of $|\psi\rangle$, $\||\psi\rangle-\sum_{\alpha,j}a_{\alpha,j}|u^\alpha\rangle|j\rangle\|$, with respect to both $a_{\alpha,j}$ and $u^\alpha_i=\langle u^\alpha|i\rangle$ (with $\langle u^\alpha|u^{\alpha'}\rangle=\delta_{\alpha\alpha'}$), we find that the u^α are the eigenvectors of ρ with the largest magnitude eigenvalues w_α.

Each w_α represents the probability of AA being in the state $|u^\alpha\rangle$, with $\sum_{\alpha=1}^{I}w_\alpha=1$. The deviation of $P_m\equiv\sum_{\alpha=1}^{m}w_\alpha$ from unity measures the accuracy of the truncation to m states.

Diagonalization of a superblock composed of p identical blocks, the configuration used in Ref. [2], is difficult for a many-particle system, since the dimension of the Hamiltonian is m^p, assuming m states per block. A better approach is shown in Fig. 1(b), where the superblock consists of two blocks and two sites. We adopt the notation $A\cdot\cdot A$ for this form of lattice. In this case the dimension of H is proportional to m^2. Here A' comes from a block plus a single site. [In a similar way, Wilson added a single interval (site) per iteration for the Kondo problem.] We found the configuration of Fig. 1(b) to be particularly efficient after trying a variety of alternative approaches. Note that open boundary conditions are used, since then the boundary between A and the rest of the system is a single point (as opposed to two points for periodic boundary conditions). In the limit of no connections between A and the rest of the system, $P_m=1$ for $m=1$. In general, the smaller this boundary, the faster P_m converges with m to unity. Note also that there are never any truncation errors from previous iterations in the representation of the two sites; this makes the iteration very stable.

The following are the steps of a single iteration of our density matrix approach in its most basic form: (1) Diagonalize the Hamiltonian of the system $A\cdot\cdot A$ using a sparse matrix algorithm, extracting the ground state. (2) Use Eq. (3) to find ρ for $A\cdot$. (3) Diagonalize ρ to find the *largest* m eigenvalues w_α and associated eigenvectors u^α. (4) Change basis and truncate using Eq. (1), with the u^α forming the rows of O. (5) Replace the first block by A' and the last by the reflection of A'.

Note that while the method generates m states for a block, these states are optimized specifically for producing *one* "target" state of $A\cdot\cdot A$ (although additional states can be targeted). For this reason, surprising accuracy is possible with very small m. However, only the target state is produced accurately.

At the fixed point of this iteration, the block A represents one-half of an infinite chain. Often it is useful to have results for a finite chain, but the above method (the infinite-system method) is not especially accurate in the early iterations. This is to be expected, since initially the density matrices used are derived from very small lattices. A variation on the method, which works very well for finite systems of size L ranging from four to several hundred sites, is illustrated in Fig. 1(c). The essential difference here is that the total length of the system $A\cdot\cdot A$ is always L (after some initial iterations of the infinite-system method to initially reach size L). This means that the first and last blocks are of different sizes, and one must keep track of a set of blocks of all sizes from 1 to L. We will explain this algorithm in detail in a subsequent paper. The calculation time is only 2 or 3 times as long as the time for the infinite-lattice method to reach size L.

As a test case for this approach, we have implemented it for antiferromagnetic Heisenberg spin chains, with $S=\frac{1}{2}$ and $S=1$, with Hamiltonian

$$H=\sum_i \mathbf{S}_i\cdot\mathbf{S}_{i+1}\,, \tag{4}$$

where we have set $J=1$. While the $S=\frac{1}{2}$ case is soluble via the Bethe ansatz, the $S=1$ case is not. The $S=1$ chain has been the subject of considerable numerical

TABLE I. Ground-state energies per site of infinite $S=\frac{1}{2}$ and $S=1$ antiferromagnetic Heisenberg chains. The exact Bethe-ansatz result for the energy of the $S=\frac{1}{2}$ chain is $-\ln 2+\frac{1}{4}=-0.443147\ldots$, and m is the number of states kept in block A (counting a triplet as three states, etc.). Results labeled ∞ are obtained from a linear extrapolation to $P_m\to 1$. Monte Carlo results are taken from Refs. [7] and [5].

	$S=\frac{1}{2}$	$S=\frac{1}{2}$	$S=1$	$S=1$
m	$E_0-E_0^{\text{exact}}$	$1-P_m$	$-E_0$	$1-P_m$
16	5.8×10^{-5}	8.0×10^{-6}	1.401089	4.8×10^{-5}
24	1.7×10^{-5}	1.9×10^{-6}	1.401380	1.6×10^{-5}
36	7.8×10^{-6}	9.0×10^{-7}	1.401437	6.6×10^{-6}
44	3.2×10^{-6}	3.6×10^{-7}	1.401476	1.1×10^{-6}
∞	1.9×10^{-7}		1.401484(2)	
MC	$\sigma=5\times10^{-4}$		1.4015(5)	

effort [5–8] since Haldane argued that the infinite system has a finite gap between the ground and first excited state [9]. Thus these two cases provide excellent tests both for the accuracy of the methods and for their competitiveness with other numerical approaches. Details of the numerical methods will be published elsewhere, as well as a more complete discussion of the results summarized below.

Table I shows results for the ground-state energies of the infinite $S=\frac{1}{2}$ and $S=1$ chains. The energy per site was determined from the difference in total energy of the system $A\cdots A$ from one iteration to the next. The procedure was iterated until the energy converged to about eight digits, about 100 iterations for the $S=1$ case.

We see from Table I that the method accurately recovers the exact energy of the $S=\frac{1}{2}$ chain to almost six digits. The truncation error $1-P_m$ appears to be an excellent estimator for the errors in the results, and can even be used to extrapolate to the exact limit $P_m\to 1$ to reduce errors further. Note the errors decrease roughly exponentially with m. The final result for the $S=1$ ground-state energy appears to be more than 2 orders of magnitude more accurate than the best available from Monte Carlo calculations.

Results for the energies of 16 and 22 site blocks for $S=\frac{1}{2}$ from the finite-lattice method are compared with exact diagonalization in Table II. This iterative diagonalization method is able to obtain energies for finite lattices with remarkable accuracy, even keeping only sixteen states. Results almost as accurate were obtained for $S=1$ chains, where we compared our results with Kennedy's exact diagonalization [6].

Recently there has been considerable interest in the $S=\frac{1}{2}$ degrees of the freedom at the ends of finite, open $S=1$ chains [6,10]. These effective spin-$\frac{1}{2}$'s have been observed experimentally in NENP systems [10,11], and are also the subject of current theoretical study [12]. As noted by Kennedy [6], these spins bind weakly on a finite open chain to form a singlet ground state with a triplet just above it (for an even numbered chain). In order to see the Haldane gap with open boundary conditions, one must look at the first excited state above this triplet. We find that the next excited state has total spin $S_T=2$, a quintuplet, and we define the Haldane gap for system size L, Δ_L, as the gap between the lowest-lying $S_T=2$ and $S_T=1$ states.

TABLE II. Relative errors $(E-E_{\text{exact}})/E_{\text{exact}}$ in ground-state energies in the indicated spin sector S_T of finite $S=\frac{1}{2}$ chains of length $L=16$ and $L=22$. The exact energies were determined by a separate exact diagonalization. Truncation errors $1-P_m$ varied from about 10^{-7} to 10^{-9}. The $L=22$, $m=24$ calculation took about 20 s of Cray time.

	$L=16$	$L=16$	$L=16$	$L=22$
m	$S_T=0$	$S_T=1$	$S_T=2$	$S_T=0$
16	9.3×10^{-8}	1.2×10^{-7}	5.9×10^{-8}	8.0×10^{-7}
24	2.2×10^{-9}	5.4×10^{-9}	4.0×10^{-9}	8.1×10^{-8}

Figure 2 shows the Haldane gap Δ_L for lattice sizes ranging from 40 to 300 using the finite-lattice method, using $m=40$ and $m=50$ and extrapolating to $P_m\to 1$. The data are fitted by the form

$$\Delta_L=\Delta+a/L^2 \tag{5}$$

quite well, with $\Delta=0.4107(3)$ and $a=67.9$. Nightingale and Blöte obtained $\Delta\approx 0.41$ by extrapolating Monte Carlo results for chains up to $L=32$.

Because the two $S=\frac{1}{2}$ degrees of freedom at the ends of an $S=1$ chain always bind to form the singlet and triplet discussed above, they are usually not directly observed numerically [6]. An interesting way to see a single $S=\frac{1}{2}$ effective spin is to attach a *real* $S=\frac{1}{2}$ spin onto one end of a finite $S=1$ chain. The ground state of this system is a spin doublet. Figure 3 shows the expectation value of S_i^z as a function of lattice site i for a sixty-site chain for the $S_T^z=+\frac{1}{2}$ ground state. The $S=\frac{1}{2}$ degree of freedom manifests itself at the *opposite end* of the

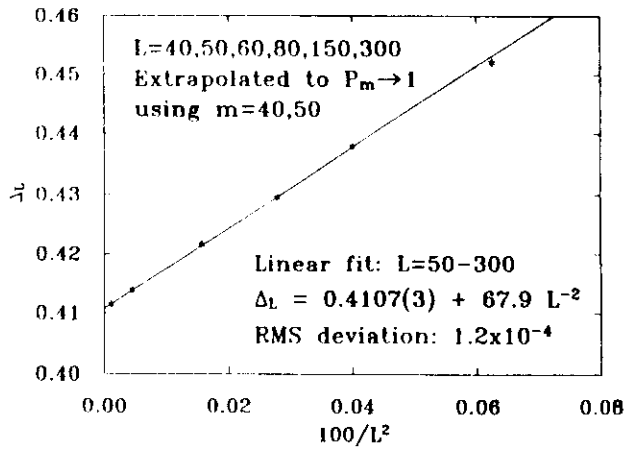

FIG. 2. The Haldane gap as a function of lattice size L.

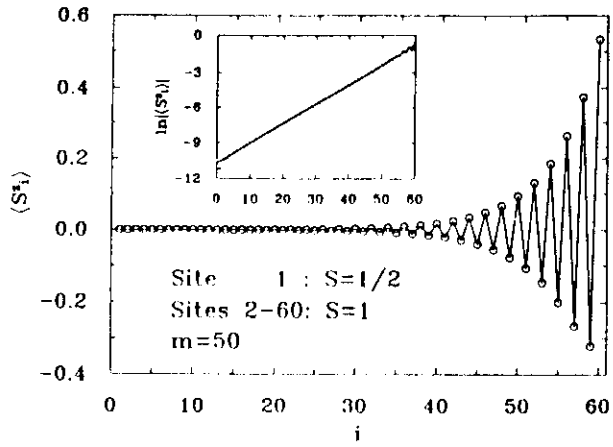

FIG. 3. Expectation value of S_i^z as a function of i for a sixty-site chain with the first site $S=\frac{1}{2}$ and all the rest $S=1$.

chain from the real $S=\frac{1}{2}$ spin. The value of S_i^z on the last site is 0.532(1), slightly larger than $\frac{1}{2}$, the result for a real $S=\frac{1}{2}$ spin, but less than the Schwinger-boson mean-field result of 0.7 [12]. We also show $\ln|S_i^z|$, which is extremely linear away from the ends, indicating almost pure exponential decay. The straight line is a linear fit to the data from 20 to 40, from which we obtain a decay length of $\xi=6.03(1)$. This result is quite close to the recent Monte Carlo result of 6.2(1) for the correlation length obtained using the two-point spin-spin correlation function [7,8]. We plan further studies of the spin-spin correlation function to determine if the decay length and correlation length are, in fact, identical.

Using this new formulation of numerical renormalization groups and iterative diagonalization, we have been able to calculate several of the most interesting properties of $S=1$ Heisenberg chains with an accuracy not achievable with other methods on today's computers. We have no reason to believe that other 1D lattice systems with short-range interactions will be substantially more difficult. This new formulation appears extremely powerful and versatile, and we believe it will become the leading numerical method for 1D systems, and eventually will become useful for higher dimensions as well.

We would like to thank R. Noack, D. Huse, C. Yu, I. Dzyaloshinski, M. P. Gelfand, D. Mills, and L. Nosanow for helpful comments and discussion. This work was supported by the Office of Naval Research under Grant No. N00014-91-J-1143 and in part by the University of California through an allocation of computer time on the UC Irvine Convex. Calculations were also performed at SDSC.

[1] K. G. Wilson, Rev. Mod. Phys. **47**, 773 (1975).
[2] S. R. White and R. M. Noack, Phys. Rev. Lett. **68**, 3487 (1992).
[3] Knowledge of $H_{A'}$ alone is not sufficient to form the block Hamiltonian at the next iteration. In addition, one needs information on how to form the interaction between two blocks. One needs, in addition to $H_{A'}$, $m\times m$ matrices representing (for spin models) matrix elements of S_i^z, S_i^+, and S_i^-, for the two sites i on the edges of a block. Using the spin operator matrices for the right-hand site i of the left block and the left-hand site $i+1$ of the right block, one can easily reconstruct the interaction $\mathbf{S}_i\cdot\mathbf{S}_{i+1}$ between the blocks. These operator matrices are treated in the same fashion as the Hamiltonian, using an analog of Eq. (1), for example.
[4] R. P. Feynman, *Statistic! Mechanics: A Set of Lectures* (Benjamin, Reading, MA, 1972).
[5] M. P. Nightingale and H. W. J. Blöte, Phys. Rev. B **33**, 659 (1986).
[6] T. Kennedy, J. Phys. Condens. Matter **2**, 5737 (1990).
[7] S. Liang, Phys. Rev. Lett. **64**, 1597 (1990).
[8] K. Nomura, Phys. Rev. B **40**, 2421 (1989).
[9] F. D. M Haldane, Phys. Lett. **93A**, 464 (1983).
[10] M. Hagiwara, K. Katsumata, I. Affleck, B. I. Halperin, and J. P. Renard, Phys. Rev. Lett. **65**, 3181 (1990).
[11] S. H. Glarum, S. Geschwind, K. M. Lee, M. L. Kaplan, and J. Michel, Phys. Rev. Lett. **67**, 1614 (1991).
[12] T. K. Ng, Phys. Rev. B **45**, 8181 (1992).

PRB 48, 10345, (1993)

December, 1992

Density Matrix Algorithms for Quantum Renormalization Groups

Steven R. White
Department of Physics, University of California, Irvine, CA 92717

A new formulation of numerical real space renormalization groups for quantum many body problems is presented and several algorithms utilizing this formulation are outlined. The methods are presented and demonstrated using $S = 1/2$ and $S = 1$ Heisenberg chains as test cases. The key new idea of the formulation is that rather than keep the lowest lying eigenstates of the Hamiltonian in forming a new effective Hamiltonian of a block of sites, one should keep the most significant eigenstates of the block density matrix, obtained from diagonalizing the Hamiltonian of a larger section of the lattice which includes the block. This approach is much more accurate than the standard approach; for example, energies for the $S = 1$ Heisenberg chain can be obtained to an accuracy of at least 10^{-9}. The method can be applied to almost any one-dimensional quantum lattice system, and can provide a wide variety of static properties.

PACS Numbers: 05.30.-d, 75.10.Jm, 02.70.+d

Typeset Using *REVTEX*

I. INTRODUCTION

Shortly after Wilson developed his numerical renormalization group (RG) procedure to solve the Kondo problem [1], there was considerable interest in applying closely related techniques to a variety of problems. In particular, it seemed that a number of quantum lattice models (such as the Hubbard and Heisenberg models), particularly in one dimension (1D), could be treated with a real-space blocking version of this technique. It was clear from the beginning that one could not hope to achieve the accuracy Wilson obtained for the Kondo problem in these other systems (c.f. Section III), but it was hoped that the method would yield qualitatively reliable results. Unfortunately, the approach proved to be rather unreliable, particularly in comparison with other numerical approaches, such as Monte Carlo, which were being developed at the same time. Until very recently, the method was only used occasionally.

Recent developments in renormalization group algorithms have changed this picture completely. The first significant advance came in the understanding of the effect of boundary conditions on the basic renormalization group procedure [2]. The standard approach of neglecting all connections to neighboring blocks during the diagonalization of the block Hamiltonian introduces large errors which cannot be corrected by any reasonable increase in the number of states kept. However, by varying the boundary conditions on a block, and keeping states from several diagonalizations with different boundary conditions, one can eliminate these errors, at least for single-particle problems. The second advance came in the development of a technique suitable for many-particle systems, using a formulation in terms of density matrices [3]. For systems such as 1D Heisenberg spin chains, the density matrix approach makes the numerical renormalization group approach not just qualitatively reliable, it makes it substantially more accurate and powerful for calculating many zero temperature properties than current quantum Monte Carlo approaches.

The main goal of this paper is to describe in some detail the density matrix

algorithms. The approach was presented in summary form in an earlier paper [3], but in insufficient detail to allow a nonexpert reader to develop his own programs for these calculations. These algorithms are somewhat more complicated than typical exact diagonalization or Monte Carlo algorithms, and a number of new ideas are involved. By reading this paper, we hope that someone with some experience in exact diagonalization calculations can develop their own density matrix program. We will illustrate and demonstrate the approach on $S = 1/2$ and $S = 1$ Heisenberg antiferromagnetic spin chains. We will present a few new results for properties of these chains, but only as examples of the power of the methods. More results on the properties of Heisenberg chains will appear in subsequent papers.

In the next section, we discuss the standard real-space renormalization group approach. In Section III, we discuss previous uses of the standard methods. In Section IV, we then present the density matrix approach, and show that it is optimal in a certain sense. In Section V we present the infinite and finite lattice density matrix algorithms. In Section VI, we discuss the measurement of a number of static quantities in these algorithms. In Section VII, we present some results for Heisenberg chains and discuss the effects of various boundary conditions on the procedure. In Section VIII we conclude and discuss future prospects.

II. STANDARD APPROACH

We first describe in detail the standard RG approach in the simplest possible context, a real space blocking approach for a 1D lattice system. The notation and many of the central ideas will be very similar in the density matrix approach described later. The Hamiltonian considered here could describe a spin system, such as the Heisenberg model, or an interacting electron system, such as the Hubbard model. The approach is relevant for zero temperature, and one obtains the ground state and some low-lying excited states.

One begins by breaking the 1D chain into finite identical blocks. It is usually convenient to start at the first iteration with blocks consisting of just one site. We

will label the blocks B and the block Hamiltonian H_B. H_B contains all terms of H involving only sites contained in B. For example, for the Hubbard model at the first iteration, where B consists of one site, $H_B = U n_{i\uparrow} n_{i\downarrow} - \mu(n_{i\uparrow} + n_{i\downarrow})$. For the Heisenberg model at the first iteration, $H_B = 0$.

Rather than describe B and H_B in the usual way by listing the sites of B and using second-quantized operator expressions for H_B, we describe B by a list of the many-body states on the block, and by quantum numbers and matrix elements between these states. We store the number of states m, and for each state we list all quantum numbers which are to be used, such as S_z and S for a spin system, or $N_\uparrow, N_\downarrow$, and S for an electron system. H_B is represented as an $m \times m$ matrix. In order to reconstruct H, additional information is needed besides H_B. The additional information describes the interactions between blocks. For a Heisenberg system with interaction

$$\vec{S}_i \cdot \vec{S}_{i+1} = S_i^z S_{i+1}^z + \frac{1}{2}(S_i^+ S_{i+1}^- + S_i^- S_{i+1}^+) \tag{1}$$

one needs to store $m \times m$ matrix representations of S_i^z, S_i^+, and S_i^- for i equal to both the left and right end sites of B. (In practice, one need not store S_i^-, since it can be obtained by taking the Hermitian conjugate of S_i^+). For a Hubbard model one would have to store matrices for $c_{i\sigma}^\dagger$ and $c_{i\sigma}$, with $\sigma = \uparrow$ and $\downarrow$, in order to reconstruct the hopping term $\sum_\sigma (c_{i+1\sigma}^\dagger c_{i\sigma} + c_{i\sigma}^\dagger c_{i+1\sigma})$.

The standard procedure is summarized in Table I. At the beginning of an iteration one forms the Hamiltonian for two blocks joined together, H_{BB}. BB has m^2 states. The states are labeled by two indices, $i_1 i_2$. For a Heisenberg system with $J = 1$ the $m^2 \times m^2$ matrix for H_{BB} is given by

$$\begin{aligned}[H_{BB}]_{i_1 i_2, i_1' i_2'} = {} & [H_B]_{i_1 i_1'} \delta_{i_2 i_2'} + [H_B]_{i_2 i_2'} \delta_{i_1 i_1'} + [S_r^z]_{i_1 i_1'} [S_\ell^z]_{i_2 i_2'} + \\ & \frac{1}{2} [S_r^+]_{i_1 i_1'} [S_\ell^-]_{i_2 i_2'} + \frac{1}{2} [S_r^-]_{i_1 i_1'} [S_\ell^+]_{i_2 i_2'}\end{aligned} \tag{2}$$

where r represents the rightmost site of the left block, and ℓ the leftmost site of the right block.

In diagonalizing H_{BB} it is useful to separate the basis states by quantum numbers, since H_{BB} is block diagonal. It is very simple to use S_z or $N_\uparrow$ and $N_\downarrow$ in this way. Utilizing the total spin S is more tedious (especially when one puts four blocks together, as we do below), and we have not used S to further reduce the dimension of H_{BB}. (The value of S for a state can easily be inferred by degeneracies for different values of S_z.)

The lowest lying eigenstates $u^\alpha_{i_\uparrow i_\downarrow}$, $\alpha = 1, \ldots m$, of H_{BB} are the states used to describe B' ($BB \rightarrow B'$). The new block Hamiltonian matrix $H_{B'}$ is diagonal. However, in the more general case where the states kept, the u^α, are not eigenstates of H_{BB} we can write

$$H_{B'} = O H_{BB} O^\dagger \tag{3}$$

where the $m \times m^2$ matrix $O_{\alpha,i_\uparrow i_\downarrow} = u^\alpha_{i_\uparrow i_\downarrow}$, i.e. the rows of O are the states kept. If O were square, this would be a unitary transformation. Since O is not square, the transformation truncates away (integrates out) the high energy states.

In order to obtain new matrices for S^z_ℓ, S^+_r, etc., it is necessary to use O again. First, one must construct the operators for S^z_ℓ, S^z_r, etc. for BB, which we denote by $\hat{S}^z_\ell$, $\hat{S}^z_r$, etc. For example

$$\left[\hat{S}^z_\ell\right]_{i_\uparrow i_\downarrow, i'_\uparrow i'_\downarrow} = [S^z_\ell]_{i_\uparrow i'_\uparrow} \delta_{i_\downarrow i'_\downarrow} \tag{4}$$

$$\left[\hat{S}^z_r\right]_{i_\uparrow i_\downarrow, i'_\uparrow i'_\downarrow} = [S^z_r]_{i_\downarrow i'_\downarrow} \delta_{i_\uparrow i'_\uparrow} \tag{5}$$

Then the new matrices for B' are given by

$$S^z_\ell = O \hat{S}^z_\ell O^\dagger \tag{6}$$

etc.

After these new operator matrices are formed, we can replace B by B' and start the next iteration. The iteration is continued until the system is large enough to represent properties of the infinite system. As our main concern here is the iterative

diagonalization procedure discussed above, we will not discuss the analysis, using fixed points, relevant and irrelevant operators, etc., of the effective Hamiltonians obtained with the procedure.

III. PREVIOUS USES

We will not attempt to give a comprehensive review of previous uses of this approach; rather, we will discuss a handful of studies which illustrate successful and unsuccessful applications.

Wilson's approach to the Kondo problem is closely related to the method described here, despite some important differences. One difference is that rather than joining two identical blocks, the degrees of freedom associated with a single interval (an "onion-layer") were added to the system at each iteration. The analogous procedure for a 1D system would be to add a single site to a block at each iteration. From a computational point of view, this has a distinct advantage in that many more states can be kept (m can be made larger) since at each iteration a system with nm states, as opposed to m^2, must be diagonalized, where n is the number of states on a single site ($n = 4$ for Hubbard models, $n = 2S + 1$ for spin models).

The most important difference between the Kondo system and a 1D system is that the couplings between adjacent layers or "sites" decreases exponentially in the Kondo system, whereas it remains constant for a 1D system. This exponential decrease is the key to the success of the method for the Kondo system and related impurity systems. More discussion concerning how the detailed form of the Hamiltonian makes the numerical approach accurate are given by Wilson [1].

Bray and Chui [4] applied the approach described in the previous section to the 1D Hubbard model. The results were quite discouraging. Even when a large number of states were kept ($m \approx 1000$), results for the energies of the lowest few levels were off by 5 - 10% for 16 site chains. Results for 32 sites or larger were not considered reliable and were not presented. The origin of the difficulties was not clearly understood.

Xiang and Gehring [5] recently applied a slight variation of the method of the

previous section to the 1D Heisenberg model. Their method added a single site to a block at each iteration, rather than doubling the block size each time. (The algorithms we present below also add a single site to a block.) This improvement gave results rather more encouraging than those of Bray and Chui; keeping about 200 states they obtained an error of about 0.5% in the ground state energy. This can be compared to our results below, where keeping fewer states we obtain the ground state energy to at least nine digits.

There have also been a number of analytical real-space RGs applied to the 1D Hubbard and related models [6]. These methods keep only a handful of states, and one generally only expects to obtain qualitative features. These will not be discussed further here.

P. A. Lee used a numerical RG method to study 2D Anderson localization. Since the model studied was non-interacting, a two dimensional calculation was feasible. It was clear from an examination of the density of states that the algorithm was not especially accurate. However, Lee argued that the errors would simply result i the system being in another realization of the random potential. Lee concluded that there was a critical amplitude for the random potential which induced localization. However, not long after Lee's work Lee and Fisher found that the 2D model is logarithmically localized even for arbitrarily small randomness using a different approach. This result is now generally accepted.

In summary, the standard numerical RG approach generally performs poorly. The exceptions to this rule involve Hamiltonians which can be put into a special form.

IV. DENSITY MATRIX APPROACH

The fundamental difficulty in the standard approach discussed in Section II lies in choosing the eigenstates of H_{BB} to be the states kept. Since H_{BB} contains no connections to the rest of the lattice, its eigenstates have inappropriate features at the block ends. This is clearly illustrated in the work of White and Noack [2], who

suggested two alternatives to the standard approach. These methods shared a common feature: the states that were kept were *not* the eigenstates of H_{BB}. They differed in how the states to be kept were chosen. In the first method, the combination of boundary conditions (CBC) approach, the lowest lying eigenstates of several different block Hamiltonians were kept. The several block Hamiltonian differed only in the boundary condition applied to a block, e.g. one Hamiltonian might have periodic boundary conditions applied and another antiperiodic. The rationale for this was that quantum fluctuations in the rest of the system effectively apply a variety of boundary conditions to the block. States from any single boundary condition cannot respond properly to these fluctuations. By applying a representative set of boundary conditions, which is in some sense "complete" enough for the problem at hand, one obtains a set of states which are able to respond to these fluctuations. This approach proved very effective for the simple single-particle problems studied by White and Noack, as well as for Anderson localization models [7].

The CBC approach appears to be ill-suited to interacting systems. It is useful to consider a noninteracting many-particle system, such as the Hubbard model with $U = 0$. An arbitrary state of this system can be described in terms of the single particle wavefunctions of each of its particles. Some of these single-particle wavefunctions may have nodes at the ends of a block, and some may have antinodes.

It is easy to choose boundary conditions with generate block states where every particle on the block has a node or every particle has an antinode, but it is difficult to get different boundary behavior for different particles. In order to properly represent the block, the states kept not only need to allow for different end behavior for different particles, they must represent a complete range of boundary behavior.

This general line of reasoning is supported by numerical tests on Heisenberg chains. We have tried to find a simple set of boundary conditions which can be used to treat the $S = \frac{1}{2}$ Heisenberg chain. We tried combinations of periodic and antiperiodic couplings between the ends of the block, as well as varying the magnitude

of the coupling between the ends of a block. We were unable to find any set of boundary conditions which was at all satisfactory.

The other approach suggested by White and Noack, the superblock method, forms the basis for the density matrix approach. In the superblock method, one diagonalizes a larger system (the "superblock", the name is analogous to "supercell", as used in electronic structure calculations) composed of three or more blocks which includes the two blocks BB which are used to form B'. The wavefunctions for the superblock are projected onto BB, and these projected states of BB are kept. For a single particle wavefunction, this projection is single-valued and trivial. The superblock method works quite well in the single-particle model, with the accuracy increasing rapidly with the number of extra blocks used. However, for a many-particle wavefunction, the "projection" of a wavefunction onto BB is many-valued, and, in fact, a single many-particle state for the entire lattice generally "projects" onto a complete set of block states. However, some of these states are more important than others; the density matrix tells us which states are the most important. (The reader is urged to review Feynman's introduction to density matrices [8] before proceeding further.)

It is very natural to use the density matrix to choose the states which we wish to keep. Consider first the following argument by analogy. For an *isolated* block at finite temperature, the probability that the block is in an eigenstate α of the block Hamiltonian is proportional to its Boltzmann weight $\exp(-\beta E_\alpha)$. The Boltzmann weight is an eigenvalue of the density matrix $\exp(-\beta H_B)$, and an eigenstate of the Hamiltonian is also an eigenstate of the density matrix. Since lowest energy corresponds to highest probability in the Boltzmann weight, we can view the standard RG approach as choosing the m most probable eigenstates to represent the block given the *assumption* that the block is isolated. (Alternatively, we can view the rest of the lattice as a heat bath at an effective inverse temperature β, to which the system is very weakly coupled.) However, in reality the block is not isolated, the density matrix

is not $\exp(-\beta H_B)$ (it is defined through Eq. (12) or (16) below), and eigenstates of the block Hamiltonian are not eigenstates of the block's density matrix. For a system which is strongly coupled to the outside universe, it is much more appropriate to use the eigenstates of the density matrix to describe the system rather than the eigenstates of the system's Hamiltonian. Thus a natural generalization of the standard approach is to choose to keep the m most probable eigenstates of the block density matrix.

This argument can be made much more precise. In particular, we can show that keeping the most probable eigenstates of the density matrix gives the most accurate representation of the state of the system as a whole, i.e., the block plus the rest of the lattice. Let us assume we have diagonalized a superblock and obtained one particular state $|\psi\rangle$, probably the ground state. Let $|i\rangle$, $i = 1, \ldots, \ell$ be a complete set of states of BB (the system) and $|j\rangle$, $j = 1, \ldots, J$ be the states of the rest of the superblock, i.e., the "universe". We can write $|\psi\rangle = \sum_{i,j} \psi_{i,j}|i\rangle|j\rangle$. We will assume for simplicity $\psi_{i,j}$ is real. We wish to define a procedure for producing a set of states of the system $|u^\alpha\rangle$, $\alpha = 1, \ldots, m$, with $|u^\alpha\rangle = \sum_i u^\alpha_i |i\rangle$, which are optimal for representing ψ in some sense. Because we allow only m states, we cannot represent $|\psi\rangle$ exactly if $\ell > m$. We wish to construct an accurate expansion for $|\psi\rangle$ of the form

$$|\psi\rangle \approx |\tilde{\psi}\rangle = \sum_{\alpha,j} a_{\alpha,j} |u^\alpha\rangle|j\rangle. \tag{7}$$

In other words, we wish to minimize

$$S = \left| |\psi\rangle - |\tilde{\psi}\rangle \right|^2, \tag{8}$$

by varying over all $a_{\alpha,j}$ and u^α, subject to $\langle u^\alpha | u^{\alpha'} \rangle = \delta_{\alpha\alpha'}$. Without loss of generality, we can write

$$|\tilde{\psi}\rangle = \sum_\alpha a_\alpha |u^\alpha\rangle|v^\alpha\rangle \tag{9}$$

where $v^\alpha_j = \langle j | v^\alpha \rangle = N_\alpha a_{\alpha,j}$, with N_α chosen to set $\sum_j |v^\alpha_j|^2 = 1$. Switching to matrix notation, we have

$$S = \sum_{ij} (\psi_{ij} - \sum_{\alpha=1}^{m} a_\alpha u_i^\alpha v_j^\alpha)^2, \tag{10}$$

and we minimize S over all u^α, v^α, and a_α, given the specified value of m. The solution to this minimization problem is known from linear algebra. We now think of ψ_{ij} as a rectangular matrix. The solution is produced by the singular value decomposition [9] of ψ,

$$\psi = UDV^T, \tag{11}$$

where U and D are $\ell \times \ell$ matrices, V is an $\ell \times J$ matrix (where $j = 1, \ldots, J$, and we assume $J \geq \ell$), U is orthogonal, V is column-orthogonal, and the diagonal matrix D contains the singular values of ψ. Linear algebra tells us that the u^α, v^α, and a_α which minimize S are given as follows: the m largest-magnitude diagonal elements of D are the a_α and the corresponding columns of U and V are the u and v. (We emphasize that the singular value decomposition is not being used here as a numerical method, only as a convenient factorization which allows us to use a theoretical result from linear algebra.)

These optimal states u^α are also eigenvectors of the reduced density matrix of the system as part of the universe. This reduced density matrix for the system depends on the state of the universe, which in this case is a pure state $|\psi\rangle$. (The universe could also be in a mixed state [see below] or at finite temperature.) The density matrix for the system in this case is given by

$$\rho_{ii'} = \sum_j \psi_{ij} \psi_{i'j}. \tag{12}$$

We see that

$$\rho = UD^2U^T, \tag{13}$$

i.e., U diagonalizes ρ. The eigenvalues of ρ are $w_\alpha = a_\alpha^2$ and the optimal states u are the eigenstates of ρ with the largest eigenvalues. Each w_α represents the probability

of the system being in the state u^α, with $\sum_\alpha w_\alpha = 1$. The deviation of $P_m \equiv \sum_{\alpha=1}^{m} w_\alpha$ from unity measures the accuracy of the truncation to m states.

To summarize, in the previous two paragraphs we have shown that when the entire lattice is assumed to be in a pure state, the optimal states to keep are the m most significant eigenstates of the reduced density matrix of the block BB, obtained from the wavefunction of the entire lattice via Eq. (12).

We can also consider the universe to be in a mixed state. This is the natural assumption for a system at finite temperature, and it is also useful to assume a mixed state when one wishes to obtain several of the lowest lying states: if we put the lattice with equal probability into each of several states, then the block states obtained from the density matrix will equally well represent each of these lattice states. We represent the mixed case by saying that the lattice has probability W_k to be in state $|\psi^k\rangle$. If the system is at a finite temperature, then the W_k are normalized Boltzmann weights. In this case the appropriate definition for the error in the representation is

$$S = \sum_k W_k \sum_{ij} (\psi_{ij}^k - \sum_{\alpha=1}^{m} a_\alpha^k u_i^\alpha v_j^{k,\alpha})^2. \tag{14}$$

Note that we are interested in determining a single set of optimal u^α, whereas we allow the rest of the universe additional freedom to choose a different v^α for each state k. Minimizing over the u^α, $v^{k,\alpha}$, and a_α^k, we find

$$\rho u^\alpha = w_\alpha u^\alpha \tag{15}$$

with

$$\rho_{ii'} = \sum_k W_k \sum_j \psi_{ij}^k \psi_{i'j}^k, \tag{16}$$

and

$$w_\alpha = \sum_k W_k (a_\alpha^k)^2 \tag{17}$$

This equation for ρ is the definition of the reduced density matrix when the universe is in a mixed state, and the u^α are the eigenstates of ρ.

Thus the conclusion when the universe is in a mixed state is identical to the result for a pure state: the optimal states to keep are the eigenvectors of the reduced density matrix with the largest eigenvalues.

V. DENSITY MATRIX ALGORITHMS

Incorporating the result of the previous section in a numerical renormalization group algorithm involves a fundamental change in the way the calculation is carried out. In the standard RG approach, to find the states to be kept, one diagonalizes only the system BB, which becomes B'. In the density matrix approach, in order to obtain any reasonable approximation to the density matrix, it is necessary to diagonalize the Hamiltonian of a larger system which includes BB, namely some sort of superblock, and then use the eigenstates of the superblock to determine the density matrix. The density matrix is then diagonalized, and its most significant eigenstates are the states kept. The number of eigenstates of the Hamiltonian of the superblock used to produce the density matrix can be as small as one; this single state produces a density matrix for BB which has many eigenstates to be used as block states to be kept.

A density matrix algorithm is defined mainly by the form of the superblock and the manner in which the blocks are enlarged (such as by doubling the block, $B' = BB$, or by adding a single site, $B' = B +$ site), and by the choice of superblock eigenstates used in constructing the density matrix (e.g., the two lowest-lying $S_z = 0$ states). An eigenstate of the superblock Hamiltonian is called a *target state* if it is used in forming the block density matrix. The most efficient algorithms use only a single target state (usually the ground state) in constructing the density matrix. By targeting only one state, the block states are more specialized for representing that state, and fewer are needed for a given accuracy. Probably the most important characteristic of a density matrix algorithm is the rate at which the accuracy increases with the number of states m. We have found that the accuracy of the representation of the target states increases roughly exponentially with m, at least for open boundary conditions. The coefficient governing the increase of accuracy with m is largest with a single target

state.

Several considerations enter in the construction of the superblock to be used in an algorithm. Generally it is more efficient to enlarge the block by adding a single site, rather than doubling a block, for the same reasons as in the standard RG approach (see Section II). A block can be represented more accurately with a given m if it connects to the rest of the chain only on one end, rather than both ends. A block can connect to the rest of the chain by only one end if it is on an end of a chain with open boundary conditions. If periodic boundary conditions are used, it is not possible for a block to connect on only one end. Below we give results of calculations which show that the open boundary condition case performs much better than the periodic boundary condition case. Our intuitive picture for this numerical result is the following: roughly speaking, each eigenstate of the block density matrix represents the response of the block to a particular quantum fluctuation in the rest of the chain. A block with two ends which connect to the rest of the system must respond to nearly independent fluctuations near each of the ends. In the case of a long block, where the ends are nearly independent, if m states are required to accurately describe a single end to a given accuracy, then approximately m^2 states would be required to accurately represent both ends. In other words, if for a given accuracy open boundary condition require m states, periodic boundary conditions require roughly m^2 states.

Figure 1 shows the superblock configuration used for most of the calculations reported here. We adopt the notation $B_\ell \bullet \bullet B_{\ell'}^R$ for this configuration, where B_ℓ represents a block composed of ℓ sites, B_ℓ^R is a reflected block (right interchanged with left) of length ℓ', $\bullet$ represents a single site, and the total length of the superblock is $L = \ell + \ell' + 2$. Here $B' = B_{\ell+1}$ is formed from the left block plus a single site, i.e. $B_{\ell+1} = B_\ell \bullet$. Open boundary conditions are used. The right-hand block and site $\bullet B_{\ell'}^R$ are only used to help form the density matrix for $B_{\ell+1}$; in the construction of the density matrix, the states of $\bullet B_{\ell'}^R$ are traced over. This configuration can be used in two different ways: in an infinite chain method, in which the chain size increases

by two at each step, and in a finite chain method, in which the chain size is fixed.

A. The infinite system method

In the first step of the infinite system method, we start with a four site chain and diagonalize the Hamiltonian of the superblock configuration $B_1 \bullet \bullet B_1^R$, where B_1 and B_1^R both represent a single site. We use the Davidson algorithm [10] for the sparse matrix diagonalization, but one could also use the more well known Lanczos method. Using the target states calculated with this configuration, we calculate a density matrix and form an effective Hamiltonian for $B_2 = B_1\bullet$. In the second step we diagonalize $B_2 \bullet \bullet B_2^R$, where we have formed B_2^R by reflecting B_2. We continue in this manner, diagonalizing the configuration $B_\ell \bullet \bullet B_\ell^R$, and setting $B_{\ell+1} = B_\ell\bullet$, and using $B_{\ell+1}$ and its reflection in the next step of the iteration. At each step, both blocks increase in length by one site, and the total length of the chain increases by two at each step of the iteration. The infinite chain method is usually used when one is interested in ground state properties of the infinite chain. Each step of the iteration pushes the ends of the chain farther from the two sites in the center. After many steps, each block approximately represents one half of an infinite chain. In order to represent one half of an infinite chain, B must not only contain many sites itself, its effective Hamiltonian must be formed from a system in which the rest of the chain has many sites. The effective Hamiltonian formed from the left-hand side $B_\ell\bullet$ depends strongly on the right-hand side $\bullet B_\ell^R$. The infinite chain algorithm converges in two senses simultaneously: in the length of B_ℓ going to infinity and in the sense that B_ℓ is adapted to respond to an infinite chain connected to it on the right.

Why not use the simpler configuration $B_\ell \bullet B_\ell^R$? In other words, why make the right-hand side $\bullet B_\ell^R$ rather than B_ℓ^R? If there is only one target state, and B_ℓ^R has m states, then from Eq. (12), the density matrix ρ for the system $B_\ell\bullet$ has at most m nonzero eigenvalues. Initially, when B_ℓ^R (and B_ℓ) consists of just a single site, it has only a few states. With this method, the number of states in $B_{\ell+1}$ could not

be larger than the number in B_ℓ^R (which is the same as the number in B_ℓ), unless one included states with density matrix eigenvalues of zero. In general, for a robust method, the number of nonzero eigenvalues of the density matrix should be larger than the number of states kept, except in the first few steps when all states of the block are kept. If more than one state is targeted, then the $B_\ell \bullet B_\ell^R$ configuration is presumably feasible, although we have not tested it. In any case, the presence of extra sites in the center which are not part of the outer blocks makes the method more accurate, since B_ℓ^R is represented by an approximate Hamiltonian, whereas the central sites are represented exactly. Thus extra sites in the center produce a more accurate density matrix. The penalty for these extra sites is that the diagonalization of the superblock is more work.

The infinite system algorithm is summarized in Table II. The representation of the blocks is identical to that of the standard algorithm: we describe a block by listing how many states it has and the quantum numbers for each state, and by storing matrices for H_B, S_i^z, etc. Once the matrix O is constructed using the most significant eigenvectors of the density matrix, the change of basis procedure it also identical to that of the standard algorithm. For the purposes of organizing the algorithm, it is easiest to think of the two sites in the middle as blocks which can be treated similarly to the two outer blocks, although they contain only a few states.

B. The finite system method

The finite system algorithm is designed to calculate accurately the properties of a finite system of size L, which we will assume for simplicity to be even. It is summarized in Table III. It begins with the use of the infinite system algorithm for $L/2 - 1$ steps, so that the final superblock used is of size L. In the infinite system method, there is no need to store B_ℓ once we have $B_{\ell+1}$, we need only store the latest block. In the finite system method, we need to store $L - 3$ blocks, B_1 to B_{L-3}, and the infinite system method is used to get initial, approximate versions of B_1 to

$B_{L/2}$. After the system $B_{L/2-1} \bullet\bullet B^R_{L/2-1}$ is used to form $B_{L/2}$, the next step is to use the configuration $B_{L/2} \bullet\bullet B^R_{L/2-2}$ to form $B_{L/2+1}$. This system, and all the other superblocks to follow, contain L sites. We continue to form the other blocks up to size $L-3$, using the superblock $B_\ell \bullet\bullet B^R_{L-\ell-2}$ to form $B_{\ell+1}$. This sequence of steps is the first iteration of the finite system algorithm.

The second and subsequent iterations use the blocks obtained from the previous iteration as the right-hand reflected blocks in each superblock. The first step starts by diagonalizing the superblock $B_1 \bullet\bullet B^R_{L-3}$, where B_1 is a single site and is always known exactly, and B^R_{L-3} is obtained from the last step of the previous iteration. Once a new B_ℓ is formed, it replaces the old B_ℓ, so that only one set of blocks need be stored. Consequently, for the second half of the iteration, starting with the superblock $B_{L/2-1} \bullet\bullet B^R_{L/2-1}$, we use a block formed in the current iteration, rather than the last iteration, as the right-hand block. On the very last iteration, we usually stop after the diagonalization of $B_{L/2-1} \bullet\bullet B^R_{L/2-1}$, and then use this wavefunction of the L-site system to measure various properties, such as the local magnetization or correlation functions.

After a few iterations each B_ℓ accurately represents an ℓ-site block which is the left hand ℓ sites of an L site chain. Usually the method converges by the middle of the second iteration, although sometimes three iterations are necessary.

An important improvement in efficiency can be made by keeping a different number of states m' in the right-hand block from the number in the left-hand block m. Fewer states are needed in the right-hand block because this block is only used to help produce the density matrix, whereas the left-hand block not only is used to produce the density matrix, it is part of the new block we are producing. Thus the left-hand block is more important, and we should take $m > m'$. This can be done quite simply by keeping only m' states in both blocks in all but the last iteration, and in the last iteration keeping m states for the left block. Assuming we stop after diagonalizing the $B_{L/2-1} \bullet\bullet B^R_{L/2-1}$ system, then this very last diagonalization will have m states

for both blocks, and it will be especially accurate. Typically we take $m/m' = 2$ or 3. If only one state is targeted, then one should not try to make $m > nm'$, where n is the number of states on a single site, since the number of nonzero eigenvalues of the density matrix cannot be more than nm' times the number of states targeted. We find that in typical cases, the accuracy of the calculation for fixed m is approximately the same using this procedure for any m' ranging from $m' \approx m/2$ to $m' = m$. Of course, the calculation time and storage is substantially less for smaller values of m'.

C. Periodic boundary conditions

To perform calculations with periodic boundary conditions, a slight variation of the finite system method can be used. In this case it is most convenient to use the superblock configuration $B_\ell \bullet B^R_{\ell'} \bullet$, with $B'_{\ell+1} = B_\ell \bullet$. This configuration is preferred over $B_\ell \bullet\bullet B^R_{\ell'}$ because it does not have the two big blocks as neighbors. If the two big blocks are neighbors, the sparseness of the Hamiltonian (measured by the average number of nonzero matrix elements per row of the matrix) for the superblock is greatly reduced (meaning more elements are nonzero). The off-diagonal terms of the Hamiltonian matrix come from operators such as $S^+_r S^-_\ell$, where r is the right-hand site of a block, say block 1, and ℓ is the left-hand site of block 2. The term in the Hamiltonian for this operator is of the form

$$[S^+_r]_{i_1 i'_1} [S^-_\ell]_{i_2 i'_2} \delta_{i_1 i'_2} \delta_{i_2 i'_1}. \tag{18}$$

The sparseness of this term is measured by the number of nonzero terms as we vary i'_1 and i'_2, keeping i_1 and i_2 fixed. If both block 1 and block 2 are blocks containing m states, the number of nonzero elements per row of the Hamiltonian matrix is proportional to m^2, whereas if block 2 is a single site, the number is proportional to m. In the case of periodic boundary conditions, these considerations are relevant because block 1 is connected to block 1, and thus one of these should be a single site. Otherwise, the periodic case is nearly identical to the open boundary case discussed above.

VI. MEASUREMENTS

Properties of the L-site system can be obtained from the wavefunctions of any of the $L-3$ superblock configurations, although we find that the symmetric configuration (with both the left and right blocks of size $L/2-1$) usually gives the most accurate results. The procedure is to use the wavefunction $|\psi\rangle$ resulting from the diagonalization of the L-site system to evaluate expectation values of the form $\langle\psi|A|\psi\rangle$. Rather complicated operators can be evaluated fairly easily, but dynamical information is not easily obtained. In order to measure A, one must have kept operator matrices for the components of A. For example, to measure the on-site spin-density S^z_j for all sites j, one must keep track of matrices $[S^z_j]_{i_1 i'_1}$ for all sites in block 1, and similarly for blocks 2, 3, and 4 (regarding the single sites in the middle as blocks 2 and 3). At each step of each iteration, these operators for blocks 1 and 4 must be updated using analogues of Eqs. (4-6). One then obtains the expectation value using

$$\langle\psi|S^z_j|\psi\rangle = \sum_{i_1 i_2 i_3 i_4 i'_1} \psi^*_{i_1 i_2 i_3 i_4} [S^z_j]_{i_1 i'_1} \psi_{i'_1 i_2 i_3 i_4}, \tag{19}$$

etc. This procedure gives *exact* evaluations of $\langle\psi|A|\psi\rangle$ for the *approximate* eigenstate $|\psi\rangle$.

For a correlation function such as $\langle\psi|S^z_j S^z_k|\psi\rangle$, the evaluation depends on whether j and k are on the same block or not. If they are on different blocks, say block 1 and block 4, then one need only have kept track of $[S^z_j]_{i_1 i'_1}$ and $[S^z_k]_{i_4 i'_4}$, and one has

$$\langle\psi|S^z_j S^z_k|\psi\rangle = \sum_{i_1 i_2 i_3 i_4 i'_1 i'_4} \psi^*_{i_1 i_2 i_3 i_4} [S^z_j]_{i_1 i'_1} [S^z_k]_{i_4 i'_4} \psi_{i'_1 i_2 i_3 i'_4}. \tag{20}$$

If j and k are on the same block, one *should not* use

$$\langle\psi|S^z_j S^z_k|\psi\rangle \approx \sum_{i_1 i_2 i_3 i_4 i'_1 i''_1} \psi^*_{i_1 i_2 i_3 i_4} [S^z_j]_{i_1 i'_1} [S^z_k]_{i'_1 i''_1} \psi_{i''_1 i_2 i_3 i_4}. \tag{21}$$

This expression does not evaluate the correlation function exactly within the approximate state $|\psi\rangle$. The sum over i'_1 should run over a complete set of states, but does not, whereas the sums over the other variables need run only over those states needed

to represent $|\psi\rangle$, since they appear as a subscript in either the $|\psi\rangle$ on the left or on the right. To evaluate this type of correlation function, one needs to have kept track of $[S^z_j S^z_k]_{i_1 i'_1}$ throughout the calculation. One then evaluates

$$\langle\psi|S^z_j S^z_k|\psi\rangle = \sum_{i_1 i_2 i_3 i_4 i'_1} \psi^*_{i_1 i_2 i_3 i_4} [S^z_j S^z_k]_{i_1 i'_1} \psi_{i'_1 i_2 i_3 i_4}. \tag{22}$$

It is usually more convenient to choose points i and j on different blocks, rather than keep track of complicated operators such as $[S^z_j S^z_k]_{i_1 i'_1}$. A convenient way to calculate a correlation function such as this as a function of $j-k$ is to always put j and k at the same distance (within a lattice spacing) from the center of the chain. As $j-k$ is increased, both points move outwards symmetrically towards the ends of the chain.

VII. RESULTS

In this section we give a brief survey of results, with the intention of illustrating features of the algorithms rather than giving a study of the model systems. Figure 2 shows the density matrix eigenvalues w_α for a 32 site system for both open and periodic boundary conditions, and for both $S=1/2$ and $S=1$, targeting one state. The figure shows the eigenvalues only for one particular size of block 1, but similar results are obtained at other steps in the iteration. The fall-off of w_α is most rapid for the open $S=1/2$ case. The figure shows that it is possible to obtain an accuracy (truncation error) of better than 10^{-7} in this case, keeping only $m=20$ states. The $S=1$ open case shows a slightly slower fall-off, with an accuracy of 10^{-7} obtained with $m=48$. The periodic cases fall off more slowly than either of the open cases. Keeping $m=50$ states yields an accuracy of roughly 10^{-5} to 10^{-6}. Even more accurate treatment of periodic systems is quite feasible; we have been able to keep as many as $m=200$ states in a calculation of a 60 site system. Degeneracies in the w_α are clearly visible, which come from spin symmetries. One must adjust m so as not to split a degenerate set of levels, since this will destroy spin symmetries that would otherwise be preserved.

In Fig. 3 we show the relative accuracy of the ground state energy of a 28

site $S = 1/2$ system as a function of the number of states kept. The error for the periodic case was obtained from comparison with an exact diagonalization calculation [12]; for the open case, we used the renormalization group calculation itself with $m = 60$, which we believe reproduces the ground state energy to better than 10^{-10}. (For smaller systems, we have verified that the open case really is this accurate by comparison with our own exact diagonalization calculations.) Again, we see that the open boundary condition case is extremely accurate even for a relatively small m. The relative error in the energy is somewhat larger than the truncation error indicated by the density matrix eigenvalues. The fall-off in the error in the energy is much slower for the periodic case; it is difficult to achieve an accuracy of better than 10^{-7} in this case. Figure 4 shows similar results for a 16 site $S = 1$ system, which is close to the largest system currently feasible with exact diagonalization. As in the $S = 1/2$ case, the error for the periodic case was obtained from comparison with an exact diagonalization calculation [13], and from the renormalization group calculation itself with $m = 140$ for the open case. The accuracy for $S = 1$ case shows the same overall behavior as the $S = 1/2$ case, although it is slightly less accurate.

Using periodic boundary conditions, we calculated the gap Δ_L between the ground state, which has $S_z^{total} = 0$, and the first excited state, which has $S_z^{total} = 1$, as a function of lattice size, Fig. 5. For the $S = 1/2$ systems we used $m = 80$, and for largest $S = 1$ systems we used $m = 200$. The gap for $S = 1$ system clearly tends to a finite value as $L \to \infty$, in agreement with Haldane's conjecture that integral-spin Heisenberg chains are gapped. The gap in the $S = 1/2$ system tends to 0 as $L \to \infty$, in agreement with the Bethe ansatz exact solution of the model. These results predict an infinite system gap for the $S = 1$ chain of 0.411(1). Using open boundary conditions (of the "soft" type discussed below) we have obtained what we believe is the most accurate value of Δ to date: $\Delta = 0.4105(1)$ [11].

It is clearly more accurate to use open boundary conditions than periodic in these calculations, but a bulk system is generally better described using periodic boundary

conditions. It is important to understand the effect of an open boundary on these systems. The effect of an open boundary is most easily seen for an $S = 1/2$ system by measuring the local bond strength $(\vec{S}_i \cdot \vec{S}_{i+1})$ as a function of site-index i. In Fig. 6(a) we show the local bond strength for a 60 site system. The open boundaries cause a strong alternation in the bond strength which decays very slowly. (We emphasize that this is the effect of the boundaries; errors in our calculation are negligible.) This effect is easily understood using the valence bond picture of the ground state of the $S = 1/2$ system. In the valence bond picture, the ground state is viewed as a resonance between two different states, one having strong singlet bonds on the even numbered links of the chain, and no bonds on the odd links, and the other with strong bonds on the odd links, and none on the even. Simple variational estimates show that this type of state is greatly preferred over a Néel ordered state. This picture strongly suggests that the system can be perturbed very easily into one of these two dimerized states. The open boundary conditions favor a strong bond on the outermost links, since that is the only way the end sites can participate in a bond.

If the system has an odd number of sites, one end favors the strong bonds on the even links, and the other favors them on the odd links; thus the system is frustrated. In Fig. 6(b) we show the local bond strength on a 61 site system. The system shows the odd links with stronger bonds on the left, and the even links stronger on the right. For other system sizes the behavior is nearly identical to that shown for $L = 60$ in the sense that there are never more than a few links in the center with almost no bond-strength alternation present, and there is approximately linear fall-off of the bond-strength in the central region. We interpret this behavior as evidence of a mobile domain wall (soliton), with a nearly uniform probability to be at any particular site in the central region. If one averages over the various positions of the domain wall, one obtains results consistent with the figure.

If we desire the accuracy of open boundary conditions, but not the bond-strength alternation which is absent in the bulk system, it is possible to considerably weaken

the alternation using "soft" boundary conditions. In Fig. 6(c) we show results from an especially simple version of these boundary conditions. In this case we weakened the two outermost exchange constants J from their bulk value $J = 1$. The strength was chosen to minimize the bond-strength alternation in the center. In the limit that these outermost couplings are zero, the even sublattice is favored, whereas in the usual case the odd sublattice is favored. Clearly for some intermediate coupling the alternation is nearly absent; in this case it is for $J = 0.236$. More work needs to be done to understand these soft boundary conditions.

The boundaries of an open system pose much less of a problem for an $S = 1$ system, and in addition, are of substantial interest. Spin-spin correlation functions decay exponentially in this system, and the effect of the open ends is also reduced exponentially as we move towards the interior. Figure 7(a) shows the local bond strength of an $S = 1$ chain. Within the central region of the chain, the bond strength is constant to very high accuracy. The open ends of $S = 1$ chains act as effective spin 1/2's. These spin 1/2's bind very weakly through the chain to form a singlet and triplet. The singlet is the ground state for even numbered chains, and the triplet is the ground state for odd numbered chains. Figure 7(b) shows the local spin magnetization for one of the triplet states of a 60 site chain, which has the spin 1/2's on both ends pointing up. As reported earlier [3], the magnetization of the ends is 0.532, as opposed to exactly 1/2 for a real spin 1/2.

The renormalization group method is most accurate when only one state is used as a target. Figure 8 shows the behavior of the density matrix eigenvalues w_α of a typical system as the number of target states is varied. It is possible to target 15 or more states and still retain reasonable accuracy for a system with open boundary conditions. In this way it is possible to map out the low-lying elementary excitations of a many-body system.

VIII. CONCLUSIONS

The density matrix algorithms for numerical renormalization group calculations

of 1D systems are very powerful. They provide extremely accurate results for the ground state and low-lying excited states, and can be used to calculate a variety of static quantities. The methods can be applied to a wide variety of systems, and work is currently underway to apply the methods to strongly interacting fermion systems, such as the Hubbard chain and the 1D Kondo lattice. In this paper we have concentrated on the description of a few algorithms, rather than giving detailed results for Heisenberg chains. We plan to publish a survey of a variety of properties of Heisenberg chains shortly.

These methods are somewhat complex and there are substantial variations possible in the construction of algorithms. More work needs to be done in exploring these variations. For example, one could use a momentum space basis instead of real space basis in setting up the calculation. This was recently done *without* the density matrix formulation for a 4×4 Hubbard lattice [14]. Applying the density matrix formulation in this case would probably substantially improve the calculation. One could apply the real-space method to coupled chains and to two dimensional systems; one would expect less accuracy than in 1D but one might still obtain valuable results. Other areas for future study include applying magnetic fields to calculate static susceptibilities; studying disordered 1D systems; and studying various types of soft boundary conditions for use with open systems.

We would like to thank R.M. Noack, D. Huse, C. Yu, I. Affleck, and M.P. Gelfand, for helpful comments and discussion. This work was supported by the Office of Naval Research under Grant No. N00014-91-J-1143 and in part by the University of California through an allocation of computer time on the UC Irvine Convex. Calculations were also performed at SDSC.

REFERENCES

[1] K.G. Wilson, *Rev. Mod. Phys.* 47, 773 (1975).

[2] S.R. White and R.M. Noack, *Phys. Rev. Lett.* **68** , 3487 (1992).

[3] S.R. White,*Phys. Rev. Lett.* **69** , 2863 (1992).

[4] J.W. Bray and S.T. Chui, *Phys. Rev.* B19, 4876 (1979).

[5] T. Xiang and G.A. Gehring, *Journal of Magnetism and Magnetic Materials* 104-107, 361 (1992); T. Xiang and G.A. Gehring, preprint.

[6] See, for example, J.E. Hirsch,*Phys. Rev.* B22, 5259 (1980); C. Dasgupta and P. Pfeuty, *J. Phys.* C14, 717 (1981).

[7] R.M. Noack and S.R. White, preprint.

[8] R.P. Feynman, *Statistical Mechanics: A Set of Lectures*, (Benjamin, Reading, MA, 1972).

[9] W.H. Press, B.P. Flannery, S.A. Teukolsky, and W.T Vetterling, *Numerical Recipes: The Art of Scientific Computing*, (Cambridge, New York, NY, 1986).

[10] E.R. Davidson, *J. Comp. Phys.* **17**, 87 (1975).

[11] S.R. White and D. Huse, to be published.

[12] D. Medeiros and G.G. Cabrera, *Phys. Rev.* B43, 3703 (1991).

[13] A. Moreo, *Phys. Rev.* **B35**, 8562 (1987).

[14] S.R. White, *Phys. Rev.* **B45**, 5752 (1992).

FIGURES

FIG. 1. The configuration of blocks used for the density matrix calculations considered here. The rectangles represent blocks containing l and l' sites, and the solid circles represent single sites.

FIG. 2. Density matrix eigenvalues w_α versus eigenvalue index α for a 32 site system for both periodic and open boundary conditions, $S = 1/2$ an $S = 1$. The eigenvalues were obtained from the $B_{16} \bullet \bullet B_{16}^R$ system. The step-like structure comes from the presence of spin degeneracies. Additional near-degeneracies in the $S = 1$ cases come from the presence of nearly free $S = 1/2$ effective spins on the ends of $S = 1$ blocks. The errors in the calculation is determined by $\sum_{\alpha=m+1}^{\infty}$, which can be estimated from the figure.

FIG. 3. Relative error in the ground state energy $\Delta E/E$ for a 28 site $S = 1/2$ system as a function of the number of states kept m, for periodic and open boundary conditions. The exact energy was obtained from [12] for the periodic case, and from the renormalization group calculation itself with $m = 58$ for the open case.

FIG. 4. Relative error in the ground state energy E for a 16 site $S = 1$ system, as a function of the number of states kept m, for periodic and open boundary conditions. The exact energy was obtained from Ref. [13] for the periodic case, and from the renormalization group calculation itself with $m = 140$ for the open case.

FIG. 5. Gaps Δ_L between the ground and first excited states for $S = 1/2$ and $S = 1$ systems with periodic boundary conditions versus the inverse length of the chain $1/L$.

FIG. 6. Local bond strength for (a) 60 site and (b) 61 site $S = 1/2$ chains with open boundary conditions. The systems try to have strong single bonds at the outermost links of the chain; this induces a domain wall in the odd-length chain. In (c), the bond strength alternation is diminished by weakening the local value of the exchange constant J on the outermost links.

FIG. 7. Local bond strength (a) and local value of S_z (b) for a $S = 1$ system with 60 sites. The $S = 1/2$ effective spins on the ends of are clearly visible in (b), which shows one of the low-lying triplet states just above the ground state.

FIG. 8. Density matrix eigenvalues w_α versus α for a 32 site $S = 1/2$ system with open boundary conditions, with various numbers of target states. When a greater number of states are targeted for a fixed value of m, the size of the w_α which are discarded is increased, and there is a reduction in the accuracy. The eigenvalues were obtained from the $B_{l\mathrm{s}} \bullet \bullet B^R_{l\mathrm{s}}$ system.

TABLE I. Standard numerical renormalization group algorithm for a 1D quantum system.

1. Isolate two blocks BB, and form H_{BB}.
2. Diagonalize H_{BB}, obtaining the m lowest eigenvectors u^α
3. Form matrix representations of S^i_l, etc., for BB from the corresponding matrices for B.
4. Change basis to the u^α, keeping only the lowest m states, using $H_{B'} = OH_{BB}O^\dagger$, etc., with $O(\alpha; i_1, i_2) = u^\alpha_{i_1,i_2}$, $\alpha = 1, \ldots, m$.
5. Replace B with B'.
6. Go to step 1.

TABLE II. Infinite system density-matrix algorithm for a 1D system.

1. Make four initial blocks, each consisting of a single site, representing the initial four site system. Set up matrices representing the block Hamiltonian and other operators.

2. Form the Hamiltonian matrix (in sparse form) for the superblock.

3. Using the Davidson or Lanczos method, diagonalize the superblock Hamiltonian to find the target state $\psi(i_1, i_2, i_3, i_4)$. ψ is usually the ground state. Expectation values of various operators can be measured at this point using ψ.

4. Form the reduced density matrix for the two-block system 1-2, using $\rho(i_1, i_2; i_1', i_2') = \sum_{i_3, i_4} \psi(i_1, i_2, i_3, i_4)\psi(i_1', i_2', i_3, i_4)$.

5. Diagonalize ρ to find a set of eigenvalues w_α and eigenvectors $u^\alpha_{i_1,i_2}$. Discard all but the largest m eigenvalues and associated eigenvectors.

6. Form matrix representations of operators (such as H) for the two-block system 1-2 from operators for each separate block (cf. Eq. (4)).

7. Form a new block 1 by changing basis to the u^α and truncating to m states using $H^{1'} = OH^{12}O^\dagger$, etc. If blocks 1 and 2 have m_1 and m_2 states, then O is an $m \times m_1 m_2$ matrix, with matrix elements $O(\alpha; i_1, i_2) = u^\alpha_{i_1,i_2}$, $\alpha = 1, \ldots, m$.

8. Replace old block 1 with new block 1.

9. Replace old block 4 with the reflection of new block 1.

10. Go to step 2.

TABLE III. Finite system density-matrix algorithm for a 1D system consisting of L sites. A calculation consists of several iterations, indexed by I, with each iteration consisting of $L - 3$ steps, indexed by ℓ, where ℓ is the size of the first block.

1. (First half of $I = 1$.) Use the infinite system algorithm for $L/2 - 1$ steps to build up the lattice to L sites. At each iteration store the block Hamiltonian and end operator matrices for block 1. Label the blocks by their size, B_ℓ, $\ell = 1, \ldots, L/2$.

2. (Start of second half of $I = 1$.) Set $\ell = L/2$. Use B_ℓ as block 1, and the reflection of $B_{L-\ell-1}$ as block 4.

3. Steps 2–8 of Table II.

4. Store the new block 1 as $B_{\ell+1}$, replacing the old $B_{\ell+1}$.

5. Replace block 4 with the reflection of $B_{L-\ell-1}$, obtained from the first half of this iteration.

6. If $\ell < L - 3$, set $\ell = \ell + 1$ and go to step 3.

7. (Start of iteration I, $I \geq 2$). Make four initial blocks, the first three consisting of a single site, and the fourth consisting of the reflection of B_{L-1} from the previous iteration. Set $\ell = 1$.

8. Steps 2–8 of Table II.

9. Store the new block 1 as $B_{\ell+1}$, replacing the old $B_{\ell+1}$.

10. Replace block 4 with the reflection of $B_{L-\ell-1}$, obtained from the previous iteration (if $\ell \leq L/2 - 1$) or the first half of this iteration (if $\ell > L/2 - 1$)

11. If $\ell < L - 3$, set $\ell = \ell + 1$ and go to step 8. If $\ell = L - 3$, start a new iteration by going to step 7. (Stop after 2 or 3 iterations.)

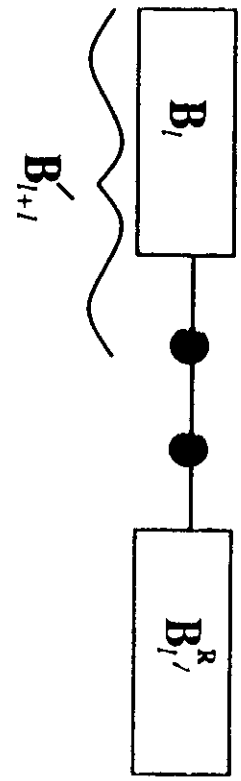
B_l
B'_{l+1}
$B^R_{l'}$

Fig. 1

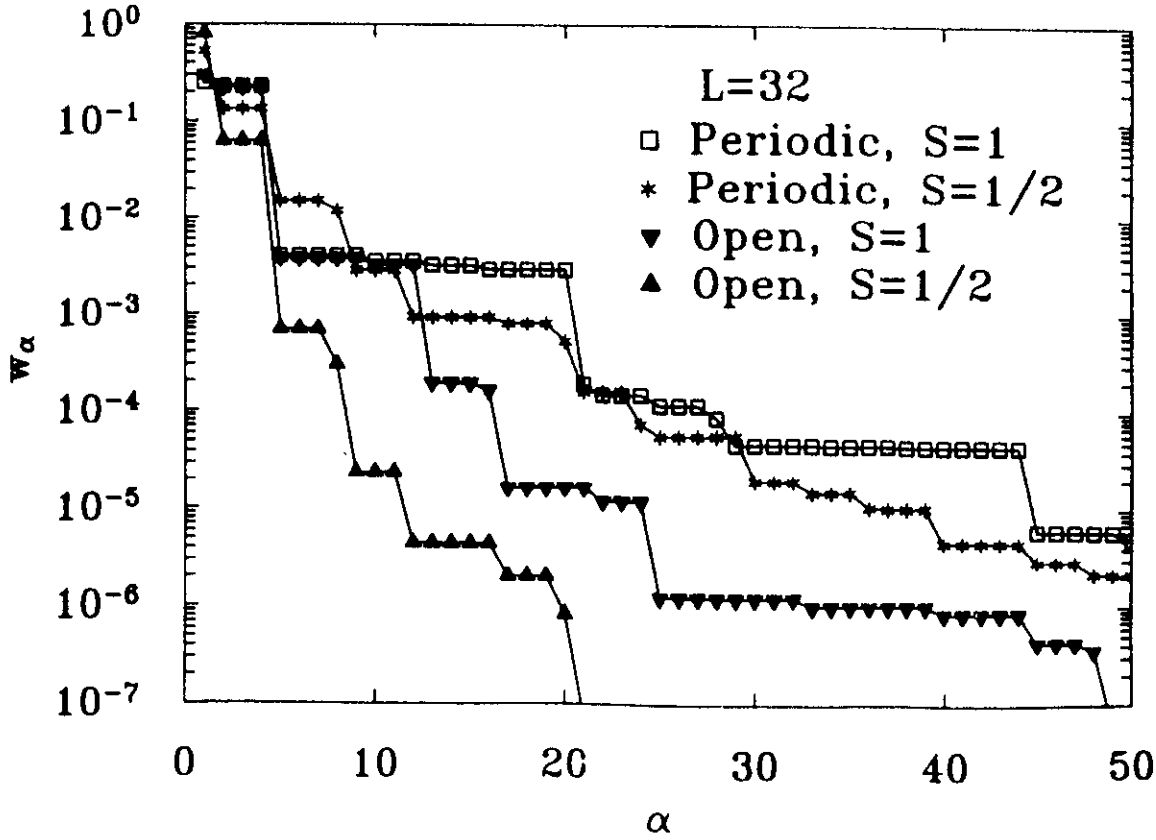
L=32
Periodic, S=1
Periodic, S=1/2
Open, S=1
Open, S=1/2
W_α
α
10^0
10^{-1}
10^{-2}
10^{-3}
10^{-4}
10^{-5}
10^{-6}
10^{-7}
0
10
20
30
40
50

Fig. 2

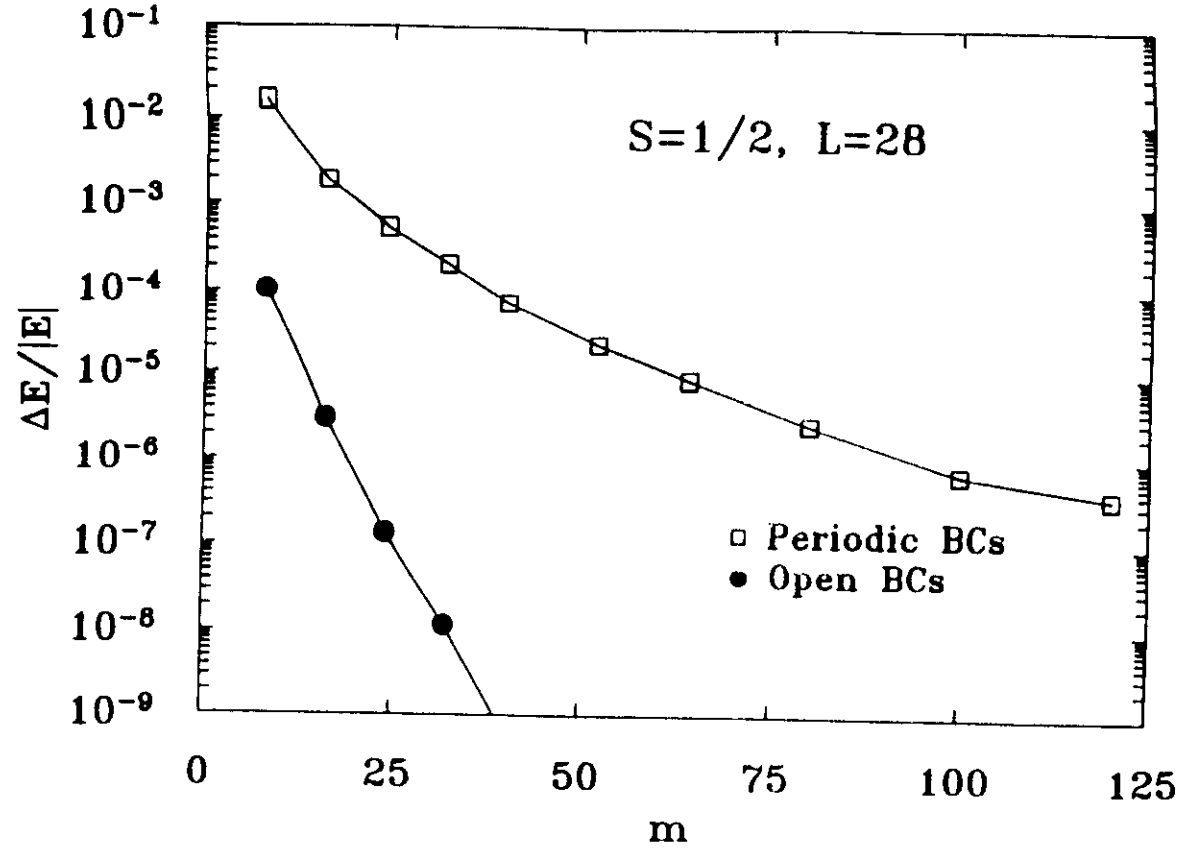
S=1/2, L=28
Periodic BCs
Open BCs
ΔE/|E|
m

Fig. 3

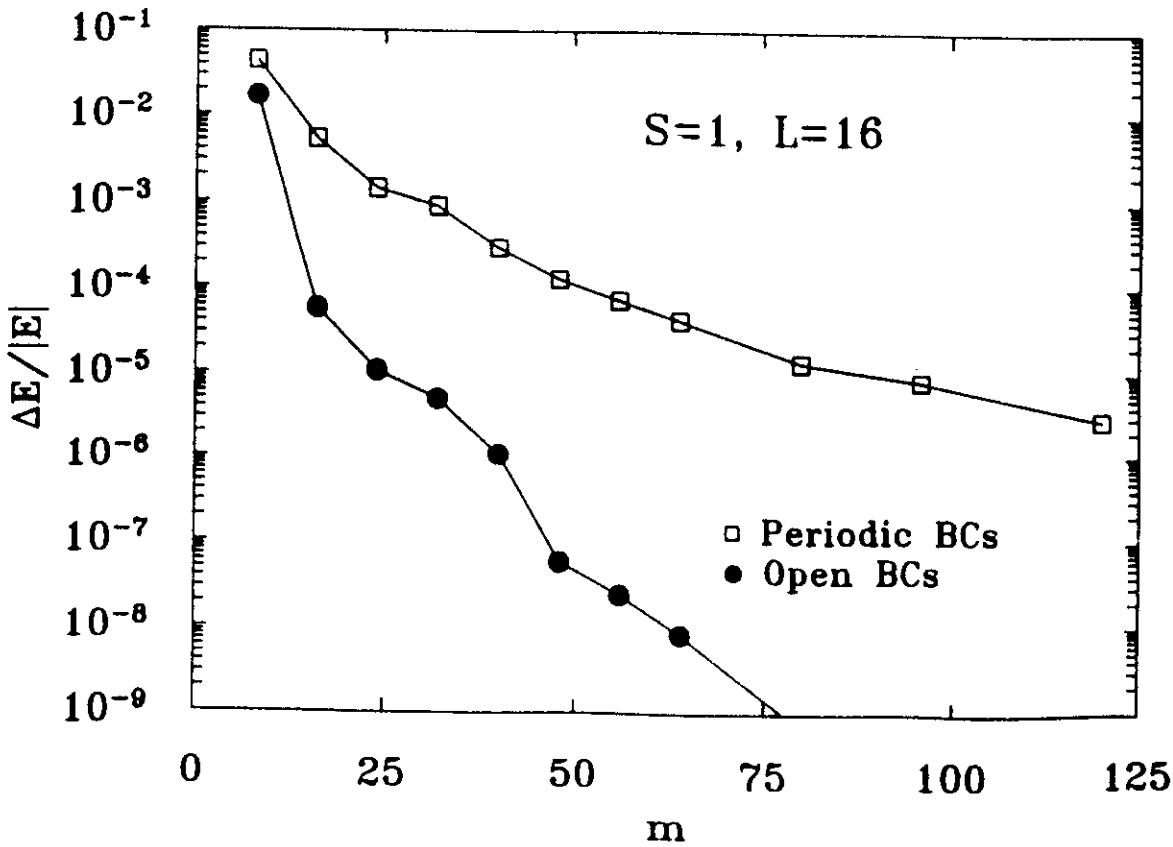
S=1, L=16
Periodic BCs
Open BCs
ΔE/|E|
m

Fig. 4

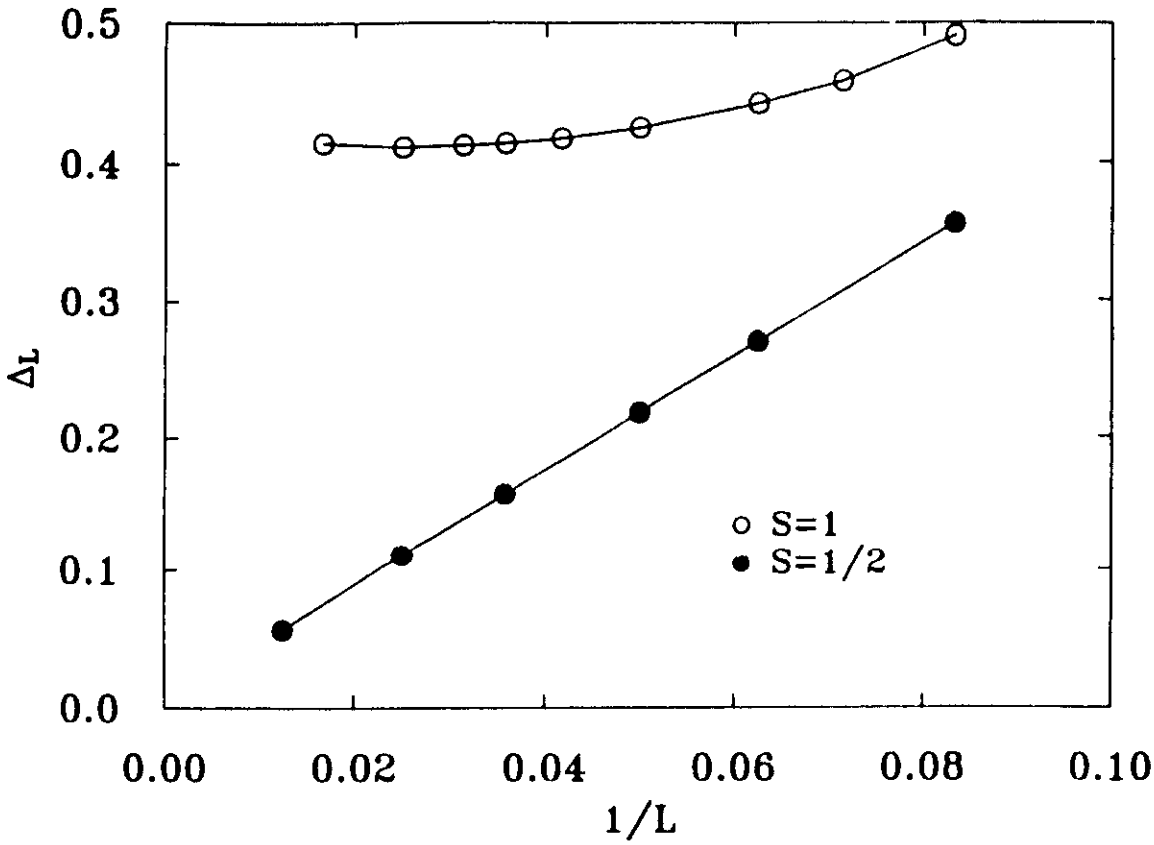
0.5
0.4
0.3
0.2
0.1
0.0
Δ_L
S=1
S=1/2
0.00
0.02
0.04
0.06
0.08
0.10
1/L

Fig. 5

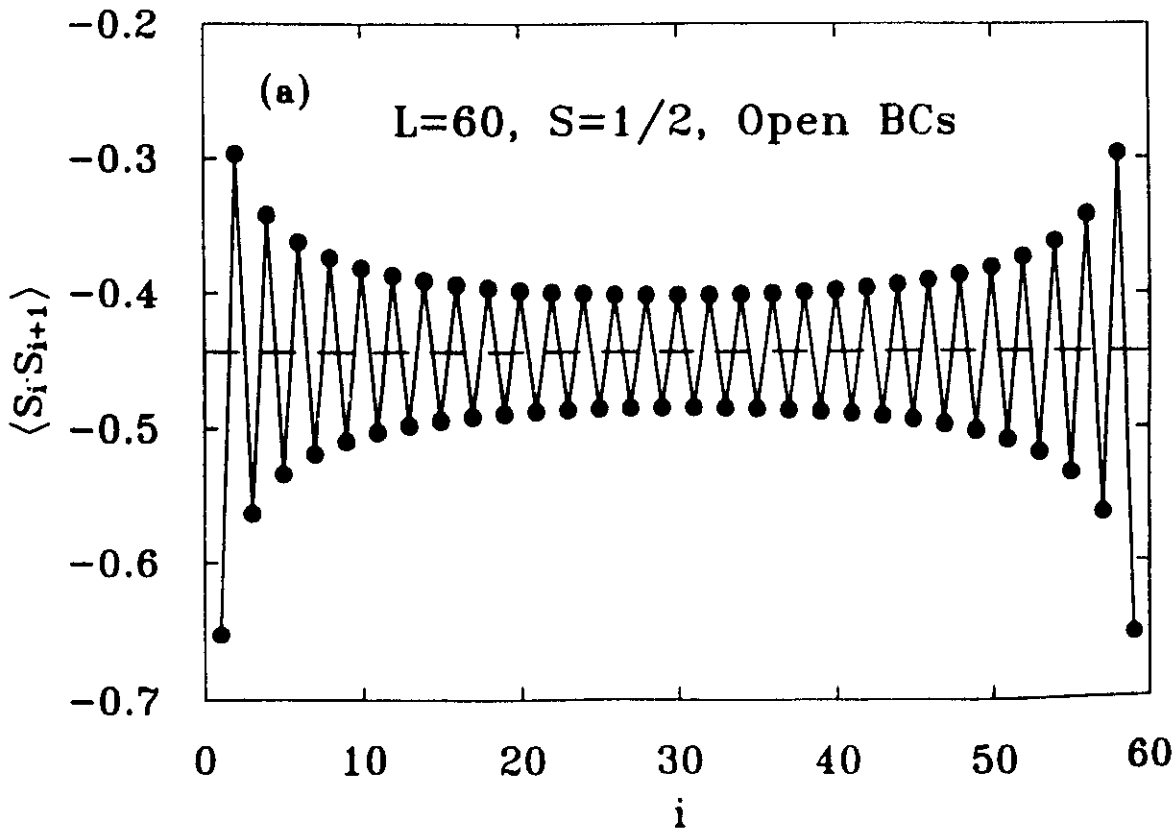
(a)
L=60, S=1/2, Open BCs
−0.2
−0.3
−0.4
−0.5
−0.6
−0.7
$\langle S_i \cdot S_{i+1} \rangle$
0
10
20
30
40
50
60
i

Fig. 6(a)

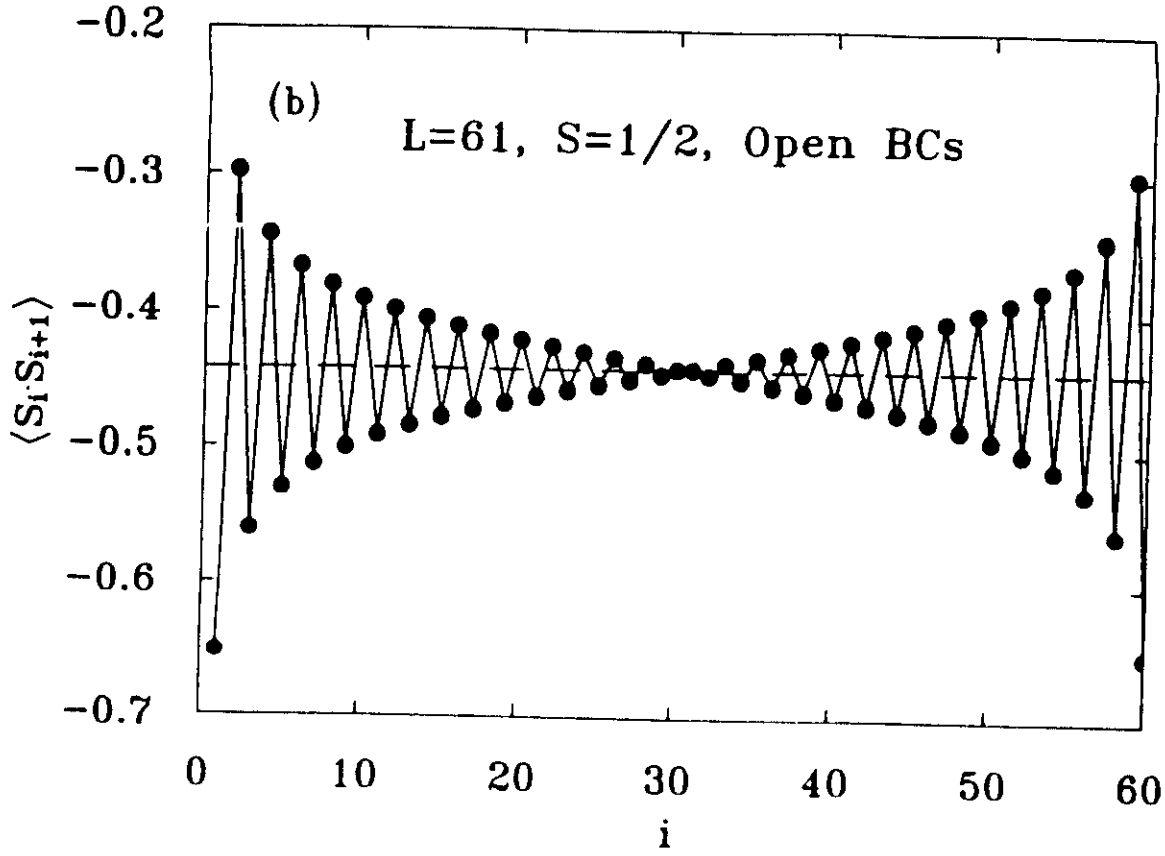
(b)
L=61, S=1/2, Open BCs
$\langle S_i \cdot S_{i+1} \rangle$
-0.2
-0.3
-0.4
-0.5
-0.6
-0.7
0
10
20
30
40
50
60
i

Fig. 6(b)

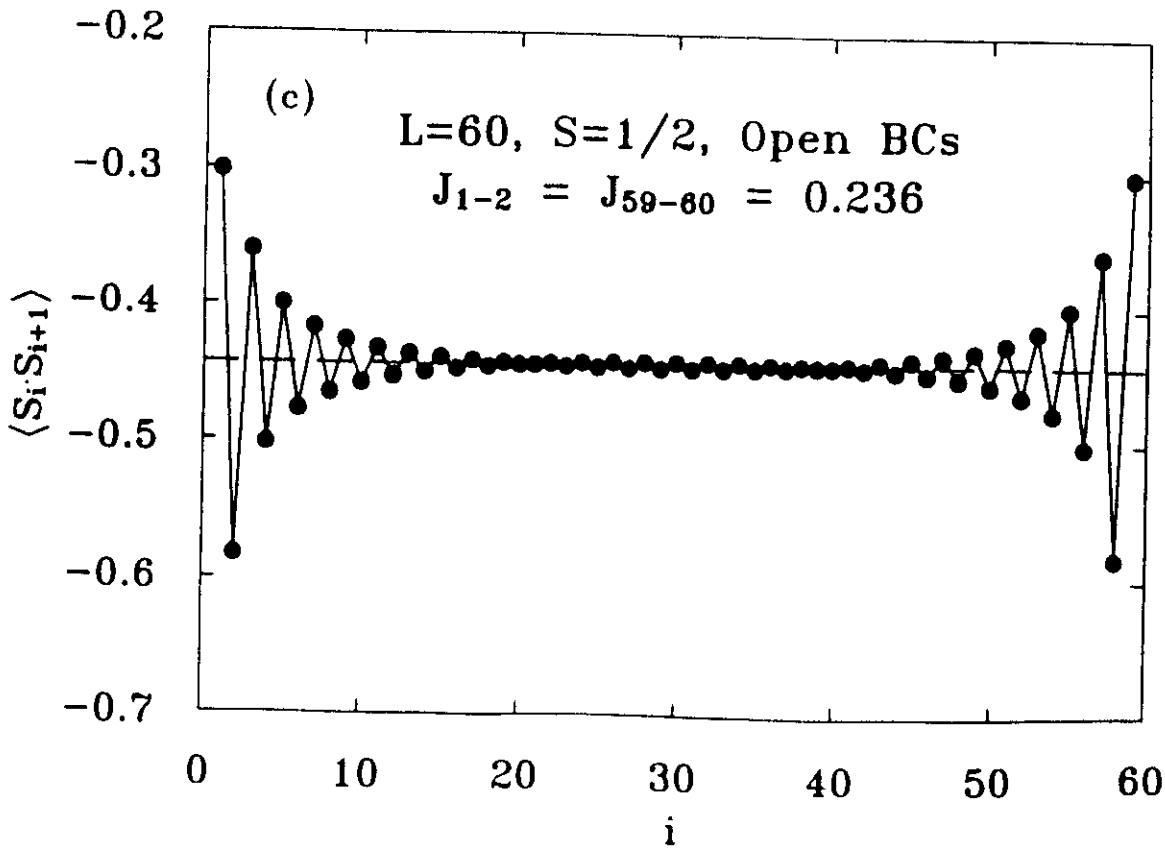
(c)
L=60, S=1/2, Open BCs
$J_{1-2} = J_{59-60} = 0.236$
$\langle S_i \cdot S_{i+1} \rangle$
-0.2
-0.3
-0.4
-0.5
-0.6
-0.7
0
10
20
30
40
50
60
i

Fig. 6(c)

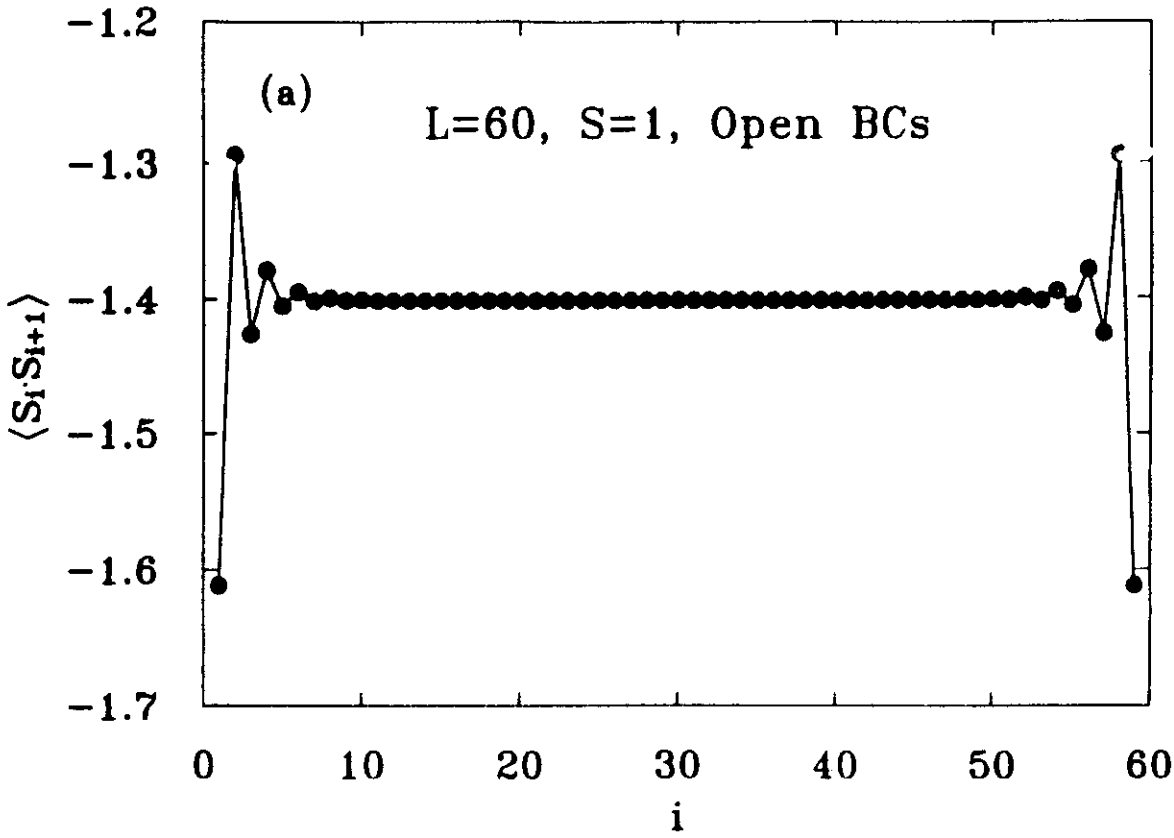
(a)
L=60, S=1, Open BCs
$\langle S_i \cdot S_{i+1} \rangle$
i
−1.2
−1.3
−1.4
−1.5
−1.6
−1.7
0
10
20
30
40
50
60

Fig. 7(a)

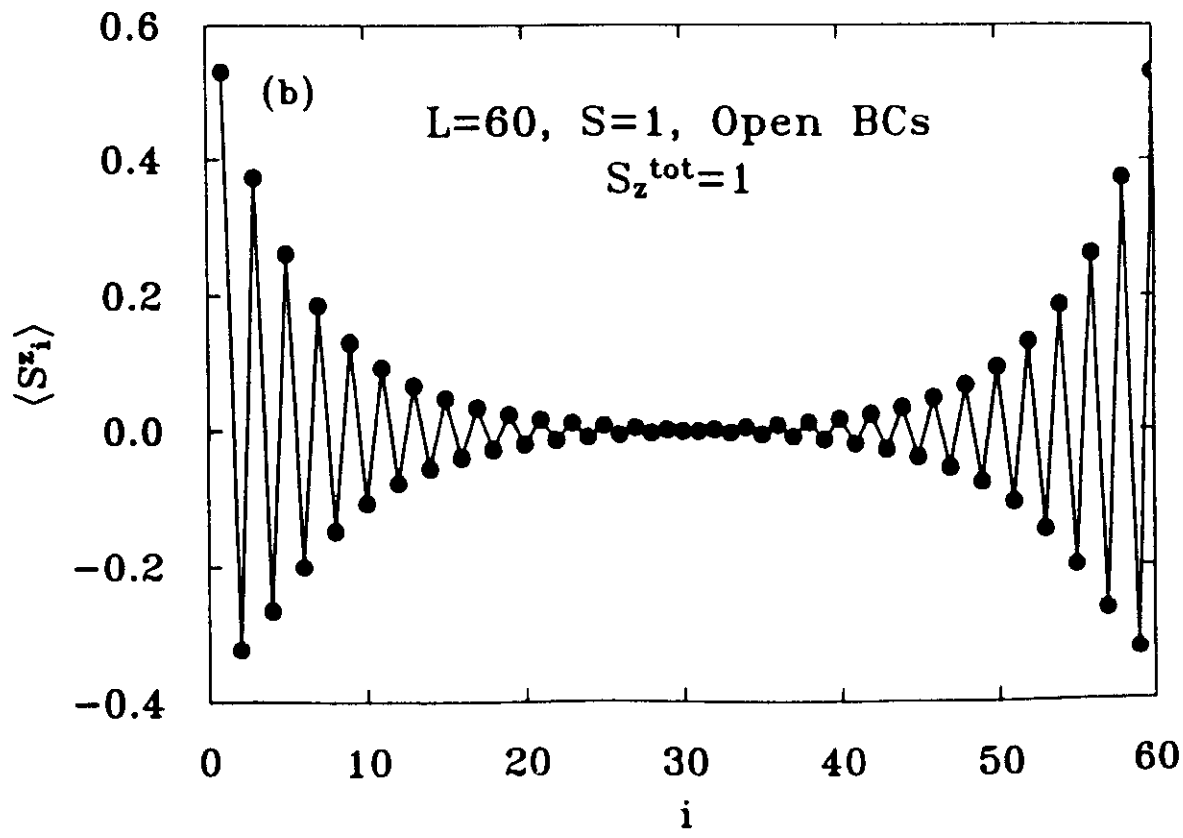
(b)
L=60, S=1, Open BCs
$S_z^{tot}=1$
$\langle S^z_i \rangle$
i
0.6
0.4
0.2
0.0
−0.2
−0.4
0
10
20
30
40
50
60

Fig. 7(b)

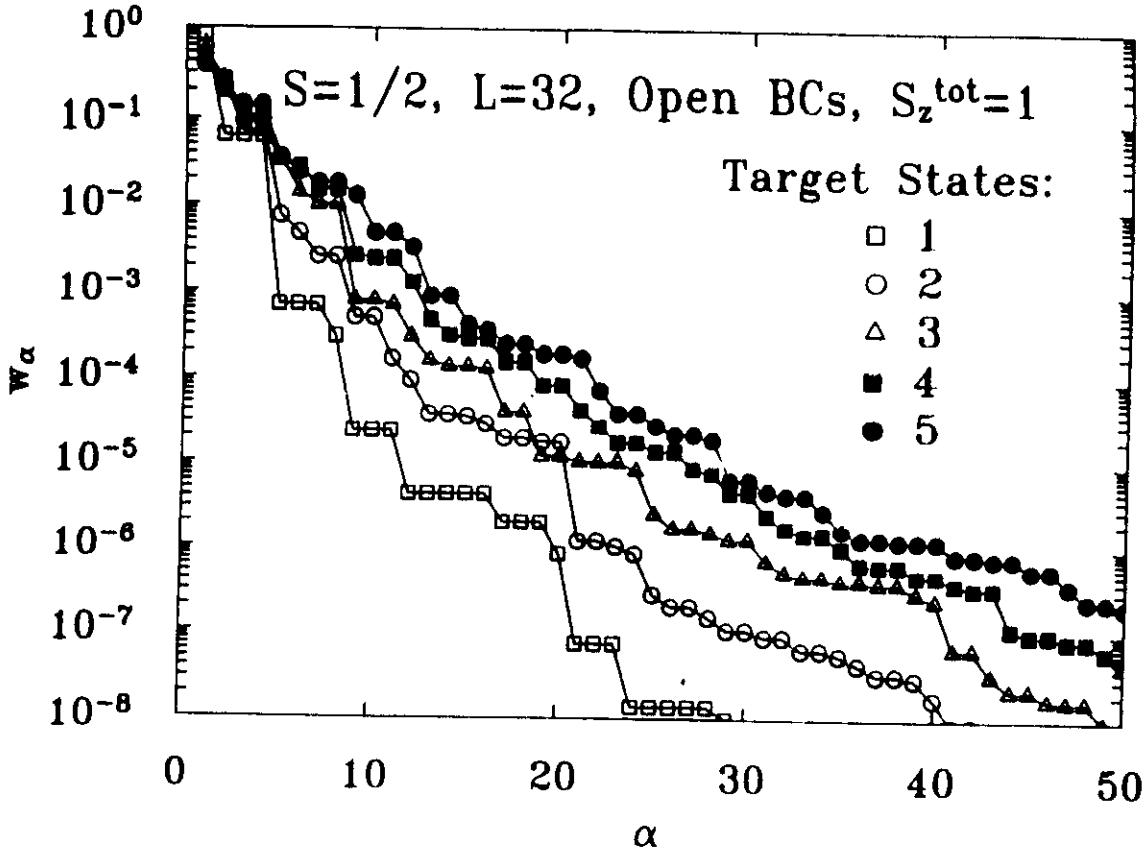
S=1/2, L=32, Open BCs, $S_z^{tot}=1$
Target States:
1
2
3
4
5
10^0
10^{-1}
10^{-2}
10^{-3}
10^{-4}
10^{-5}
10^{-6}
10^{-7}
10^{-8}
W_α
0
10
20
30
40
50
α

Fig. 8

Numerical renormalization-group study of low-lying eigenstates of the antiferromagnetic $S = 1$ Heisenberg chain

Steven R. White
Department of Physics, University of California, Irvine, California 92717

David A. Huse
AT&T Bell Labs, Murray Hill, New Jersey 07974

(Received 3 February 1993; revised manuscript received 23 April 1993)

We present results of a numerical renormalization-group study of the isotropic $S = 1$ Heisenberg chain. The density-matrix renormalization-group techniques used allow us to calculate a variety of properties of the chain with unprecedented accuracy. The ground state energy per site of the infinite chain is found to be $e_0 \cong -1.401\,484\,038\,971(4)$. Open-ended $S = 1$ chains have effective $S = 1/2$ spins on each end, with exponential decay of the local spin moment away from the ends, with decay length $\xi \cong 6.03(1)$. The spin-spin correlation function also decays exponentially, and although the correlation length cannot be measured as accurately as the open-end decay length, it appears that the two lengths are identical. The string correlation function shows long-range order, with $g(\infty) \cong -0.374\,325\,096(2)$. The excitation energy of the first excited state, a state with one magnon with momentum $q = \pi$, is the Haldane gap, which we find to be $\Delta \cong 0.410\,50(2)$. We find many low-lying excited states, including one- and two-magnon states, for several different chain lengths. The magnons have spin $S = 1$, so the two-magnon states are singlets ($S = 0$), triplets ($S = 1$), and quintuplets ($S = 2$). For magnons with momenta near π, the magnon-magnon interaction in the triplet channel is shown to be attractive, while in the singlet and quintuplet channels it is repulsive.

I. INTRODUCTION

Recent improvements in real-space numerical renormalization group (RG) techniques[1–3] have made this method competitive with, and in many ways superior to, other numerical methods, such as quantum Monte Carlo and exact diagonalization, for studies of one-dimensional (1D) quantum systems. The main advance involves the reformulation of the method in terms of density matrices.[2] In the original formulation of the real-space RG method, a block of sites is diagonalized and the lowest-lying eigenstates of the block Hamiltonian are used to construct a new effective Hamiltonian, which one hopes is valid for the low-lying states of the whole lattice. In the density-matrix method we form the new effective Hamiltonian out of the most probable eigenstates of the block density matrix. This change makes the method tremendously more accurate than the original approach. However, finding the density matrix of the block requires one to diagonalize a larger section of the lattice which includes the block, in order to incorporate the effects of the rest of the lattice on the block. Efficient density-matrix algorithms have been developed for finite chains with open or periodic boundary conditions, as well as for an infinite chain, where the chain length steadily increases with each iteration. These methods have been described in detail elsewhere.[3]

In this paper we report results of a density-matrix RG study of the antiferromagnetic $S = 1$ Heisenberg chain, which has been the subject of a large amount of work in the last decade. Besides exhibiting the well-known Haldane gap, this system has been found to have several other fascinating features. For example, the ground state of an open $S = 1$ chain has an effective $S = 1/2$ spin at each end. These effective spins have been observed in real systems containing $S = 1$ chains, such as $Ni(C_2H_8N_2)_2NO_2ClO_4$ (NENP), using magnetic-resonance techniques.[4] The ground state also exhibits a surprising form of topological long-range order, related to a similar type of order found in fractional quantum-Hall-effect systems. There have been a number of theoretical and experimental studies of the spectrum of low-lying excited states of this system.[6–8]

The density-matrix algorithms used here give much more accurate results using open boundary conditions than with periodic boundary conditions. With periodic boundary conditions, each block has two ends which interact with the rest of the lattice, whereas with open boundary conditions, a block has only one active end if it contains either the right or left end of the chain. The effective Hamiltonian of the block must be made from a larger number of states if it must represent two active ends. Thus the results we report here are all for open chains. It is possible, however, to accurately reproduce bulk properties with open chains because we can study very large chains—up to several hundred sites.

A simple understanding of the ground state of the antiferromagnetic Heisenberg spin-1 chain was presented by Affleck, Kennedy, Lieb, and Tasaki (AKLT).[5] Each spin-1 may be viewed as two spin-1/2 spins that combine on site in a fully symmetric triplet wave function. Now let one spin 1/2 on each site pair with one of the spin-1/2 spins on the next site to the left in an antisymmetric singlet wave function, while the other spin-1/2 pairs with a

0163-1829/93/48(6)/3844(9)/$06.00

spin 1/2 on the next site to the right. The unique singlet wave function of the entire chain resulting from this construction captures much of the essential physics of the ground state. (In fact this wave function is the exact ground state of a closely related Hamiltonian with additional biquadratic nearest-neighbor interactions.[5]) With simple free ends, one thus has unpaired spin 1/2's left at each end of the chain. The interaction between these extra half-spins falls off exponentially with the length of the chain, and so in the limit of a long chain one has a four-fold degenerate ground state due to these two free-end spins. Although this and other end effects are quite interesting in their own right and can be captured very accurately using density-matrix algorithms, in this paper we will focus on properties in the bulk of the chain, away from the ends, and so we would like to remove this inconvenient degeneracy.

If one adds a real spin-1/2 spin at each end of the chain, these can each form singlets with half of the last spin 1 in the chain, thereby removing the ground-state degeneracy. Thus for a chain of length L sites our Hamiltonian is

$$H = \sum_{\ell=1}^{L-1} J(\ell)\vec{S}_\ell \cdot \vec{S}_{\ell+1}, \tag{1}$$

where $\vec{S}_1$ and $\vec{S}_L$ are spin-1/2 spins, while all other spins are of spin 1. The couplings are $J(\ell) = 1$ in the bulk of the chain, but may be adjusted at or near the ends of the chain. By varying the couplings at the ends of the chain we may attempt to choose the best boundary conditions for the task at hand. Examples of this are illustrated below. We generally only adjust the final couplings, taking $J(1) = J(L-1) \equiv J_{\rm end}$ and leaving all other couplings at unity.

The total spin commutes with the Hamiltonian (1). We work in an S^z basis in which the good quantum numbers are total S^z and total spin. The couplings will generally be taken to be symmetric, $J(\ell) = J(L-\ell)$, under parity (reversal of the chain), and so parity is an additional good quantum number.

II. GROUND-STATE PROPERTIES

We have examined the ground state of (1) for various boundary conditions. As long as we have the spin-1/2 spins on the ends and only antiferrromagnetic couplings, $J(\ell) > 0$ for all ℓ, the ground state is a singlet (zero total spin). The parity of the ground state is opposite to the parity of the number of sites, L, as is expected from the above AKLT wave function. Most of our results are for even L where the ground state is thus odd under parity.

We are interested in the properties of the translationally invariant infinite chain, and so when we study the ground state we should choose a boundary condition that induces minimal nonuniformity in the ground state away from the ends. To do this we can measure the ground-state expectation value of the local energy,

$$e(\ell) \equiv \langle \vec{S}_\ell \cdot \vec{S}_{\ell+1} \rangle , \tag{2}$$

and ask that this be perturbed as little as possible by the boundary condition. Near the end of the chain, $e(\ell)$ does show nonuniformities due to end effects which decay rapidly as one moves away from the end, as illustrated in Fig. 1. When we adjust the end coupling, the minimum end effect is seen at $J_{\rm end} \cong 0.7$ (see Fig. 1).

The ground-state energy can then be obtained by measuring $E(\ell)$ in the center of the chain. However, a significantly more accurate estimate is obtained by measuring energy differences using the infinite-lattice algorithm. In the infinite-lattice method, the size of the lattice grows by 2 at each step. The two additional sites are added in the center of the chain. The total energy of the chain increases in one step by the energy associated with these two sites. Using $J_{\rm end} = 0.7$, the additional energy added in a step divided by two converges very rapidly with increasing L to a very accurate estimate of the ground-state energy per site. The error in the energy due to finite L quickly becomes negligible compared to the truncation error $1 - P(m)$,[3] where m is the number of states kept per block. $P(m)$ is defined as the sum of the first m density-matrix eigenvalues; the corresponding eigenvectors are used in constructing the effective Hamiltonian of a block. Each density-matrix eigenvalue represents the probability of that particular eigenstate, and $1 - P(m)$ thus gives the fractional error involved in representing a block by only m states. Of course, in the course of a calculation the density matrix is diagonalized for a variety of blocks of different sizes; we report the largest value of $1-P(m)$ appearing in the last iteration. (In this case the earlier iterations can be considered merely preliminary to the last iteration.)

Because of the very rapid decrease of $1 - P(m)$ with m, our determination of the ground-state energy is ultimately limited in accuracy by accumulated round-off error in the various parts of the calculation due to the use of 64-bit ("real*8" in FORTRAN) precision. The accuracy of the density-matrix eigenvectors begins to degrade when the associated eigenvalues become less than about

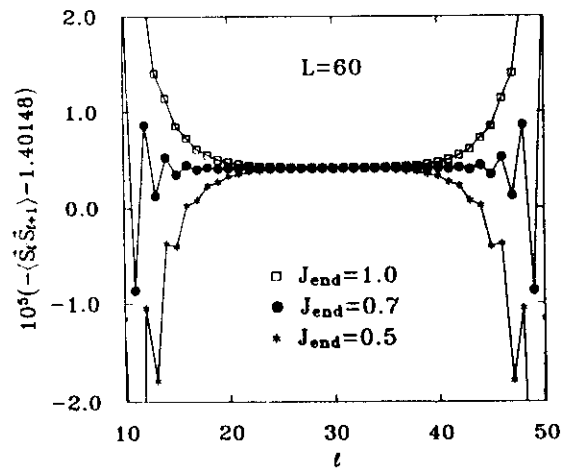

FIG. 1. Local energy in the ground state vs distance along the chain ℓ for a chain of length $L = 60$ and various values of $J_{\rm end}$. The end effect is minimized for $J_{\rm end} \cong 0.7$. Note the highly expanded scale on the vertical axis.

10^{-12}. The primary effect of using these inaccurate eigenvectors is a slight slowdown in the rate of convergence of quantities such as the energy with m. As long as the set of eigenvectors used to represent a block is kept orthonormal to machine precision, which is not difficult, we do not expect any errors associated with including these approximate eigenvectors, only a somewhat slower reduction in the truncation errors. In the case of the ground-state of the $S = 1$ Heisenberg chain, for $m \leq 110$, round-off error is negligible. Table I shows the ground-state energy per spin, e_0, for various values of m, having converged with lattice size in each case. For m ranging from 36 to 86, the error in the energy (determined using the larger-m results) is roughly proportional to $1 - P(m)$, with a coefficient of about 5. Using this slope to correct the results for $m = 110$ gives a corrected estimate of the energy of $e_0 \cong -1.40148403895$. This correction also can be used as an estimate of the uncertainty in the final result; we find (using $m \leq 110$) $e_0 \cong -1.4014840390(2)$. A more accurate result is obtained by correcting the $m = 180$ results in a similar way, yielding $e_0 \cong -1.401484038971(4)$. This last result may be affected by round-off errors larger than the stated error (which is a generous estimate of the truncation error); to estimate the round-off error we would need to run the calculations with higher numerical precision.

The spin-spin correlation function $C(i - j) = \langle S_i^z S_j^z \rangle$ can be measured in a symmetrical fashion on a finite chain by putting i and j equal distances from the center of the chain, and varying their separation. This calculation can be carried out with either the finite-lattice or infinite-lattice method. The correlation function is expected to behave for large ℓ as

$$C(\ell) \approx A(-1)^\ell K_0(\ell/\xi) \approx A(-1)^\ell (\pi\xi/2\ell)^{1/2} e^{-\ell/\xi}, \qquad (3)$$

where A is a constant, K_0 is the modified Bessel function, ξ is the correlation length, and the second form holds for $\ell >> \xi$. Figure 2 shows $C(\ell)$ from an infinite-lattice calculation with $m = 180$. The correlation function cannot be measured as accurately as the energy, with the errors as large as 10^{-6} for $\ell \approx 30$. Nevertheless, our results are substantially more accurate than those from quantum Monte Carlo calculations.[9] Unlike the errors in quantum Monte Carlo calculations, the truncation errors from finite m are systematic, rather than random. Figure 3 shows $\xi_\ell \equiv -1/\ln[-C(\ell)/C(\ell-1)]$, which is a measure of a local correlation length, with the true correlation length given by $\xi = \xi_\infty$. For any value of m, the behavior becomes purely exponential for large ℓ, but the limiting correlation length is not especially accurate. The presence of prefactors modifying the simple exponential, as in (3), makes a direct determination of ξ (with no assumptions about prefactors) difficult from this data.

Also shown as the top trace in Fig. 3 is the equivalent decay length for the decay of $\langle S_\ell^z \rangle$ away from the effective $S = 1/2$ spin on an open end of a $S = 1$ chain, i.e., one without a real $S = 1/2$ on the end to remove the degeneracy; here we take the ground state with total

TABLE I. Ground-state energy per site as a function of the number of states kept m. The energy was obtained using the infinite-lattice method, where the lattice size was increased until convergence of all digits shown was obtained. Also shown is the truncation error $1 - P(m)$.

m	e_0	$1 - P(m)$
36	-1.40148379810	5.61×10^{-8}
48	-1.40148401407	4.13×10^{-9}
60	-1.40148403106	1.23×10^{-9}
72	-1.40148403623	3.42×10^{-10}
86	-1.40148403729	1.34×10^{-10}
100	-1.40148403872	2.66×10^{-11}
110	-1.40148403887	1.27×10^{-11}
160	-1.401484038968	4.4×10^{-13}
180	-1.401484038970	1.4×10^{-13}

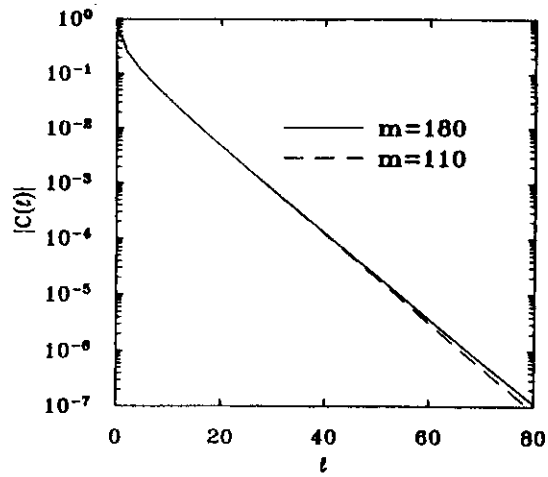

FIG. 2. Spin-spin correlation function $C(\ell)$ as a function of ℓ for two different values of m, the number of states kept per block.

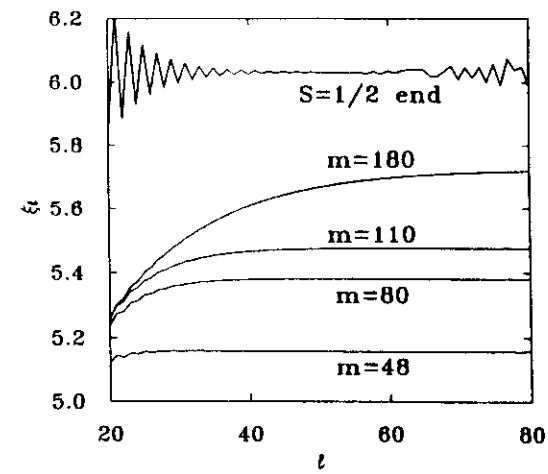

FIG. 3. Local correlation length $\xi_\ell \equiv -1/\ln[-C(\ell)/C(\ell-1)]$ for various m. Also shown is the equivalent decay length for an effective $S = 1/2$ spin at the end of an $S = 1$ chain (with $\langle S_\ell^z \rangle$ replacing $C(\ell)$ in the formula for ξ_ℓ).

$S^z = 1/2$. The decay in this case is expected to be almost purely exponential,[12] in contrast to an earlier report,[11] and our results support this. (The irregular behavior for large ℓ is due to truncation error.) In this case it is easy to determine a decay length of $\xi \cong 6.03(1)$, as was reported earlier.[2] Given that we can measure this decay length accurately, an interesting question is whether this decay length is the same as the correlation length governing the decay of $C(\ell)$. To this end we analyze the data for $C(\ell)$ in a similar manner to Nomura.[10] Figure 4 shows $C(\ell)$ divided by $A(-1)^\ell K_0(\ell/\xi)$, with $\xi = 6.03$ and $A = 0.19934$, for various m. The factor A was determined by requiring the fit to be exact for $\ell = 30$ for the $m = 180$ data. For small ℓ the calculated $C(\ell)$ is very accurate and gives corrections to the assumed form. For intermediate ℓ the data and the assumed form agree extremely well. For large ℓ, the data show systematic deviations, with the value of ℓ for which the deviations appear increasing with m. We conclude that the assumed form works very well for $\ell \geq 15$ and that the decay length and the correlation length are indeed the same, $\xi \cong 6.03$.

It has been conjectured,[13] and limited numerical evidence has supported,[14–19] that a particular type of topological long-range order exists in the spin-1 chain. This order can be measured by the string correlation function

$$g(\ell) = \left\langle S_0^z \left(\prod_{k=1}^{\ell-1} e^{i\pi S_k^z} \right) S_\ell^z \right\rangle. \tag{4}$$

Despite its complicated form, this function is easily measured with the infinite-lattice algorithm. In this algorithm, the left-hand block is built up site by site by adding a site to its right-hand side. (The right-hand block is obtained at each step by reflecting the left-hand block.) The matrix representation of the operator in the brackets of Eq. (4) is built up site by site also. As site k is added to the block, the matrix for the operator $e^{i\pi S_k^z}$ is multiplied onto the right-hand side of $S_0^z(\prod_{l=1}^{k-1} e^{i\pi S_l^z})$, which was formed during earlier steps. The starting point for the buildup of this operator is not the first site of the chain; it is a site far enough from the left end to avoid end effects. At each step of the calculation, we obtain either of two possible measurements of $g(\ell)$: one where we terminate the product at one of the center sites $k+1$ by applying S_{k+1}^z, and one where we couple this string operator with its reflection in the right-hand block to get a measurement of $g(i-j)$ with i and j symmetrically located about the center of the chain. At each step of the iteration, two more sites are added to the center of the chain and the separation $i-j$ grows by 2.

Figure 5 shows the string correlation function $g(\ell)$ as a function of ℓ. The long-range order is clearly evident. The function settles down to its limiting value very rapidly. We have continued the calculation to larger values of ℓ than is shown in the figure; the results stay at the limiting value. For $m = 180$, we find $g(\infty) = -0.374325096(2)$, with convergence to this accuracy starting at $\ell = 50$. For comparison, keeping only $m = 110$ states we find $g(\infty) = -0.374325104$. Exact-diagonalization calculations[14] have estimated $g(\infty) \cong -0.38$ based on a 14-site lattice.

III. ONE-MAGNON EXCITED STATES

Now let us turn to the excited-state spectrum of the antiferromagnetic spin-1 Heisenberg chain. For a uniform chain, momentum is a good quantum number. A sketch of the expected spectrum of low-lying excited states of an infinite chain is shown in Fig. 6. The figure shows only positive momentum; the spectrum is symmetric under momentum reversal (parity). The excitation energy of the lowest-lying excited state is the Haldane gap Δ. This excited state is a triplet with total spin 1 and momentum π in units where the spacing along the chain is $a = 1$. This state is the bottom of the magnon band, whose energy vs momentum is illustrated in Fig. 6. These magnons are the elementary excitations in this system. The rough shape of the magnon dispersion in Fig. 6 is based on the diagonalizations by Parkinson and Bonner[6] and the quantum Monte Carlo results of Takahashi.[7] Below we demonstrate that for momentum near π, the

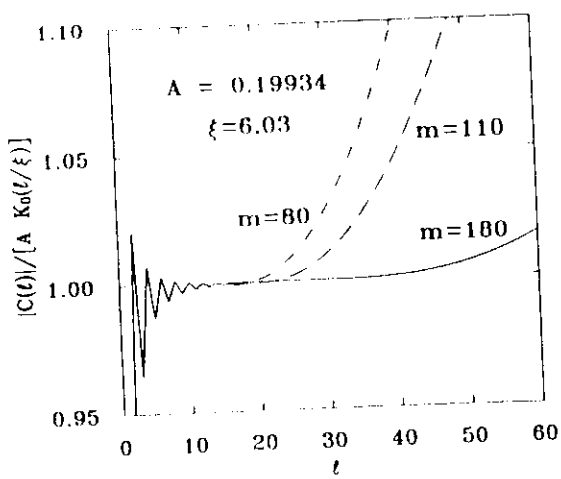

FIG. 4. Ratio of $|C(\ell)|$ to the approximate form $AK_0(\ell/\xi)$ for various values of m, with $A = 0.19934$ and $\xi = 6.03$.

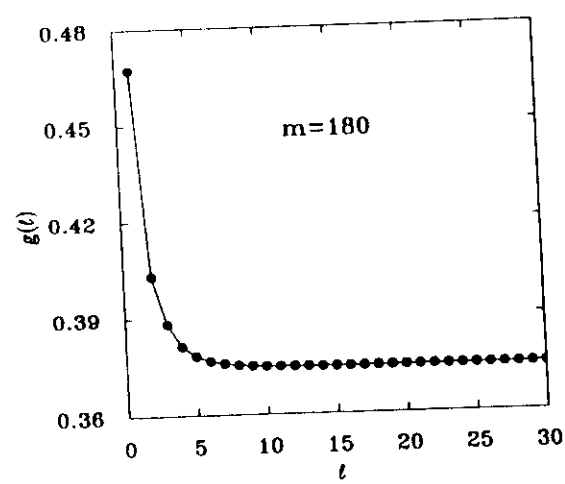

FIG. 5. String correlation function $g(\ell)$.

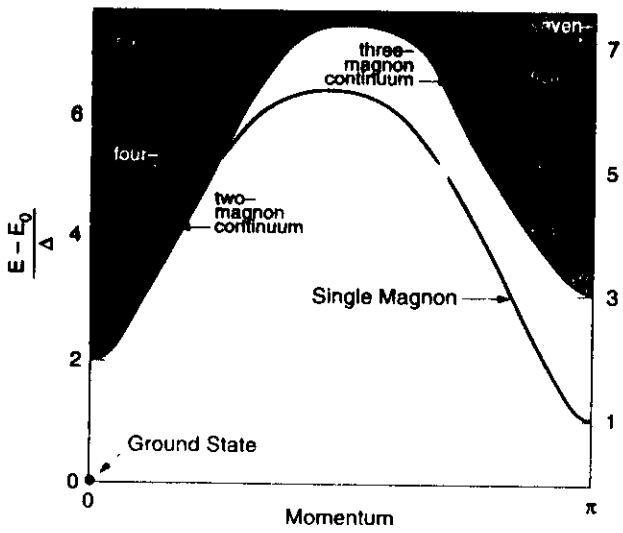

FIG. 6. Schematic of the spectrum of low-lying states for an infinite chain. E is the energy of the excited state, E_0 that of the ground state, and Δ is the Haldane gap. Note that for a given momentum, the one-magnon state, when present, is separated from the continua above it by a gap where there are no excited states.

magnon is indeed a particlelike excitation, and we accurately measure its dispersion relation near π. Inelastic neutron scattering from the qausi-one-dimensional spin-1 antiferromagnet NENP has seen quantitatively the same dispersion, with a splitting of the triplet due to the weak anisotropies in that system.[8]

One may also excite two or more magnons. This results in the multimagnon continua illustrated in Fig. 6. The continua are labeled by the maximum number of magnons that a state of that total excitation energy and total momentum can decay into. Thus, for example, the magnon band disappears into the two-magnon continuum near momentum 0.3π. At this point the single magnon with momentum near 0.3π becomes unstable to decay into two magnons, each with momentum near -0.85π, with the same total energy and the same total momentum modulo 2π. We discuss the two-magnon excited states in some detail below. The multimagnon continua have not yet been detected experimentally.

The wave function of the one-magnon state with momentum q and $S_z = \alpha$ in an infinite chain is expected to be of the form

$$|q,\alpha\rangle = \sum_{\ell} e^{iq\ell} c^{\dagger}_{q,\alpha}(\ell)|0\rangle, \tag{5}$$

where $|0\rangle$ is the ground state. The magnon creation operator $c^{\dagger}_{q,\alpha}(\ell)$ consists of spin operators and products of spin operators in the vicinity of site ℓ. If the magnon were truly a point particle, the creation operator would be simply a spin operator at site ℓ. The true magnon creation operator $c^{\dagger}_{q,\alpha}(\ell)$ also contains products of spin operators away from site ℓ. The weight of these multisite terms presumably decays as one moves away from site ℓ with some characteristic length which is thus a measure of the size of the magnon as a particle. If this particle size is smaller than the length of our finite chain, we expect the magnon to propagate as a free particle in the bulk of the chain, scattering only at the ends of the chain where translational invariance is broken.

For our finite-length chains with spin 1/2's on the ends the lowest-lying few excited states are single-magnon triplet states, with the magnons having particle-in-a-box spatial wave functions. This can be seen by examining the spin density $\langle S^z_i \rangle$ in the $S^z = 1$ states; some examples are illustrated in Fig. 7. We label these single-magnon states by their principal quantum number n. For $J_{\rm end} \geq 0.51$ the principal quantum number counts the number of maxima in the smooth part of $\langle S^z_i \rangle$. The patterns in Fig. 7 are those expected for the probability densities (the square of the modulus of the wave function) for the eigenstates of a particle in a box. Note for Fig. 7 we have adjusted the end coupling to $J_{\rm end} = 1.5$ where the amplitude of the wave function is minimal at the ends to minimize scattering into other states. That the magnons are behaving as particles of finite size carrying energy and spin is seen by noting that the excess energy above the ground state is distributed along the chain with the same pattern as the spin and these patterns are just those expected for particle-in-a-box eigenstates. Although momentum is not a good quantum number in this chain with ends, the nice periodicity of the spin density away from the ends shows that the magnon wave function is, to a good approximation, a sum of two momentum eigenstates with equal and opposite momenta, thus producing a standing wave. The magnitude of the deviation of the momentum from zero or π can thus be deduced from the period of the spin pattern. To distinguish between momenta near zero and momenta near π, one must look at the sign of the wave function, which is not detected by the spin density. For even length chains the parity operation exchanges sublattices, and so a state's eigenvalue under parity can be used to determine whether the momentum is near zero or near π.

The interaction of the magnon with the ends of the

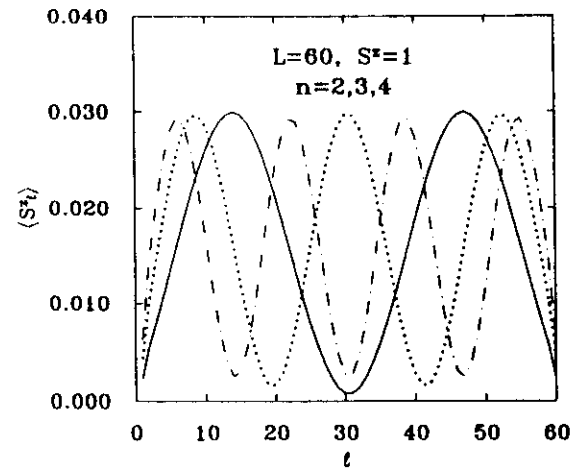

FIG. 7. Local spin densities for the one-magnon excited states with principal quantum numbers $n = 2$, 3, and 4, and total $S^z = 1$, for a chain of length $L = 60$ and $J_{\rm end} = 1.5$.

chain can be adjusted via the coupling at the ends, J_{end}. Thus we do not have just a particle in a box with simple hard walls. The potential energy of the magnon is uniform in the bulk of the chain, infinite outside the chain, but may be either negative (attractive) or positive (repulsive) near the chain ends. By adjusting J_{end} we can adjust this potential near the chain ends and thereby the momenta of the magnon eigenstates. In particular, we have found the end coupling, $J_{end} = 0.5088$, which makes the spin and energy densities of the lowest single-magnon state most uniform near the middle of the chain, as shown in Fig. 8. This effectively puts the magnon into the lowest state in the magnon band, with momentum π. The energy of this lowest magnon is the Haldane gap Δ and can be estimated from the ratio of the excess energy density to the spin density near the middle of the chain where end effects are minimal. Results for Δ for various m and L are shown in Table II. From chains with length up to $L = 130$ we estimate $\Delta = 0.41050(2)$. The estimated error comes from the same sort of analysis using $1 - P(m)$ used for the ground-state energy.

At the end of the chain, momentum is not conserved and so single magnons with momenta near π can scatter into virtual two-magnon states with total momenta near zero. These evanescent two-magnon states beat against the one-magnon state, producing the oscillations with spatial period 2 that are seen in Fig. 8. To minimize this end effect and thus get the purest single-magnon particle-in-a-box states we may adjust the end coupling to $J_{end} = 1.5$ where the spin density seems smoothest near the ends, as in Fig. 7. We would like to map out the entire single-magnon band, and hope to find techniques to target high-lying states in that band, but here we only report our results for the readily accessible low-lying states in that band.

To determine these low-lying states, at each step of the calculation we must diagonalize to find several of the lowest-lying states for a particular S^z, not just the lowest state.[3] Each of these states contributes equally in forming the density matrix of a block, which is then diagonalized in the usual way to get the states to be kept. Up to about 20 states can be targeted in this fashion. To facilitate finding singlet states in the channel $S^z = 0$ in the presence of numerous triplet states, we have incorporated spin-inversion symmetry ($S^z \rightarrow -S^z$) into the program. For even-length chains we find states with $S = 0, 2, \ldots$ have an eigenvalue $I = -1$ under spin inversion, while states with $S = 1, 3, \ldots$ have $I = 1$. Spin inversion is not a symmetry for $S^z \neq 0$. Thus we can obtain the lowest up to 20 states in each symmetry sector: $S^z = 0$ and $I = -1$, $S^z = 0$ and $I = 1$, $S^z = 1$, $S^z = 2$, etc.

The case we have examined in most detail is $L = 60$ and $J_{end} = 1.5$, where we have accurate results for the lowest eight single-magnon states. (The rest of the excited states obtained are two-magnon states.) For shorter chains we can obtain fewer one-magnon states, but, nev-

TABLE II. Estimated Haldane gap Δ as a function of the number of states kept m and length of chain L. Also shown is the truncation error $1 - P(m)$.

m	L	Δ	$1 - P(m)$
48	120	0.4123234	2.894×10^{-7}
64	120	0.4115262	4.346×10^{-8}
80	120	0.4108767	1.291×10^{-8}
100	120	0.4105433	1.900×10^{-9}
120	100	0.4105079	6.783×10^{-10}
120	120	0.4105073	7.152×10^{-10}
120	130	0.4105072	7.291×10^{-10}
140	120	0.4105020	2.916×10^{-10}

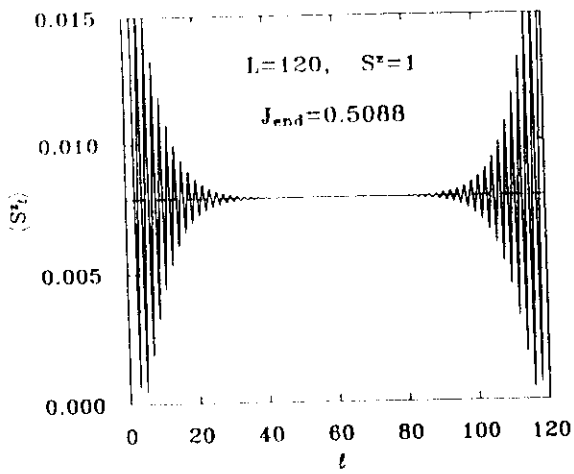

FIG. 8. Local spin density for the lowest-lying one-magnon state with total $S^z = 1$, $L = 120$, and $J_{end} = 0.5088$.

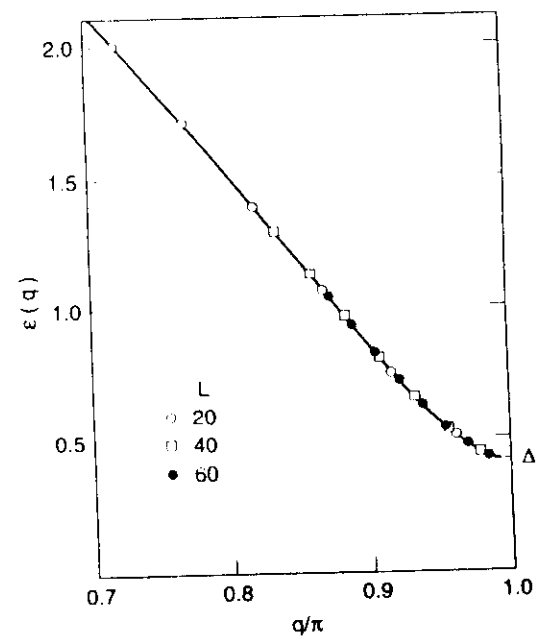

FIG. 9. Single-magnon energies $\epsilon(q)$ from the low-lying one-magnon states for $L = 20, 40$, and 60 with $J_{end} = 1.5$. The absolute value of the momentum q is obtained from the wavelength of these standing-wave eigenstates.

ertheless, these states extend to higher energies: The dispersion obtained from $L = 20, 40$, and 60 with $J_{end} = 1.5$ is shown in Fig. 9. Note the inflection point in the dispersion, which occurs near momentum 0.85π; this inflection point plays an important role in the two-magnon states, as is discussed below.

The parity of the lowest-lying single-magnon state for these even length chains is even, and thus opposite to that of the ground state. This shows that the smooth-looking densities in Fig. 7 arise from a magnon wave function that indeed does have a momentum near π, thus changing sign between adjacent sites while its amplitude slowly varies. Since the spin density is roughly proportional to the square of the modulus of the local wave function, it does not detect the alternation in sign. The parities alternate with increasing principal quantum number n in the discrete series of single-magnon states for a given L, as expected for a series of particle-in-a-box eigenstates.

IV. TWO-MAGNON STATES AND MAGNON-MAGNON INTERACTIONS

Let us now consider the two-magnon continuum, whose minimum is at energy 2Δ and zero momentum. The first question we must address is, what are the statistics of the magnons? The naive, and correct, expectation is that since they are spin-1 particles, they must be bosons. The local operators that create or annihilate a magnon are, as discussed above, presumably linear combinations of the spin operators in that region and higher-order composites of those spin operators. Since spin operators on different sites commute, we expect that the local magnon operators at two well-separated locations do commute. Thus the statistics should be bosonic and the full wave function symmetric under exchange of two magnons. The magnon operators will not commute when the magnons are close; this reflects the magnon-magnon interactions.

A two-magnon state may have a total spin of $S = 0$, 1, or 2. The spin wave function is antisymmetric under magnon exchange for $S = 1$, and so the spatial wave function must also be antisymmetric to make the full wave function symmetric. For $S = 0$ and $S = 2$ the spin and spatial wave functions are both symmetric. We have been able to access the lowest-lying two-magnon states in each spin channel. We have the fewest two-magnon states (typically five or six) for the triplet ($S = 1$) channel, because the one-magnon states have the same quantum numbers and must be produced at the same time. Each two-magnon state can be identified as the scattering state of two of the elementary one-magnon particle-in-a-box states by using the quantum numbers, parity, and total energy. The energy of interaction is the difference between the sum of the excitation energies of the two one-magnon states and that of the two-magnon state. This identification of the two-magnon states is fairly straightforward because the energies of interaction are mostly smaller than the gaps (due to the finite chain length) between the one-magnon states. We find that the magnons interact attractively in the triplet channel ($S = 1$) and repulsively in the other two spin channels. For the case of $L = 60$ and $J_{end} = 1.5$, the interaction energies are listed in Table III. Note that when the two magnons are in the same "orbital" they can only make a symmetric spatial wave function, and so there is no such $S = 1$ two-magnon state.

The fact that the magnons attract in the triplet channel and repel in the other channels can be understood as a sort of "Hund's rule" for spin-1 bosons. If there is a strong on-site repulsion between magnons, this will not affect the interaction energy in the triplet channel, where the spatial wave function is antisymmetric and thus has a node when the magnons are on the same site. Such an on-site repulsion will lead to repulsion in the other two channels. If, in addition, there is a weaker attraction when the magnons are on nearby but not identical sites, this will make the net interaction in the triplet channel attractive, while the other two channels remain repulsive.

TABLE III. Energies of one- and two-magnon states for $L = 60$ and $J_{end} = 1.5$. The first two rows of the table show the absolute value of the momentum and the excitation energy of the lowest five one-magnon states, indexed by their principal quantum numbers n. The remainder of the table shows the energy of interaction for the two-magnon states with total spin S made from magnons with principal quantum numbers n and n'. For example, the lowest-lying two-magnon state is $n = 1$, $n' = 2$, and $S = 1$ with excitation energy $0.4265 + 0.4723 - 0.009 \cong 0.890$. NSS ("no such state") denotes states that do not exist, and NA denotes states that we did not access.

		n				
		1	2	3	4	5
	q/π	0.9851	0.9698	0.9543	0.9385	0.9225
	$\epsilon(q)$	0.4265	0.4723	0.5415	0.6272	0.7239
	$S = 0$	0.052	0.078	0.100	0.116	NA
$n' = 1$	$S = 1$	NSS	-0.009	-0.015	-0.022	NA
	$S = 2$	0.041	0.061	0.075	0.083	0.038
	$S = 0$	0.078	0.081	0.104	NA	NA
$n' = 2$	$S = 1$	-0.009	NSS	-0.020	-0.026	NA
	$S = 2$	0.061	0.059	0.073	0.081	NA
$n' = 3$	$S = 2$	0.075	0.073	0.070	0.078	NA

We have not thought of a reason for why the repulsion is stronger in the singlet ($S = 0$) channel than it is in the quintuplet ($S = 2$) channel.

We have also found some three-magnon states. These can be easily found for total $S^z = 3$, where they are the lowest-lying states. For short enough chains we can also access three-magnon states for smaller S^z. The three-magnon states occur only at energies above 3Δ, as expected. We have not looked at enough three-magnon states to provide a useful characterization of the three-magnon interactions.

One interesting feature of the two-magnon continuum is the formation of a bound state in the triplet channel that occurs near momentum 0.3π and energy 5Δ. We have not been able to directly observe this part of the spectrum because it is too high in energy. The number of states rapidly proliferates once one enters the three-magnon continuum, and so the highest-energy triplet excited states we have been able to access are those near the bottom of the three-magnon continuum, which is well below the energy where the bound state first forms. However, we do know the one-magnon dispersion $\epsilon(q)$ fairly well, and that the magnons attract in the triplet channel, while they repel in the other two channels.

Thus let us take a phenomenological approach to the two-magnon states. The magnons are particlelike excitations above the ground state. Let us view the ground state as the vacuum, the magnons as particles, and assume the interactions are weak. We consider the phenomenological two-magnon Hamiltonian

$$H = \int dq \epsilon(q) c_\alpha^\dagger(q) c_\alpha(q) + \int dQ dq_1 dq_2 c_\alpha^\dagger(q_1) c_\beta^\dagger(Q - q_1) \times V_{\alpha\beta\gamma\delta}(Q, q_1, q_2) c_\gamma(q_2) c_\delta(Q - q_2), \quad (6)$$

where $c_\alpha(q)$ creates a magnon with $S^z = \alpha$ and momentum q, etc., and the repeated subscripts $\alpha, \beta, \ldots$ are summed over -1, 0, and $+1$. This phenomenological Hamiltonian explicitly conserves total momentum Q as it must, and the interaction $V_{\alpha\beta\gamma\delta}$ must be such that it conserves total spin. It also conserves magnon number, which is an approximation. We will use this phenomenology near the bottom of the two-magnon continuum at total momenta less than $\pi/2$; we will also consider the one-magnon state that forms at the high end of this momentum range to be a bound state of two magnons. Thus processes that do not conserve magnon number here involve states in the three- or more-magnon continua, which are well above the bottom of the two-magnon continuum in this regime. We assume the interactions are weak enough that the approximation of neglecting these high-energy magnon nonconserving processes is appropriate.

The single-magnon dispersion relation $\epsilon(q)$ has inflection points near $|q| = 0.85\pi$ that separate regions of upward curvature or positive effective mass, and downward curvative or negative effective mass. The bottom of the two-magnon continuum reflects this in having inflection points near $|Q| = 0.3\pi$. For total momenta below the inflection point the two-magnon state at the bottom of the continuum consists of two magnons with identical momenta $|q| = \pi - |Q|/2$ and positive effective mass. If we go to the "center-of mass" frame, considering only the relative coordinates and momenta of the magnons, our two-magnon problem then becomes a single particle in a potential. For this one-dimensional system, if the potential is at all attractive in the spatially symmetric scattering state, a bound state will form. But we have found that the interaction is repulsive in the symmetric channels, and so we do not expect any bound states there. For finite, positive effective mass, a bound state in the antisymmetric channel will not form for arbitrarily small attraction, but only above a threshold. Thus it is consistent to have an attraction in the triplet channel, but no bound state, as is the case here at low enough $|Q|$.

At the inflection point in the magnon band the fourth derivative of the magnon energy $\epsilon(q)$ with respect to q is positive. This means that at the inflection point in the bottom of the two-magnon continuum, the two-magnon state at the bottom still consists of two magnons with identical momenta. But here once one goes to the "center-of-mass" frame, the single particle now has a k^4 dispersion, where k is the relative momentum. With this dispersion, a bound state must form for arbitrarily small attraction even in the antisymmetric channel. Thus we conclude that the triplet bound state must first form at a total momentum below that of the inflection point in the bottom of the two-magnon continuum. This result is consistent with what is known so far about this part of the spectrum, but it would be interesting to somehow get more accurate information about this regime to develop and test this phenomenological approach more thoroughly.

V. CONCLUSIONS

Using density-matrix numerical renormalization-group techniques, we have calculated a variety of properties of the Heisenberg chain with unprecedented reliability and accuracy. The results we have obtained largely support conclusions obtained from a variety of other methods over the last decade. In the case of the Haldane gap Δ, previous numerical work had established with reasonable certainty the existence of a gap, in agreement with Haldane's conjecture, with $\Delta \cong 0.41$. Our results must remove all remaining doubt, and provide an accurate value for the gap, $\Delta = 0.41050(2)$. We were able to determine the ground-state energy per site of the infinite chain to especially high accuracy, $e_0 \cong -1.401484038971(4)$. The correlation length was found to be identical to the decay length of the local spin moment away from the effective $S = 1/2$ spins on the ends of open $S = 1$ chains, with $\xi \cong 6.03(1)$.

In the case of the string correlation function $g(\ell)$, which measures a form of topological long-range order similar to that found in fractional quantum-Hall-effect systems, previous numerical work had been limited to exact diagonalizations of chains with at most 14 sites. These results suggested that there was long-range topological order, with $g(\infty) \cong -0.38$. We were able to verify the exis-

tence of long-range order beyond any doubt and found $g(\infty) = -0.374325096(2)$.

We were able to determine the properties of a number of the lowest-lying excited states, including one- and two-magnon states, for several different chain lengths, including the determination of the magnon-magnon interactions for magnons with momenta near π. The magnon-magnon interaction in the triplet channel is attractive, while in the singlet and quintuplet channels it is repulsive. Since the numerical techniques used here use a real-space basis, total momentum is not available to use as a quantum number and high-lying one-magnon states with momentum near $\pi/2$ could not be studied. We hope to develop techniques for studying these states in the future.

Note added in proof. We have received a paper from Erik Sorensen and Ian Affleck that shows that the low-lying multimagnon excited states are well approximated by the eigenstates of hard-core bosons. These hard-core boson eigenstates are in turn simply related to those of noninteracting spinless fermions. This introduces a different, and physicaliy more appropriate, way of labeling the multimagnon states than we use above. The classification we have used, i.e., in Table III, is implicitly based on noninteracting bosons as the reference states. For multimagnon wave functions that are fully antisymmetric in space, such as the triplet ($S = 1$) two-magnon states, the eigenstates are identical in the noninteracting and hard-core limits because they vanish whenever two magnons are on the same site. However, for the other states the eigenfunctions in the two limits differ substantially. For example, the singlet ($S = 0$) or quintuplet ($S = 2$) two-magnon eigenstate in the noninteracting limit with orbitals n and n' occupied, with $n' \geq n$, evolves continuously as an on-site repulsion is turned on into the hard-core boson eigenstate which is obtained from the two-fermion eigenstate with orbitals $n_1 = n$ and $n_2 = n' + 1$ occupied. Thus in the labeling scheme of Sorensen and Affleck that derives from this hard-core limit, the lowest-lying two-magnon state in each channel has orbitals $n_1 = 1$ and $n_2 = 2$ occupied. It is clear from the results of Sorensen and Affleck, as well as our results, that the noninteracting limit is actually a rather poor approximation for multimagnon eigenstates that are not spatially fully antisymmetric. Thus we feel that Sorensen and Affleck's method of classifying multimagnon states based on hard-core boson eigenstates should be preferred over the labeling scheme we used in this paper. We thank them for communicating their results prior to publication.

ACKNOWLEDGMENTS

This work was supported by the Office of Naval Research under Grant No. N00014-91-J-1143 (S.R.W.) and in part by the University of California through an allocation of computer time on the UC Irvine Convex. Calculations were also performed at SDSC.

[1] S.R. White and R.M. Noack, Phys. Rev. Lett. **68**, 3487 (1992).
[2] S.R. White, Phys. Rev. Lett. **69**, 2863 (1992).
[3] S.R. White (unpublished).
[4] S. H. Glarum, S. Geschwind, K. M. Lee, M. L. Kaplan, and J. Michel, Phys. Rev. Lett. **67**, 1614 (1991).
[5] I. Affleck, T. Kennedy, E. H. Lieb, and H. Tasaki, Phys. Rev. Lett. **59**, 799 (1987).
[6] J. B. Parkinson and J. C. Bonner, Phys. Rev. B **32**, 4703 (1985).
[7] M. Takahashi, Phys. Rev. Lett. **62**, 2313 (1989).
[8] S. Ma, C. Broholm, D. H. Reich, B. J. Sternlieb, and R. W. Erwin, Phys. Rev. Lett. **69**, 3571 (1992).
[9] S. Liang, Phys. Rev. Lett. **64**, 1597 (1990).
[10] K. Nomura, Phys. Rev. B **40**, 2421 (1989).
[11] M. Hagiwara, K. Katsumata, I. Affleck, B.I. Halperin, and J.P. Renard, Phys. Rev. Lett. **65**, 3181 (1990).
[12] I. Affleck (private communication).
[13] K. Rommelse and M. den Nijs, Phys. Rev. Lett. **59**, 2578 (1987).
[14] S.M. Girvin and D. P. Arovas, Phys. Scr. T **27**, 156 (1989).
[15] Y. Hatsugai, J. Phys. Soc. Jpn. **61**, 3856 (1992).
[16] F.C. Alcaraz and Y. Hatsugai, Phys. Rev. B **46**, 13914 (1992).
[17] Y. Hatsugai and M. Kohmoto, Phys. Rev. B **44**, 11789 (1991).
[18] K. Hida, Phys. Rev. B **45**, 2207 (1992).
[19] M. Kohmoto and H. Tasaki, Phys. Rev. B **46**, 3486 (1992).

The Density Matrix Renormalization Group for Fermion Systems

R.M. Noack and S.R. White
Department of Physics
University of California, Irvine, CA 92717

D.J. Scalapino
Department of Physics
University of California, Santa Barbara, CA 93106

Abstract. We discuss techniques of the density matrix renormalization group and their application to interacting fermion systems in more than one dimension. We show numerical results for equal-time spin–spin and singlet pair field correlation functions, as well as the spin gap for the Hubbard model on two chains. The system is a gapped spin liquid at half-filling and shows weak algebraic d-wave–like pair field correlations away from half-filling.

1 Introduction

The numerical renormalization group was developed by Wilson [1] and used by him to solve the one impurity Kondo problem. The technique was subsequently applied to a number of quantum lattice systems [2, 3] such as the Hubbard and Heisenberg models, but with little success. A suggestion by Wilson [4] to investigate why the technique fails for the simplest quantum lattice system, the one-dimensional electron gas, led to the development of a number of new techniques to overcome the difficulties of the numerical RG for this simple system [5]. White [6] was able to generalize one of these techniques to interacting systems, applying it successfully to one dimensional quantum spin systems. This technique has come to be known as the density matrix renormalization group (DMRG).

This paper describes our our current efforts to apply the DMRG to fermion systems in more than one dimension, and in particular to the Hubbard model. So far, we have successfully applied the method to the Hubbard model on one and two chains [7]. Here we discuss the details of the methods we have developed for the two-chain Hubbard model and show results for equal-time pair field and spin–spin correlation functions and for the spin gap for the half-filled and doped systems on lattices of up to 2×32 sites.

At half-filling, both pair field and spin-spin correlations decay exponentially, with the spin correlations having a longer correlation length. There is a spin gap present at half filling which gets smaller as the system is doped, but persists down to band fillings of $\langle n \rangle = 0.75$. For the doped system, the largest pair field correlations are ones in which a spin singlet pair is formed on adjacent sites on different chains. The pair field symmetry is d-wave-like in that the pair field wave function has opposite sign along and between the chains. The form of the decay of the pair field correlations for the doped system is algebraic with a form close to that of the noninteracting system, which decays as ℓ^{-2}.

2 The Density Matrix Renormalization Group

The goal of the procedures discussed here is to find the properties of the low-lying states of a quantum system on a particular finite lattice. One way to do this would be to diagonalize the Hamiltonian matrix using a sparse matrix diagonalization method such as the Lanczos technique. However, for interacting quantum lattice systems, the number of states grows exponentially with the size of the lattice. Since exact diagonalization techniques must keep track of all the states, the maximum possible lattice sizes for interacting Hamiltonians is severely limited. It is therefore desirable to develop a procedure in which the Hilbert space of the Hamiltonian can be truncated in a controlled way so that only states that are important in making up the low-lying states of the system are included in a diagonalization. The DMRG provides a procedure for building up such a representation of the Hamiltonian matrix, which is then diagonalized to provide the properties of the low-lying states of the finite system.

The strategy of the DMRG is to build up a portion of the system (called the system block) using a real-space blocking procedure and then truncate the basis of its Hamiltonian after each blocking. In this way, the size of the Hilbert space is kept manageable as the system block is built up. The key idea is the method of truncating the Hilbert space of the system block in a controlled way. This is done by forming the reduced density matrix for the system block, given an eigenstate of the entire lattice. Let us first examine this procedure.

2.1 The Density Matrix Projection

Consider a complete system (the "universe"), divided into two parts, the "system", labeled by coordinate i, and the "environment" [8], labeled by coordinate j. If we knew the exact state ψ_{ij} of the universe, (assuming the universe is in a pure state) the prescription for finding the state of the system block would be to form the reduced density matrix of the system as part of the universe,

$$\rho_{ii'} = \sum_j \psi_{ij} \psi^*_{i'j}. \tag{1}$$

The state of the system block is then given by a linear combination of the eigenstates of the density matrix with weight given by the eigenvalues. It is shown in Ref. [6] that the optimal reduced basis set for the system block is given by the eigenstates of the density matrix with the largest weights. The sum of the density matrix weights of the discarded states gives the magnitude of the truncation error.

3 Algorithms

The density matrix projection procedure gives us a way of truncating the basis set of the matrix for the system block in a controlled way as degrees of freedom are added to the system. The projection procedure of the previous section assumes that the wavefunction ψ_{ij} of the system is known. Of course, finding ψ_{ij} is the goal of the DMRG procedure, so effective algorithms must iteratively improve approximations to ψ_{ij}. We will first discuss the algorithms for one-dimensional systems, as developed in Ref. [6].

In order to perform the density matrix projection procedure, we form the Hamiltonian for a "superblock" which is an approximation to the universe of the previous section. In this case, the superblock will describe a one-dimensional lattice of L sites, with, for example, a Heisenberg or Hubbard Hamiltonian. The superblock configuration used for the one–dimensional algorithms developed in Ref. [6] is shown in Fig. 1. The superblock is formed from an approximate Hamiltonian for the system block containing ℓ sites (labeled by B_ℓ), the Hamiltonians for two single sites which can be treated exactly, represented by solid circles, and an approximate Hamiltonian for the rightmost ℓ' sites, labeled by $B^R_{\ell'}$. Thus, the superblock contains $L = \ell + \ell' + 2$ sites. The algorithm proceeds as follows:

1. The superblock Hamiltonian is diagonalized using a Lanczos or similar exact diagonalization technique to find a particular target eigenstate ψ_{ij}.

2. The reduced density matrix is formed for the system block $B'_{\ell+1}$ using Eq. (1).

3. The density matrix is diagonalized using a dense matrix diagonalization.

4. The Hamitonian for $B'_{\ell+1}$ is transformed to a truncated basis formed by the m highest weighted eigenstates of the density matrix.

5. This approximate Hamiltonian, labeled by $B_{\ell+1}$ is used as a starting point for the next iteration, starting with step 1.

Initially we choose ℓ to be small enough (a single site, for example) so that the Hamiltonian for B_ℓ can be treated exactly. The system block then grows by a single site at each iteration, but the dimension of its Hilbert space remains m. A single site only is added to B_ℓ in order to minimize the size of the superblock

Hamiltonian, whose dimension will be n^2mm' where n is the number of states per site, and m' is the size of the basis for $B^R_{\ell'}$.

3.1 The Infinite System Procedure

The method we use to choose $B^R_{\ell'}$ at each step divides DMRG algorithms into two classes, the infinite system procedure and the finite system procedure. In the infinite system procedure, $B^R_{\ell'}$ is chosen to be the spatial reflection of B_ℓ so that $\ell = \ell'$. This means that the size L of the superblock grows by two sites at each iteration. The procedure can be iterated until the energy, calculated in the superblock diagonalization, converges.

The advantage of the infinite system procedure is that calculated quantities scale to their infinite system values. In this sense, this procedure is in the spirit of the original real-space renormalization group. The disadvantages of the infinite system procedure are that for a given system size, it is less accurate than the finite system procedure, and that it cannot easily be generalized to two-dimensional systems. For a two-dimensional system, if a single site is added to the system block at each step, an environment block of the proper geometry cannot in general be formed from the reflected system block.

3.2 The Finite System Procedure

In the finite system procedure, the superblock is formed so that it describes the same finite lattice at each iteration. In other words, the block $B^R_{\ell'}$ is chosen so that $L = \ell + \ell' + 2$ remains fixed. We can do this if we repeat the procedure (which we call a sweep through the lattice) in which the system block is built up from $\ell = 1$ to $\ell = L - 3$ more than once. After one sweep, the system block can be built up from the other side of the lattice, and the stored set of system blocks from that sweep can be used as environment blocks for the next sweep. The procedure is analogous to zipping a zipper back and forth once through the lattice, where the location of the zipper is the location of the single site added to B_ℓ. The sweeps can be repeated until the energy or some other quantity of interest converges. In practice, we have found that it only takes a few sweeps through the lattice to achieve convergence to within truncation error for a given m. The power of this procedure lies in the iterative improvement of the environment block.

On the initial sweep of the finite system procedure, the environment blocks are undefined. For one dimensional systems, however, one can build up the superblock size using the infinite system procedure and use reflections of the stored blocks B_ℓ for $B^R_{\ell'}$ on the initial sweep.

There are a number of advantages to the finite system procedure. First, since the environment blocks are iteratively improved with each sweep through the lattice, the finite system procedure gives much more accurate results for a particular lattice size than the infinite system procedure, although the infinite

system procedure can give results that are closer to the thermodynamic limit. It might be possible to combine the two procedures in a hybrid algorithm to get more accurate results for a given m in the thermodynamic limit.

Second, since the environment block no longer must be a reflection of the system block, it is possible to study lattices that are no longer reflection symmetric. This is useful, for example, in studying systems with impurities or disorder.

Third, in the finite system procedure, the target state of the superblock is the same at each iteration, with unchanging quantum numbers, unlike in the infinite system procedure. For the one-dimensional Heisenberg model calculations described in Ref. [6], the states are labeled only by the z component of the total spin, S_z, so it is easy to find a state with the appropriate quantum number for different lattice sizes. For fermion systems such as the Hubbard model, however, $N_\uparrow$ and $N_\downarrow$, the number of spin up and spin down fermions, are good quantum numbers. Since $N_\downarrow$ and $N_\uparrow$ must be integers, it is impossible to choose them so that the overall occupation stays constant on all different lattice sizes, except at half-filling. The best one can do is to target one or more states closest to the proper density, and this leads to reduced accuracy for non-half-filled systems.

Fourth, it is much easier to extend the finite system procedure to lattices of more than one dimension.

3.3 Extension to Higher Dimensions

One way to extend these algorithms to more than one dimension would be to replace the single sites added between the blocks with a row of sites. However, the extra degrees of freedom added to the system at each real-space blocking would make size of the superblock Hilbert space prohibitively large. Therefore, the two-dimensional algorithms we have developed still involve adding single sites at a time to the system block. This can be done by adding sites in a connected one-dimensional path through the two-dimensional lattice, i.e. by folding the one-dimensional zipper into two dimensions. A typical superblock configuration for the two-dimensional algorithm is shown in Fig. 2. The site added to the system block is enclosed by a dashed line and the dotted line shows the order in which sites are added to the system block for a sweep. One can see that it is not possible to reflect the system block into an environment block of the proper geometry at every iteration, so the finite system algorithm must used. The two-dimensional procedure differs from the one-dimensional finite size procedure only in that there are additional connections between the system and environment blocks along the boundary.

For one-dimensional lattices, we use the infinite system procedure to build up the superblock to the proper size on the first sweep through the lattice. Since this can no longer be done for higher dimensional lattices, we must formulate a procedure for the initial sweep through the lattice. The simplest procedure

is to use an empty environment block on the first sweep. One can diagonalize the Hamiltonian for the system block and keep the m states of lowest energy. This procedure is equivalent to Wilson's original numerical renormalization group procedure, and is not very accurate even for the one–dimensional single electron on a lattice, as shown in Ref. [5]. In addition, for fermion systems, one must adjust the chemical potential μ so that states with the proper $N_\uparrow$ and $N_\downarrow$ quantum numbers have the lowest energy. The procedure is quite sensitive to these adjustments. Thus, this initialization technique thus tends to be inaccurate and hard to use for fermion systems.

Liang [9] has tried two other techniques for the initial sweep. In the first, he performs an initial infinite system sweep for a one-dimensional lattice, then turns on the additional couplings needed to make the lattice two dimensional on subsequent finite system sweeps. In the second, he uses as the environment block an approximate Hamiltonian for a one–dimensional system of the size of the row length. Both of these procedures depend on representing portions of two-dimensional states by one-dimensional states, and thus give poor representations of the superblock initially.

The technique which we find works best for the initial sweep is a hybrid procedure in which the finite system procedure for a smaller lattice size is repeated for a few iterations, until the system block is big enough so that its reflection can be used for the environment block of a superblock that is a row larger. Thus, the superblock is extended a row at a time. Initially, the first row can be built up with a one-dimensional infinite system procedure. This procedure minimizes problems with target states with inappropriate quantum numbers and provides a reasonable representation for two–dimensional states.

We have found that the accuracy of the initial sweep is not critical as long as the first set of environment blocks has a set of states with appropriate quantum numbers. In most cases, a few sweeps of the finite system procedure will improve the environment blocks sufficiently so that the procedure will converge.

3.4 Performance Considerations

The number of states needed to maintain a certain truncation error in the density matrix projection procedure depends strongly on the number of operators connecting the two parts of the system. Best accuracy is obtained when the number of connections between the system and environment blocks is minimized. Therefore, we study systems with open rather than periodic or antiperiodic boundary conditions. Also, we find that the number of states m needed to maintain a given accuracy depends strongly on the width and weakly on the length of the system.

Just how rapidly the truncation error increases with the width of the system is not clear in general. Liang [9] studied the error in the energy as a function of width for a gas of noninteracting spinless fermions and found that the number of

states needed to maintain a given accuracy grew exponentially with the width of the system. In an interacting system such as the Hubbard model, the detailed structure of the energy spectrum seems to be important. For example, in the two chain Hubbard model at half-filling, where there is a spin and pairing gap, the truncation error for a given m is much smaller than away from half-filling, where the spin gap is reduced and the gap to pairing excitations is no longer present. For multiple Hubbard or Heisenberg chains, the presence or absence of a gap in the spin spectrum depends on whether the number of chains is even or odd[10], so the truncation error for a given m depends on the number of chains in a complicated way. Also, increasing the strength of on-site interactions can reduce the truncation error. The Hubbard model DMRG is most accurate for large U and least accurate for $U = 0$.

For systems of more than one dimension, it is therefore important to be able to keep as many states m per block as possible. We have been able to improve the performance of the algorithm in a number of ways. One way of doing this is to minimize the size of the superblock Hilbert space, whose dimension is n^2mm'. For fermion systems, one can reduce the number of states per site n from four to two by treating the spin degree of freedom on the same footing as a spatial coordinate. A site for a particular spatial coordinate and spin can have an occupancy of zero or one fermion. While this makes the path through the lattice (which now has an added dimension) somewhat more complicated, we have found that by adding these "half-sites" instead of full spatial sites on the last few sweeps through the lattice we can increase the accuracy by increasing m. We have also found that m' can be made smaller than m without losing much accuracy in the truncation[6]. Since the representation the approximate block Hamiltonians is poor on the first few sweeps through the lattice, making m large initially does not improve the representation very much. Therefore, the most efficient procedure is to increase m after every sweep through the lattice, so that m' is m from the previous sweep.

We have made a major effort to write the code in an efficient way in C++. We store only the nonzero parts of operators that link states with particular quantum numbers. These matrices are dense in general because the basis transformation at each step mixes matrix elements. This representation minimizes memory usage and makes it possible to optimize highly the multiplication of a vector by the Hamiltonian, the basic step needed for the Lanczos diagonalization. However, the resulting data structures are complicated and are variable in size, so that it has been useful to take advantage of the object-oriented data structures and dynamic memory allocation available in C++. The code is currently limited more by memory usage than by computer time, although we minimize memory usage by writing to disk all operators not needed for a particular superblock diagonalization step. The current version of the code can handle $m = 400$ or more whereas the original Fortran code used in Ref. [6] for the computationally less demanding Heisenberg spin problem could keep at most $m = 200$. We have found that $m \approx 400$ is necessary in order to obtain

accurate results for the two–chain Hubbard model away from half–filling.

4 Results for the two–chain Hubbard model

The two-chain Hubbard model is described by the Hamiltonian

$$\begin{aligned} H = \quad & -t_y \sum_{i,\lambda\sigma} (c^\dagger_{i,\lambda\sigma} c_{i+1,\lambda\sigma} + c^\dagger_{i+1,\lambda\sigma} c_{i,\lambda\sigma}) \\ & -t_x \sum_{i,\sigma} (c^\dagger_{i,1\sigma} c_{i,2\sigma} + c^\dagger_{i,2\sigma} c_{i,1\sigma}) + U \sum_{i,\lambda} n_{i,\lambda\uparrow} n_{i,\lambda\downarrow}. \end{aligned} \tag{2}$$

We think of the lattice as beinging a ladder aligned with the y axis so that $c^\dagger_{i,\lambda\sigma}$ creates an electron of spin σ at rung j and side $\lambda = 1$ (left) or 2 (right), the hopping along a chain is t_y, the hopping between chains on a rung is t_x, and U is the on-site Coulomb repulsion. This system is thought to be relevant to a number of anisotropic two–dimensional systems, including $(VO)_2P_2O_7$ [11] and $Sr_2Cu_4O_6$ [12, 13], which have weakly coupled ladder–like structures arranged in planes. Here we will concentrate on a parameter regime relevant to the latter class of substances: $U/t_y = 8$, and $t_x = t_y$. We will explore the phase diagram as a function of band filling as the half-filled system is doped with holes.

At half–filling, the Hubbard model maps to the Heisenberg model in the large U/t_y limit. Therefore, the dominant correlations should be antiferromagnetic spin correlations. However, it is known that in the Heisenberg model on two chains [14, 15, 16], there is spin gap leading to an exponential decay of the spin correlation function. The origin of the spin gap is easy to understand in the limit of strong coupling across the rungs. In this case, the only only interaction will be an antiferromagnetic coupling between the two spins on a rung. This two spin system forms a spin singlet state and a higher energy triplet state with an energy separation of the Heisenberg coupling J. Away from half–filling, it is not clear what correlations dominate the behavior. Some authors [17, 18] have predicted that singlet superconductivity with a partial d-wave symmetry should be the dominant order.

In order to resolve these issues, we have calculated equal time spin–spin and pair field correlation functions $S_{\lambda\lambda'}(i,j) = \langle M^z_{i,\lambda} M^z_{j,\lambda'} \rangle$, $D_{xx}(i,j) = \langle \Delta_{xi} \Delta^\dagger_{xj} \rangle$, and $D_{yx}(i,j) = \langle \Delta_{yi} \Delta^\dagger_{xj} \rangle$ with

$$\begin{aligned} M^z_{i,\lambda} &= n_{i,\lambda\uparrow} - n_{i,\lambda\downarrow} \\ \Delta^\dagger_{xi} &= c^\dagger_{i,1\uparrow} c^\dagger_{i,2\downarrow} - c^\dagger_{i,1\downarrow} c^\dagger_{i,2\uparrow} \\ \Delta^\dagger_{yi} &= c^\dagger_{i+1,2\uparrow} c_{i,2\downarrow} - c^\dagger_{i+1,2\downarrow} c^\dagger_{i,2\uparrow}. \end{aligned} \tag{3}$$

Here $S_{11}(i,j)$ and $S_{12}(i,j)$ measure the spin-spin correlations along a chain and between the chains respectively, and $D_{xx}(i,j)$ measures the singlet pair field correlations in which a singlet pair is added at rung j and removed at rung i. In addition, $D_{yx}(i,j)$ measures the pair field correlations in which a singlet pair is added to rung j and removed from the right–hand chain between rungs i and $i+1$. The relative phase of the pair wave function across the ith rung to

along one chain from i to $i+1$ is given by comparing the phase of $D_{xx}(i,j)$ to $D_{yx}(i,j)$. This turns out to be negative, corresponding to the mean field result obtained in Ref. [17]. However, the non-interacting $U=0$ result at a filling $\langle n\rangle = 0.875$ is also negative.

Fig. 3 shows the logarithm of the antiferromagnetic spin–spin correlation function $(-1)^{|i-j|}S_{11}(i-j)$ and the cross-chain pairing correlation function $D_{xx}(i-j)$. Both the correlation functions decay exponentially with $|i-j|$, but the pair field correlations decay much more rapidly. The correlation length, calculated from the slope of the lines in the semilog plot, is plotted as a function of U/t_y in the inset. The spin-spin correlation length decreases as U is increased, saturating at a value near 3 lattice spacing for large U. We have calculated the spin-spin correlation length for the isotropic two chain Heisenberg model using the DMRG [10] and find a value of 3.19 lattice spacings, consistent with the large U limiting value. The pair field correlations decay with a correlation length of the order of a lattice spacing and are thus negligible at half-filling.

In order to determine the behavior of the spin correlations as the system is doped below half-filling, we have calculated the magnetic structure factor $S(q_x,q_y)$ by taking the fourier transform of $S_{\lambda\lambda'}(i,j)$. Since the lattice is long in the y direction and the spin-spin correlation function decays exponentially with $|i-j|$, one can take a continuous fourier transform in the y direction without introducing much error. Since there are two chains, q_x can take on the values 0 and π. Only the $S(\pi,q_y)$ branch is interesting, because the correlations are always antiferromagnetic across the rungs. This function is plotted in Fig. 4 for the fillings, $\langle n\rangle = 1.0, 0.9875, 0.875, 0.75$, corresponding to doping 0, 2, 8, and 16 holes into the half-filled 2×32 lattice. As the system is doped away from half-filling, $S(\pi,q_y)$ peaks at a wavevector $q_y = \langle n\rangle$. The residual peak at $q_y=\pi$ present for $\langle n\rangle = 0.875$ and $\langle n\rangle = 0.75$ is present only for even numbers of hole pairs and thus probably disappears in the thermodynamic limit. Therefore, we see that the spin-spin correlations develop incommensurate structure as the system is doped away from half-filling.

One can calculate the spin gap directly, by calculating the difference in energies between the ground state, which has total spin $S=0$, and the lowest lying $S=1$ state. We calculate the ground state energy for $N_\uparrow$ spin up electrons and $N_\downarrow$ spin down electrons, $E_0(N_\uparrow,N_\downarrow)$. The spin gap for a system with $N_\uparrow = N_\downarrow = N$ electrons is then given by $\Delta_{spin} = E_0(N+1,N-1) - E_0(N,N)$. The spin gap plotted as a function of filling is shown in Fig. 5. It is largest at half filling and becomes smaller as the system is doped with holes and seems to be present at least down to fillings of $\langle n\rangle = 0.75$. We show the spin gap for 2×16 and 2×32 lattices to show the size of the finite size effects and argue that they are small enough that the gap is present in the thermodynamic limit for two chains.

We now turn to the behavior of the pair field correlations as the system is doped away from half filling. We have seen that the pairing correlations with cross chain symmetry decay exponentially in the half-filled system. This is

true for all symmetries of the pair field wavefunction. Fig. 6 shows the pair field correlations $D_{xx}(i-j)$ and $D_{yx}(i-j)$ plotted as a function of $|i-j|$ for $\langle n \rangle = 1.0$ and $\langle n \rangle = 0.875$. One can see that $D_{xx}(i-j)$ and $D_{yx}(i-j)$ have opposite signs, as one would expect for d-wave like symmetry, at both fillings and are significantly enhanced for the doped system.

In order to determine the strength of the pairing correlations, one must consider their ℓ-dependence at large distances. For a quasi–one–dimensional system, we expect that any pairing correlation will at best decay as a power of ℓ and can in some cases decay exponentially, as we have seen for the half-filled system. For two chains, one can compare with the the non-interacting $U = 0$ ladder, for which

$$D_{xx}(\ell) = (1/2\pi\ell)^2 \left[2 - \cos(2k_f(0)\ell) - \cos(2k_f(\pi)\ell)\right]. \tag{4}$$

Here $k_f(0) = \cos^{-1}(t_x + \mu)/2$ and $k_f(\pi) = \cos^{-1}(t_x - \mu)/2$ are the Fermi wave vectors corresponding to the bonding and antibonding bands of the two coupled chains with μ the chemical potential. The pair correlations, $D_{xx}(\ell)$ are shown in Fig. 7, plotted on a log-log scale. The correlations of the interacting system decay approximately as ℓ^{-2} and do not seem to be significantly enhanced over those of the non–interacting system, as given by Eq. (4).

5 Conclusion

We have discussed techniques we have developed to apply the density matrix renormalization group to Fermion systems in more than one dimension. In particular, we have been able to obtain accurate results for energy gaps and equal-time correlation functions for the Hubbard model on two coupled chains.

The two–chain Hubbard model is a gapped spin liquid at half–filling. Both spin–spin and pair field correlations decay exponentially, with the spin–spin correlations having the longest correlation length. As the system is doped with holes, the spin–spin correlations become incommensurate at a wave vector proportional to the filling and the spin gap becomes smaller, but persists in the thermodynamic limit. The pairing correlations are enhanced with a d-wave–like symmetry and decay algebraically with an exponent close to that of the non interacting, $U = 0$ system.

Acknowledgements

The authors thank N. Bulut, T.M. Rice, A. Sandvik, M. Vekic, E Grannan, and R.T. Scalettar for useful discussions. R.M.N. and S.R.W. acknowledge support from the Office of Naval Research under grant No. N00014-91-J-1143 and D.J.S. acknowledges support from the National Science Foundation under grant DMR92-25027. The numerical calculations reported here were performed at the San Diego Supercomputer Center.

References

[1] K.G. Wilson, *Rev. Mod. Phys.* 47, 773 (1975).

[2] J.W. Bray and S.T. Chui, *Phys. Rev.* **B19**, 4876 (1979); S.T. Chui and J.W. Bray, *Phys. Rev.* **B18**, 2426 (1978); J.E. Hirsch,*Phys. Rev.* **B22**, 5259 (1980); C. Dasgupta and P. Pfeuty, *J. Phys.* **C14**, 717 (1981).

[3] P.A. Lee, *Phys. Rev. Lett.* **42** , 1492 (1979).

[4] K.G. Wilson, in an informal seminar.

[5] S.R. White and R.M. Noack, *Phys. Rev. Lett.* **68** 3487, (1992).

[6] S.R. White, *Phys. Rev. Lett.* **69**, 2863 (1992), *Phys. Rev. B* **48**, 10345 (1993).

[7] R.M. Noack, S.R. White, and D.J. Scalapino (to be published).

[8] The term "environment" block is due to Shoudan Liang.

[9] S. Liang (to be published).

[10] S.R. White, R.M. Noack, and D.J. Scalapino (to be published).

[11] D.C. Johnston *et al.*, *Phys. Rev. B* **35**, 219 (1987).

[12] M. Takano, Z. Hiroi, M. Azuma, and Y. Takeda, Jap. J. of Appl. Phys. Series **7**, 3 (1992).

[13] T.M. Rice, S. Gopalan, and M. Sigrist, Europhys. Lett. **23**, 445 (1993).

[14] E. Dagotto, J. Riera, and D.J. Scalapino, *Phys. Rev. B* **45**, 5744 (1992).

[15] T. Barnes et al., *Phys. Rev. B* **47**, 3196 (1993).

[16] S.P. Strong, and A.J. Millis, *Phys. Rev. Lett.* **69**, 2419 (1992).

[17] M. Sigrist, T.M. Rice, and F.C. Zhang (to be published); Sudha Gopalan, T.M. Rice, and M. Sigrist (to be published).

[18] H. Tsunetsugu, M. Troyer, and T.M. Rice (to be published).

Figure 1: The superblock configuration for the one–dimensional algorithms. The solid circles represent single sites treated exactly and the boxes represent approximate Hamiltonians representing ℓ and ℓ' sites.

Figure 2: The superblock configuration for the two–dimensional algorithm. The order in which sites are added to the system block on a series of iterations is given by the dotted line, and the site added to the approximate system block Hamiltonian is outline by the dashed line.

Figure 3: Semilog plot of the spin–spin correlation function $S_{11}(i-j)$ and the pair field correlation function $D_{xx}(i-j)$ at half–filling and $U/t_y = 8$. The insert shows the correlation lengths in units of the lattice spacing obtained from similar plots for various U/t_y values.

Figure 4: The fourier transform $S(\pi, q_y)$ of the spin–spin correlation function $S_{\lambda\lambda'}(\ell)$. Here $t_x = t_y$ and $U/t_y = 8$ and the calculations were made on a 2×32 lattice.

Figure 5: The spin gap Δ_{spin} plotted as a function of band filling $\langle n \rangle$ on a 2×32 lattice for $U/t_y = 8$ and $t_x = t_y$.

Figure 6: The pair field correlation functions $D_{xx}(i-j)$ and $D_{yx}(i-j)$ versus $|i-j|$ on a 2×32 lattice with $U/t_y = 8$ and $t_x = t_y$.

Figure 7: Log-log plot of the rung-rung single pair field correlation function $D_{xx}(i-j)$ versus $|i-j|$ for a 2×32 cluster with $U/t_y = 8$ and an infinite two chain system with $U = 0$. In both cases $\langle n \rangle = 0.875$. The dashed line shows $|i-j|^{-2}$.

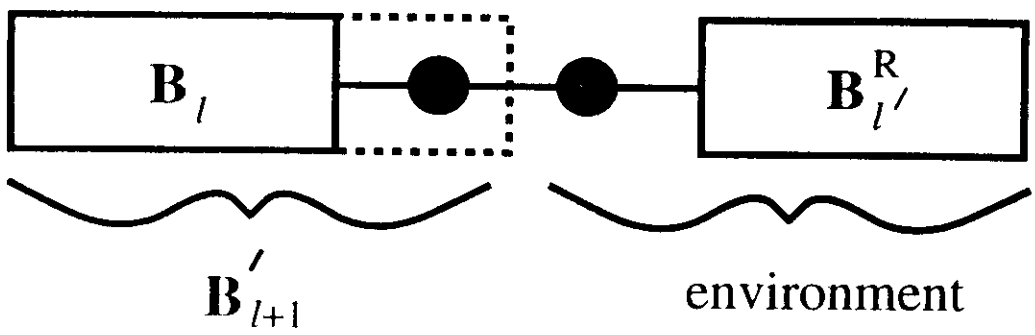
$\mathbf{B}_l$
$\mathbf{B}^R_{l'}$
$\mathbf{B}'_{l+1}$
environment

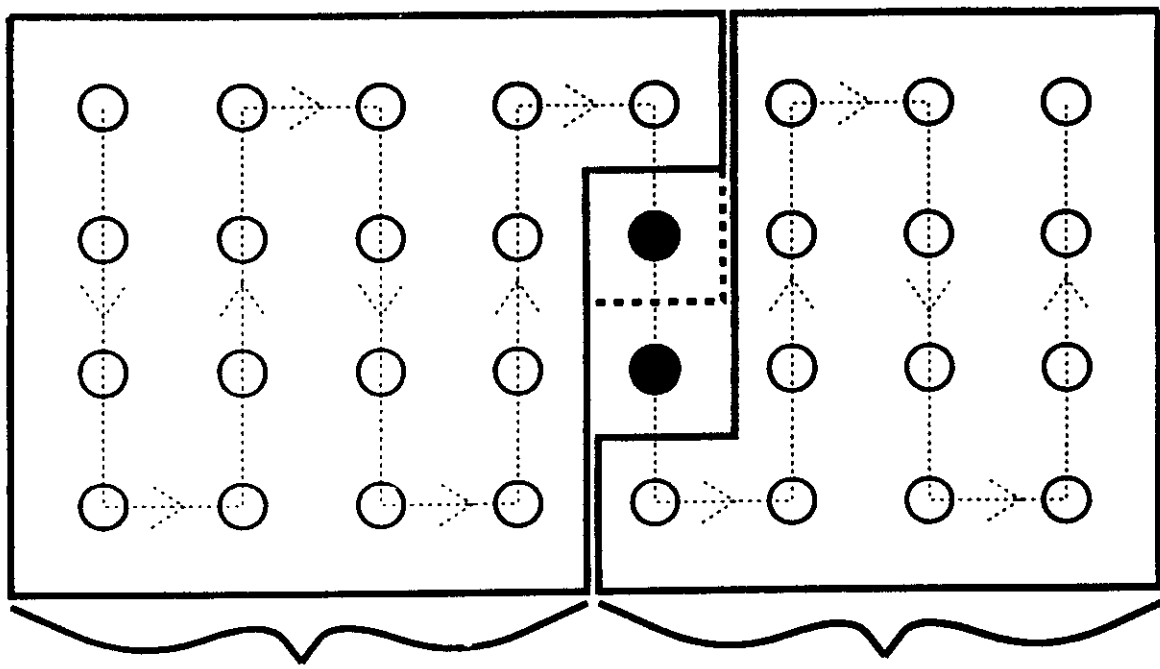
system
environment

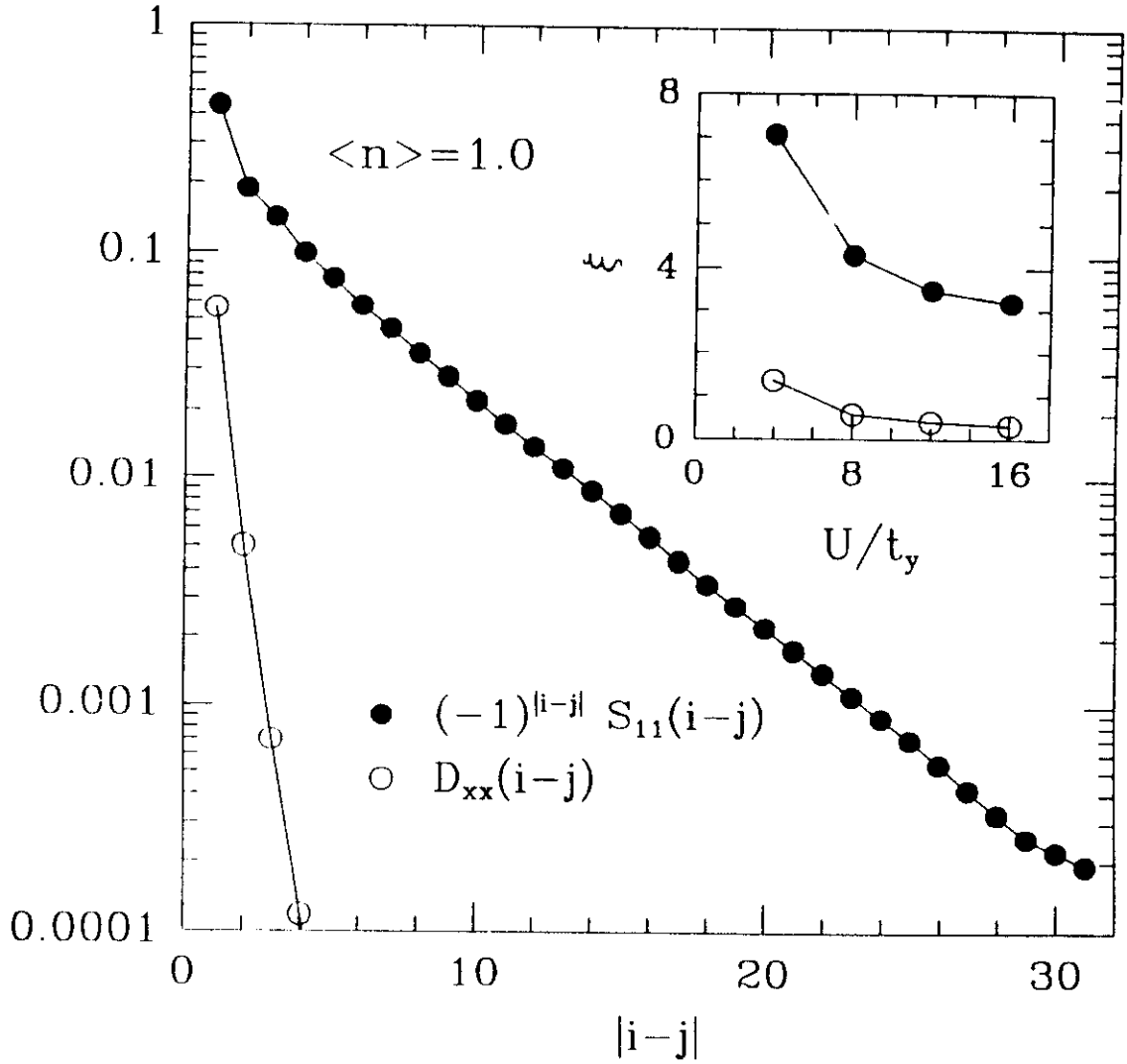
1
0.1
0.01
0.001
0.0001
0
10
20
30
|i−j|
<n>=1.0
(−1)^|i−j| S11(i−j)
Dxx(i−j)
8
4
0
0
8
16
U/ty

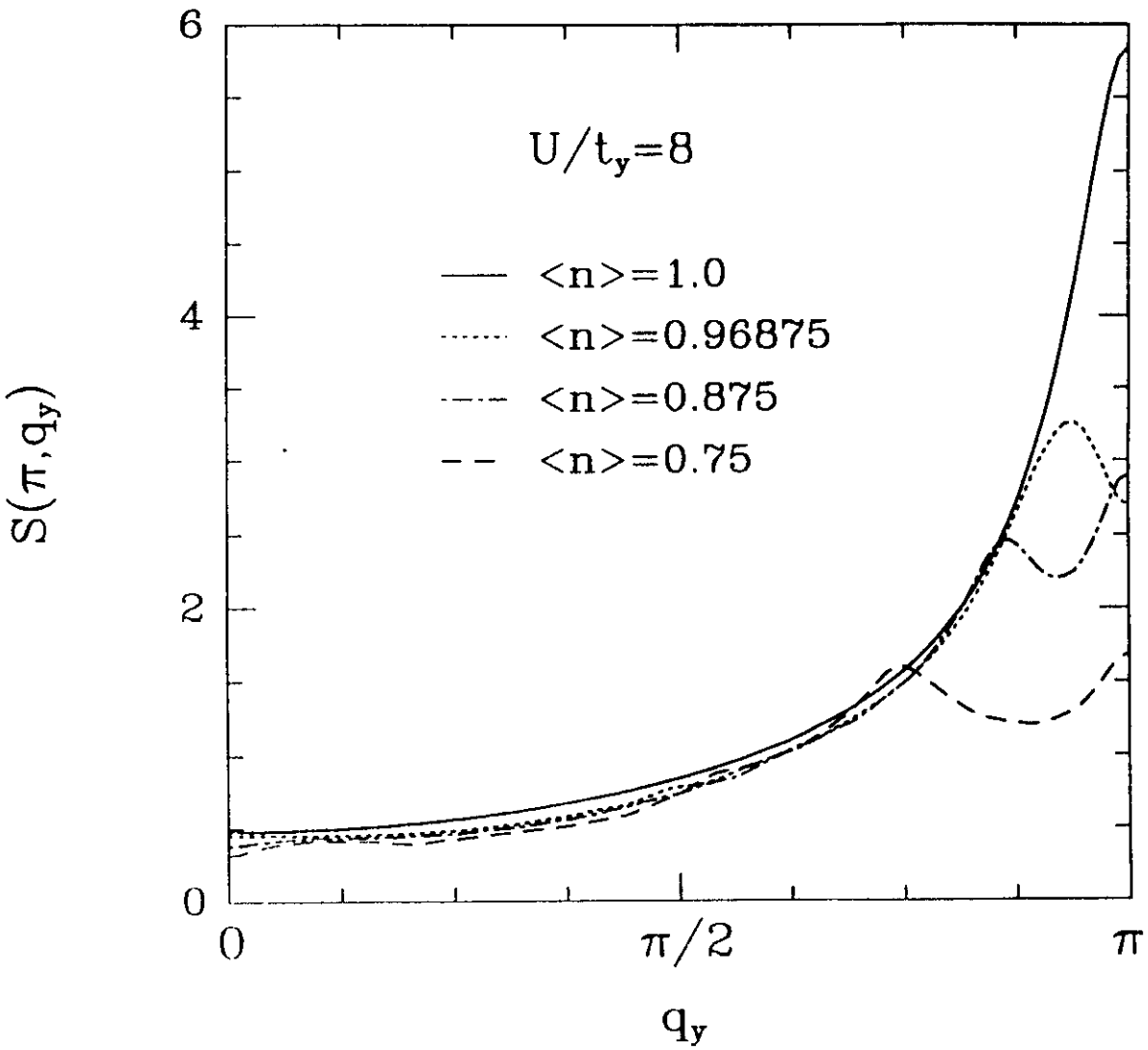
6
4
2
0
0
π/2
π
q_y
$S(\pi, q_y)$
$U/t_y=8$
<n>=1.0
<n>=0.96875
<n>=0.875
<n>=0.75

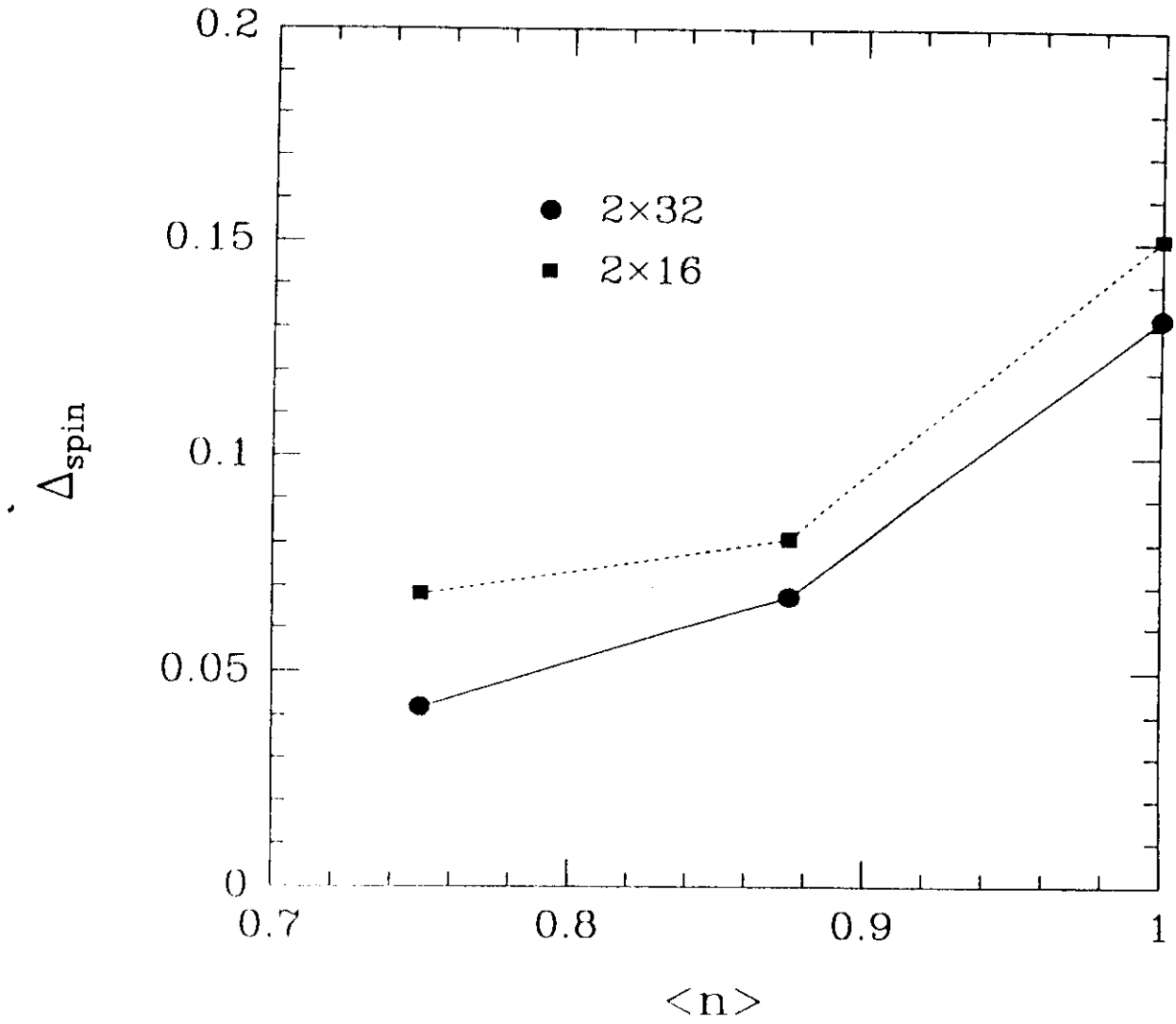
0.2
0.15
0.1
0.05
0
0.7
0.8
0.9
1
Δ_{spin}
<n>
2×32
2×16

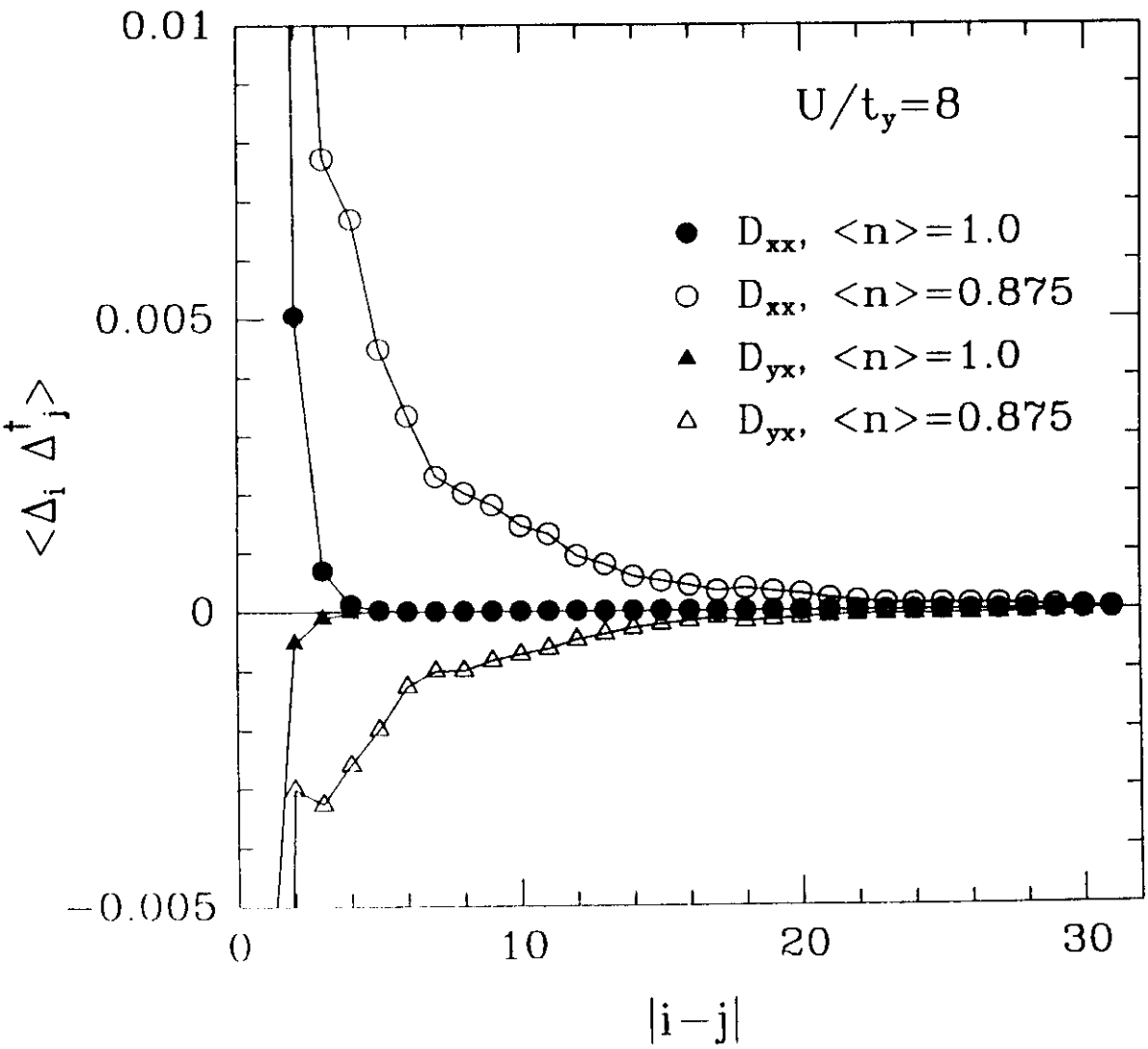
0.01
0.005
0
−0.005
0
10
20
30
$\langle \Delta_i \Delta_j^\dagger \rangle$
|i−j|
$U/t_y=8$
D_{xx}, <n>=1.0
D_{xx}, <n>=0.875
D_{yx}, <n>=1.0
D_{yx}, <n>=0.875

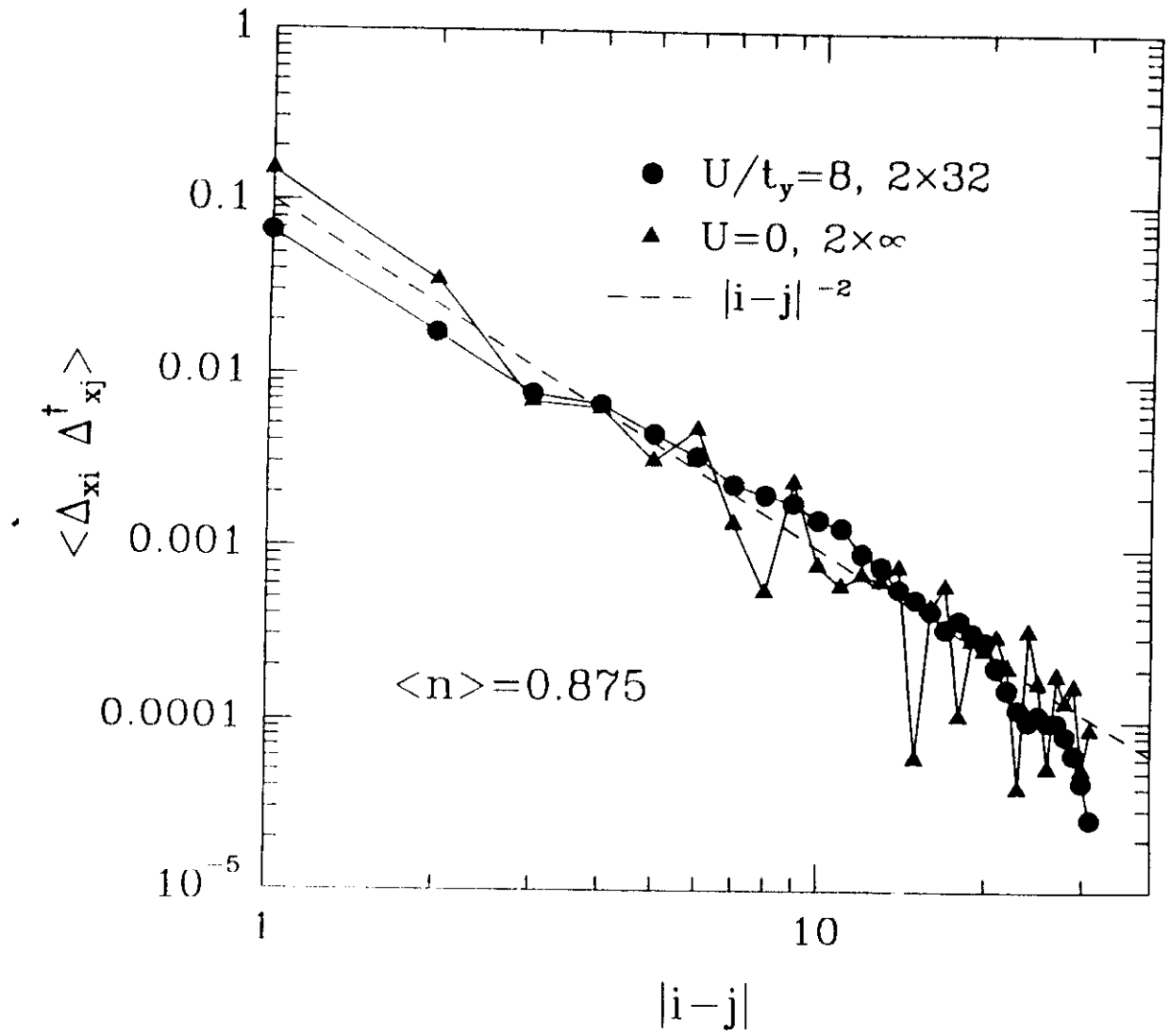
1
0.1
0.01
0.001
0.0001
10^{-5}
1
10
$|i-j|$
$<\Delta_{xi}\ \Delta^{\dagger}_{xj}>$
$U/t_y=8,\ 2\times32$
$U=0,\ 2\times\infty$
$|i-j|^{-2}$
$<n>=0.875$

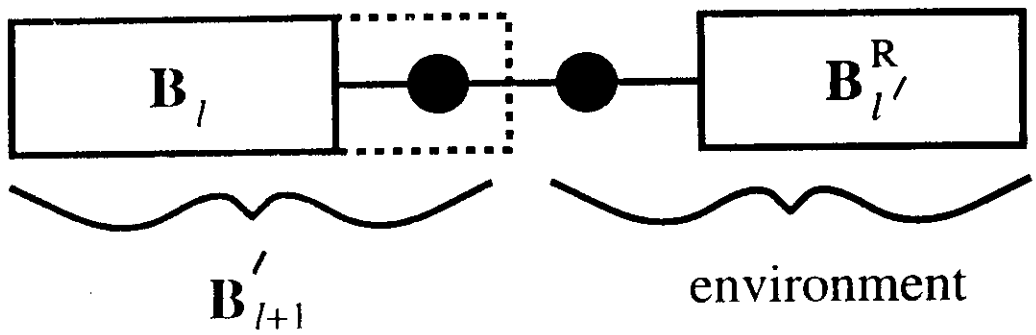

Fig. 1

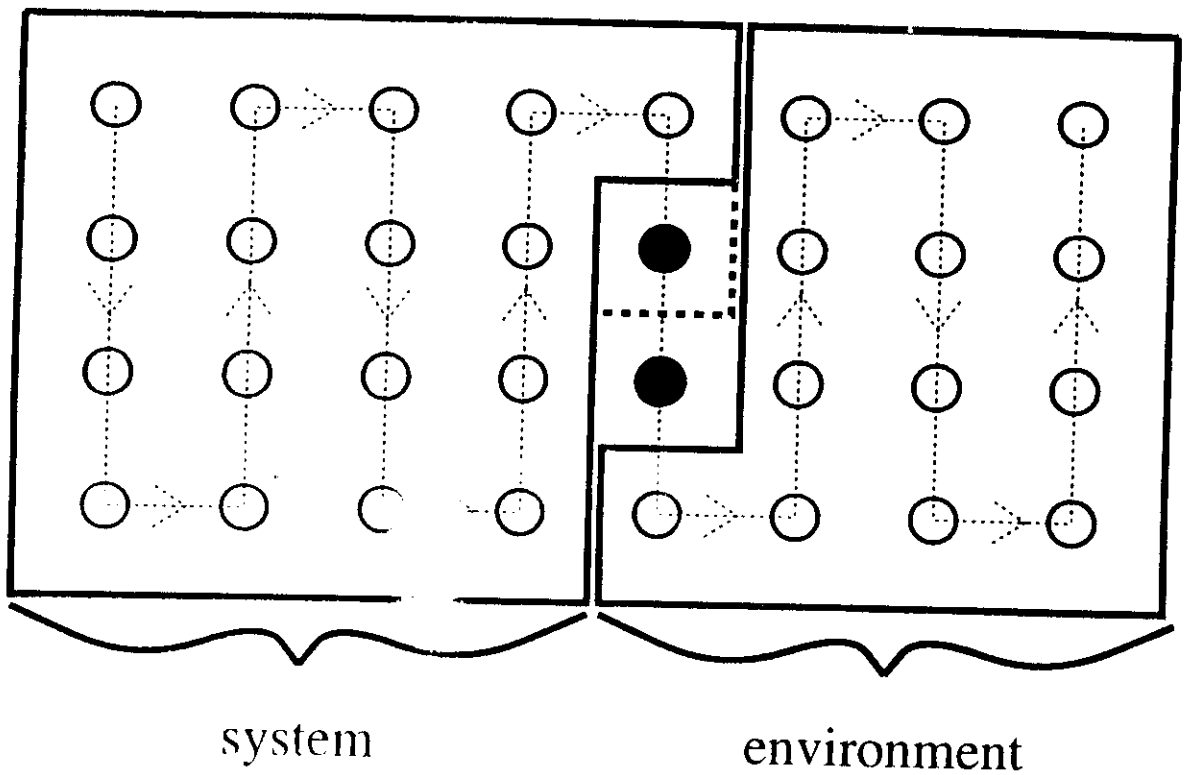

Fig. 2

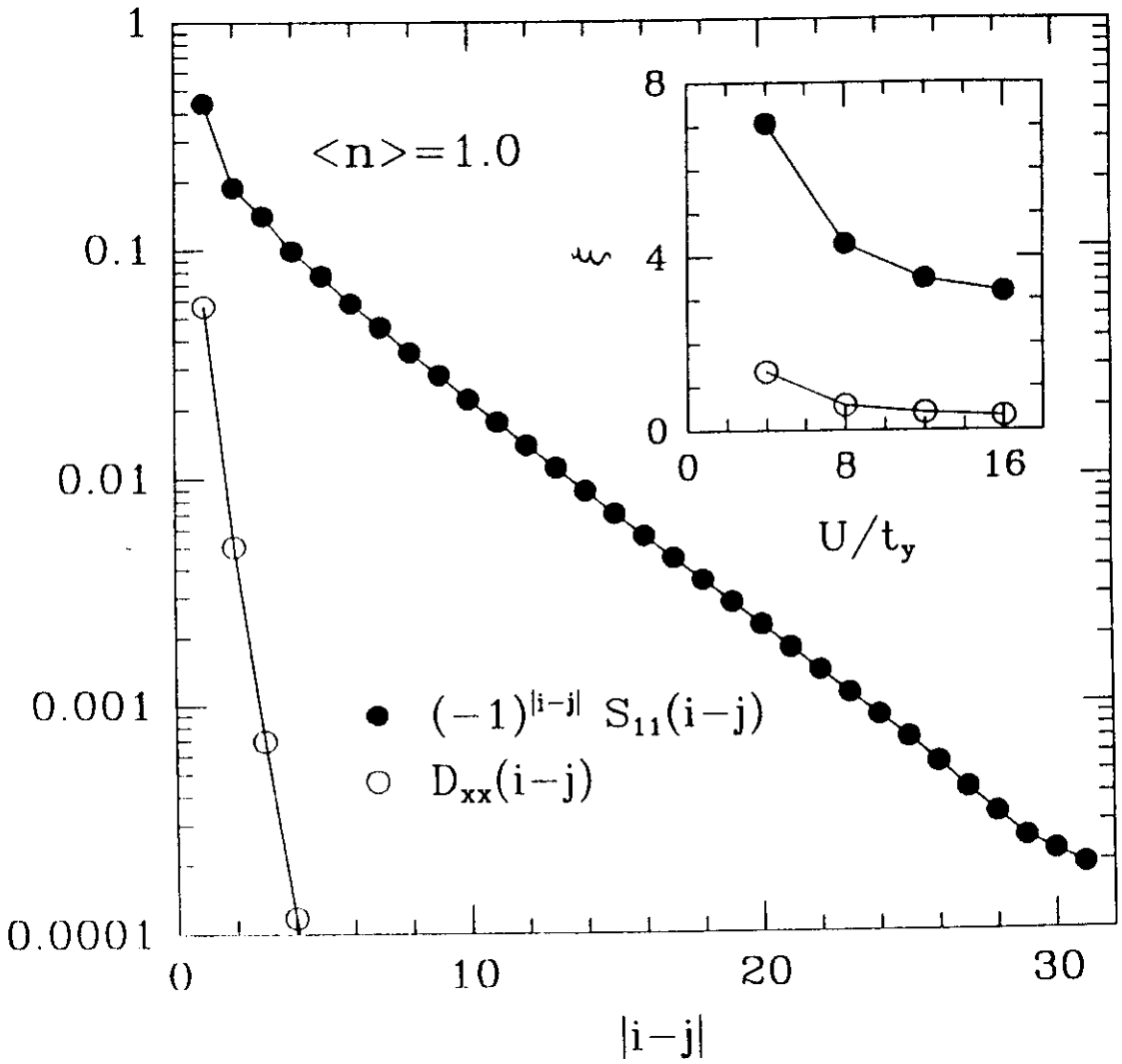
1
0.1
0.01
0.001
0.0001
0
10
20
30
|i−j|
<n>=1.0
(−1)^|i−j| S11(i−j)
Dxx(i−j)
8
4
0
0
8
16
U/ty

Fig. 3

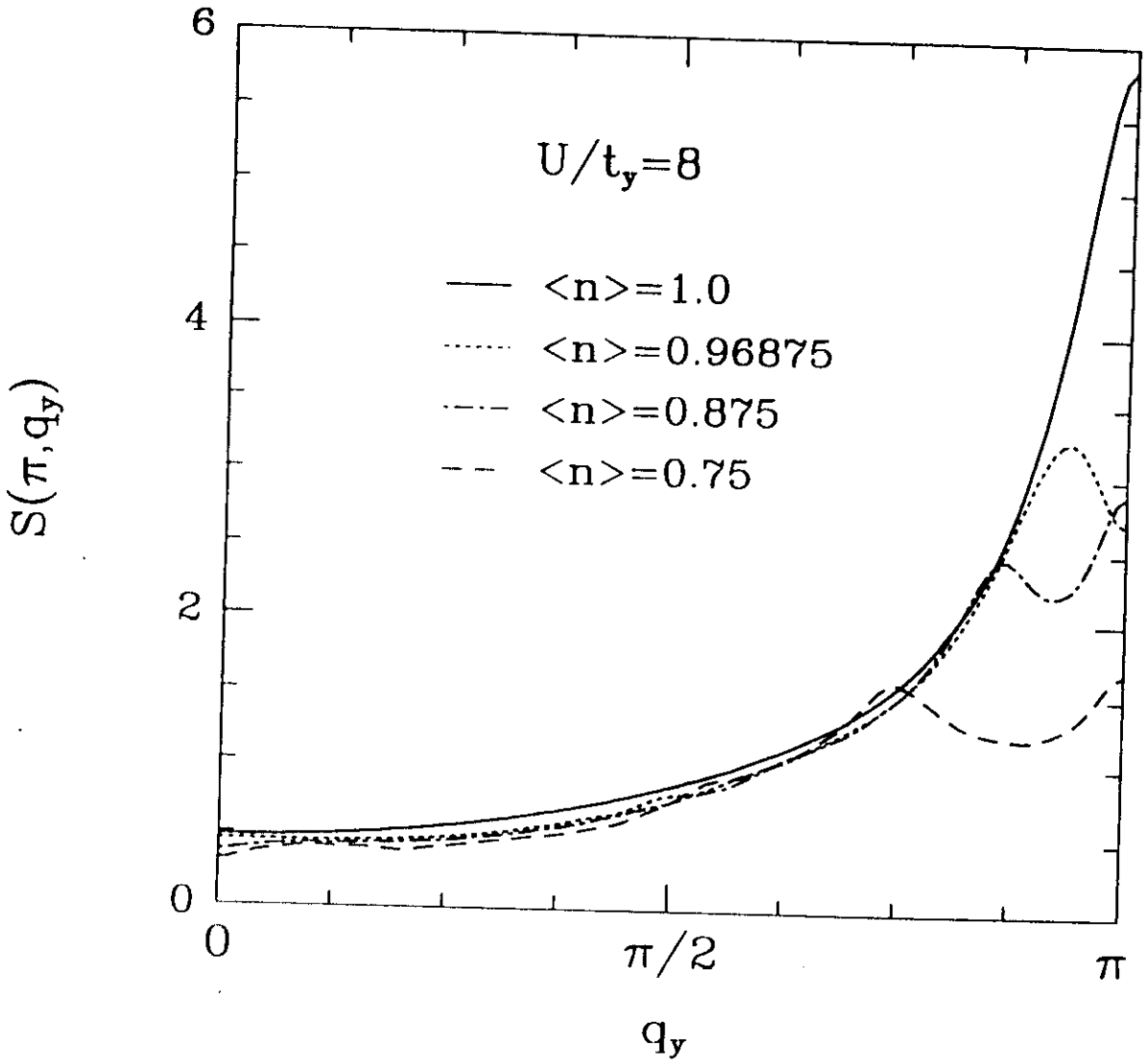

Fig. 4

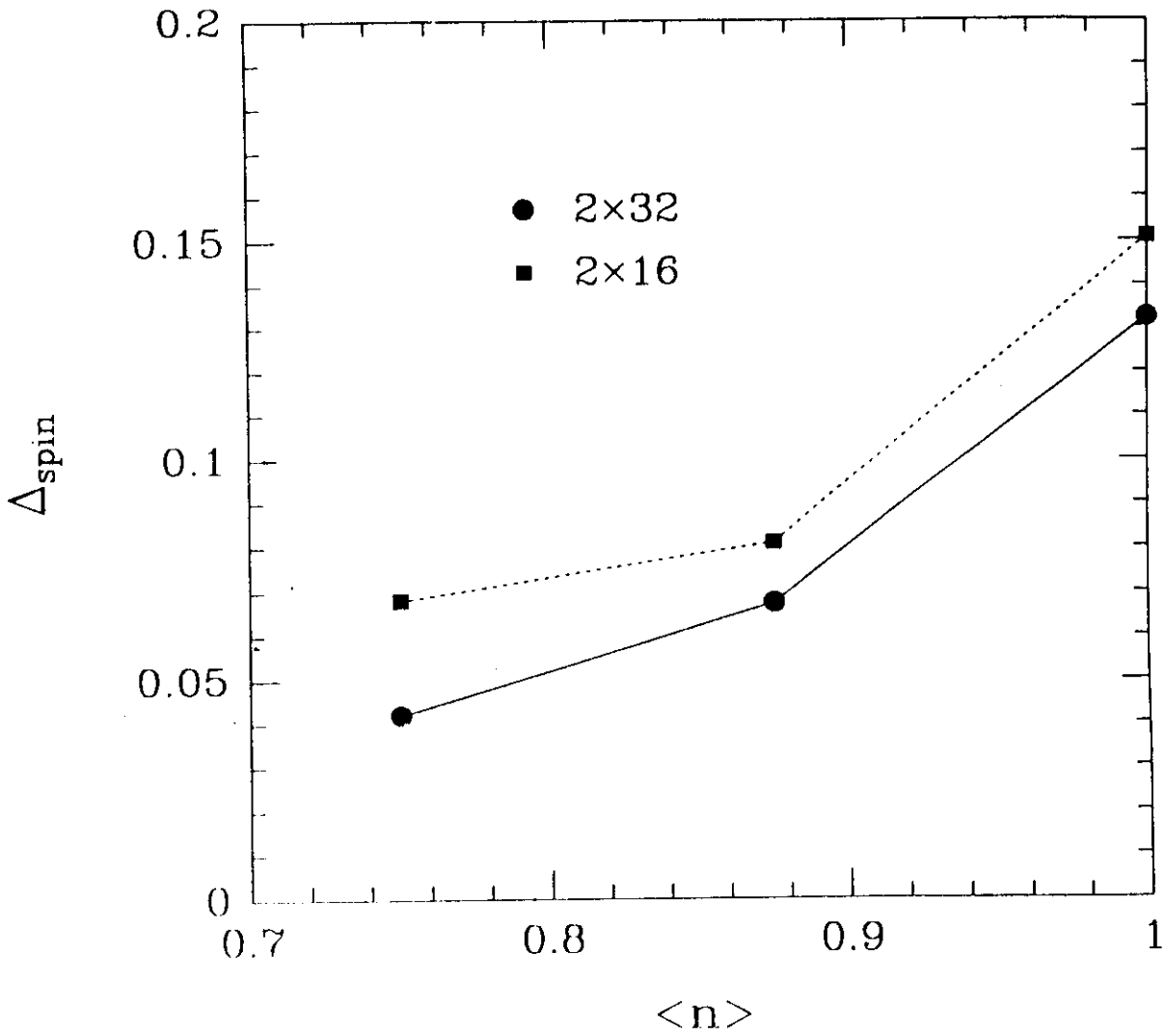

Fig. 5

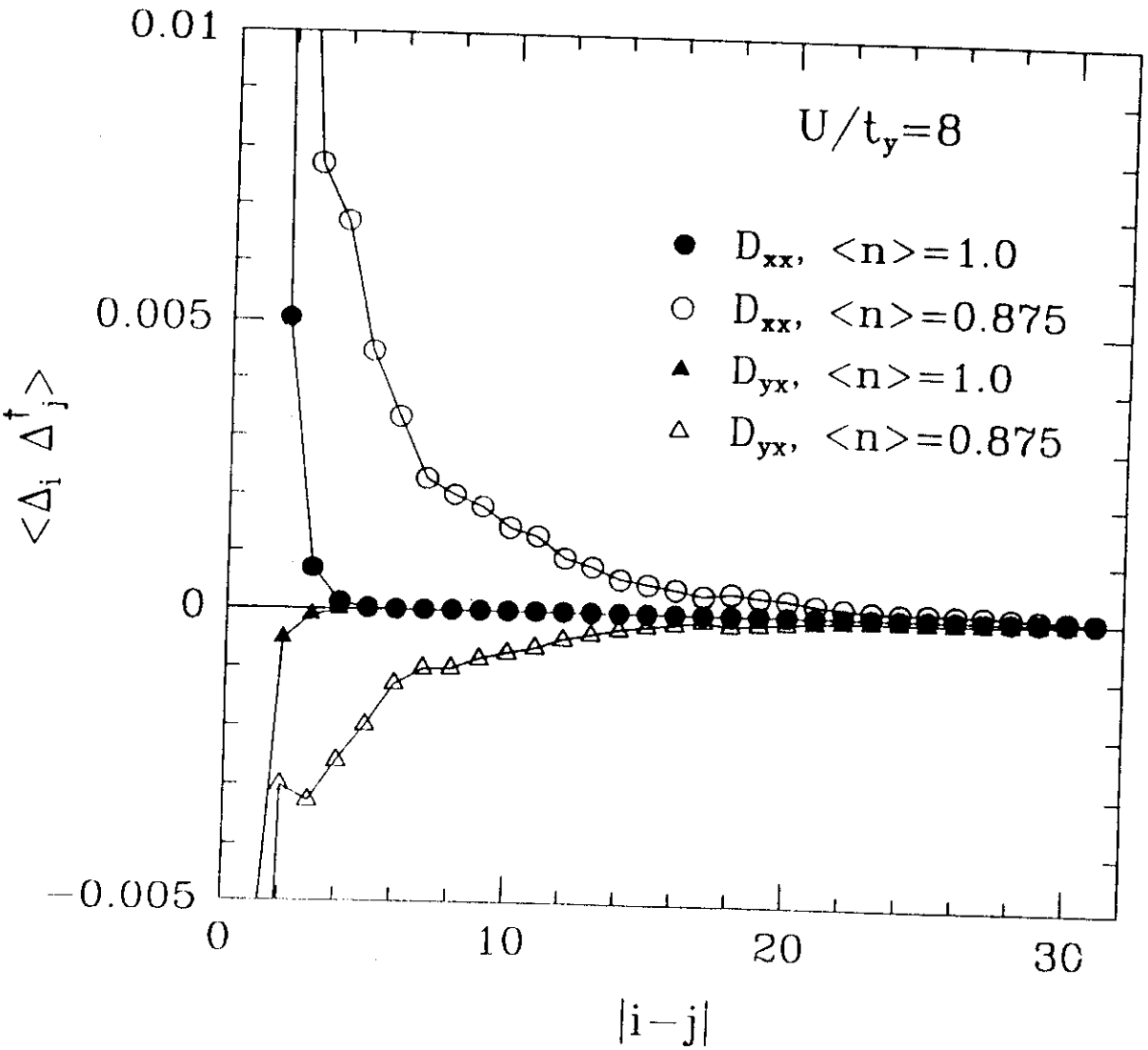
0.01
0.005
0
−0.005
0
10
20
30
|i−j|
$\langle \Delta_i \Delta_j^t \rangle$
$U/t_y=8$
D_{xx}, <n>=1.0
D_{xx}, <n>=0.875
D_{yx}, <n>=1.0
D_{yx}, <n>=0.875

Fig. 6

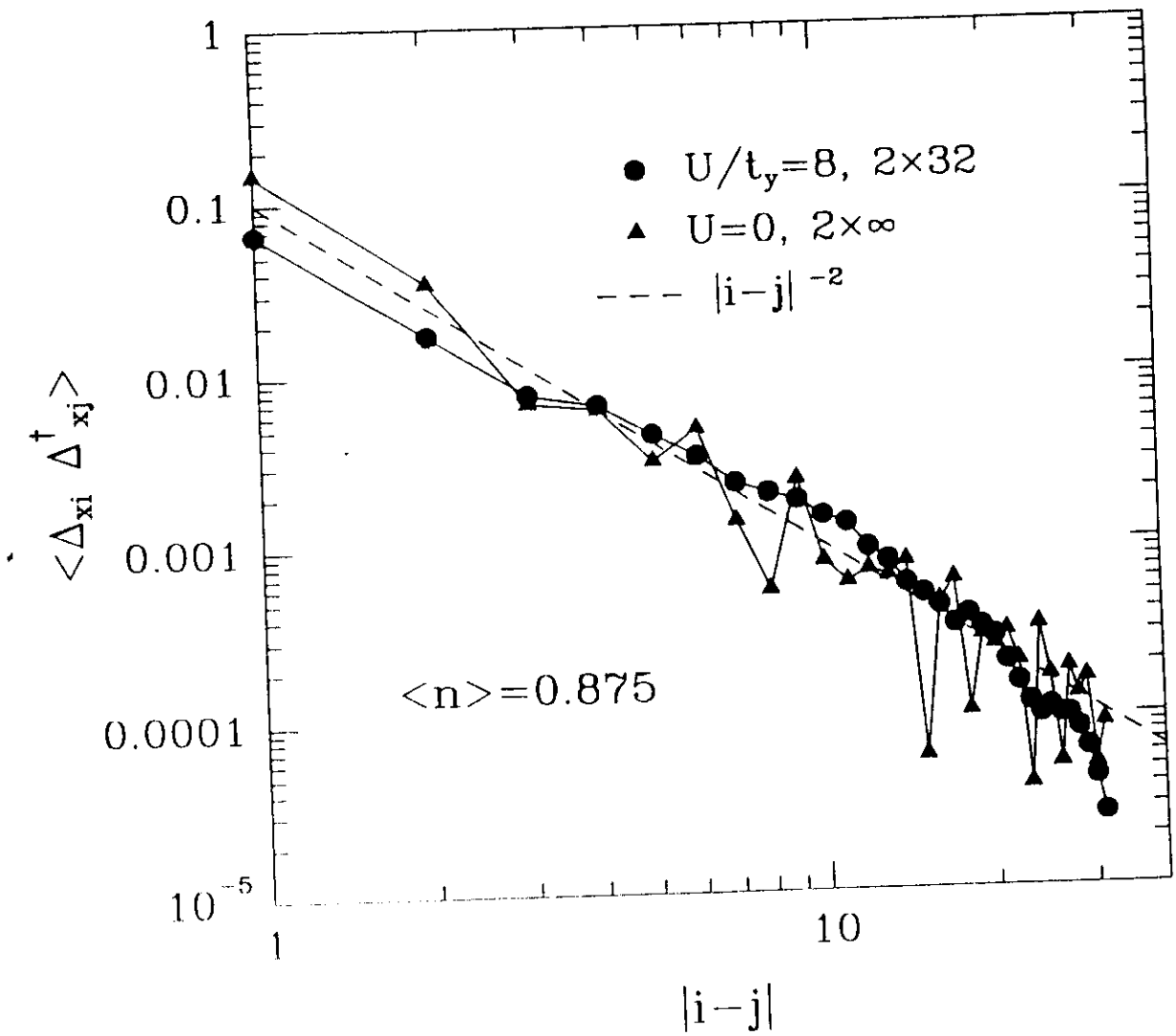
1
0.1
0.01
0.001
0.0001
10^{-5}
1
10
$|i-j|$
$\langle \Delta_{xi}\ \Delta^{\dagger}_{xj} \rangle$
● $U/t_y=8,\ 2\times32$
▲ $U=0,\ 2\times\infty$
--- $|i-j|^{-2}$
$\langle n \rangle=0.875$

Fig. 7